Driving Mechanisms for Cataclysmic Variable Evolution.

Thesis

Faculty of Science, The Open University

Driving Mechanisms for Cataclysmic Variable Evolution

John Barker BSc. Hon.

Submitted for the degree of Doctor of Philosophy

August 2003

Submission date: 27 August 2003
Award date: 8 December 2003

ProQuest LLC.
789 East Eisenhower Parkway
P.O. Box 1346
Ann Arbor, MI 48106 – 1346

CONTENTS

LIST OF FIGURES

LIST OF TABLES

Driving Mechanisms for Cataclysmic Variable Evolution

John Barker BSc. Hon.
August 2003

Faculty of Science, The Open University
Submitted for the degree of Doctor of Philosophy

Cataclysmic variables are interacting binary systems in which the evolution of the system is driven by the loss of orbital angular momentum. In this thesis I investigate possible angular momentum loss mechanisms and try to reconcile the differences between the observed and theoretically predicted minimum period and the orbital period distribution for systems with orbital periods below the period gap. Specifically I use a general consequential angular momentum loss mechanism (CAML) which depends linearly upon the mass transfer rate in the system, and a deformation mechanism which bloats the donor star. Numerical models to include the effects of circumbinary discs and irradiation driven winds from the donor star on the evolution of CVs were developed, the circumbinary disc model is able to raise the minimum period to the observed value. Systems subject to irradiation driven winds and high CAML efficiencies exhibit mass transfer cycles; these could explain the range of mass transfer rates observed in CVs with similar orbital periods. I also consider the possibility that the observed minimum period is purely an age effect.

I model possible parent distributions by using an additional intrinsic angular momentum loss to set the minimum period to the observed value, with different spectra of donor star masses, white dwarf masses, efficiencies for the CAML and bloating mechanisms. A statistical test was developed and used to calculate a probability that the observed distribution is drawn from the modelled parent distribution. None of the calculated distributions gives a better fit than that for a flat distribution. This is suggestive of some additional evolutionary mechanism or selection effect.

I also investigate the apparent difference between the distributions of magnetic and non-magnetic CVs over the period range ($1.3 \leq P/hr \lesssim 15$), concluding that it is likely that these systems evolve via different mechanisms for orbital periods above the lower edge of the period gap.

ACKNOWLEDGEMENTS

I would first like to thank my supervisors, Ulrich Kolb, for all his help, interesting input, interesting conversations and understanding over the past few years and Andrew Norton for some interesting ideas and listening when I needed a sounding board. I also thank Andrew Conway and Chris Jones for their help with my statistical mathematics. Without these people I would have found the working on and the writing of this thesis a much harder task. I also thank Derek Richards[1] and John Cannizzo[2] for the helpful descussions into my circumbinary disc model.

A special thanks must go to Diana Maxwell who was not only my office mate for the first two years, keeping me sane through those dark days, but for 'the help what she gave me' to improving the English in this thesis. Also to Chris Brockwell, Dave (I'm a big boy now!!) Lott, Lisa Blake and once again Andrew Conway who all started around the same time as me and with whom I had so many great times with both in and out of the university. All the great parties, all the hard work and fun of the OU robot wars / technogames experience's, 'CV will live on'. I thank Sandra Mills, Roger Bence and Martin Pearce for all their help with the robot projects and the science marketing department whom without their financial support the projects would have never reached fruition. Ben Eves and Stephen Justham who have put up with me as my office mates through thick and thin over the past two years, to you I leave 'MY' office, desk and chair make sure my replacement treats them well.

I would like to acknowledge the computer staff Geoff Bradshaw and Read Short for all their help and hard work on maintaining and upgrading of the system, whilst contending with my occasional disruption of the system due to runaway programs and the destruction of various machines. To the many other members, not least Craig Powel for being Craig and Robin Barnard for being incomprehensible even when I understood the words, of this great department for making this such a nice relaxed environment to work in you will all be sorely missed.

And finaly I must thank Dan Rolfe who was also my office mate for the first two years, the coloured home made bread will stick in my mind forever, what else can you say about Dan?

[1]The Open University, Dept:- Maths and Computing

[2]NASA Goddard Space Flight Center, Laboratory for High Energy Astrophysics, Code 661, Greenbelt, MD 20771; and The University of Maryland, Baltimore County.

DEDICATION

I dedicate this thesis to my partner Elisa 'my anchour', my four wonderful daughters Joanna, Sarah, Lynn and Mary for sticking with me and ridding all the mood swings, from elation to despair during the writing of this work, and to my mother Trudy Barker for always being there at the other end of the phone to encourage and support me when I needed a shoulder to cry on.

Well a black hole is this realy big thing, well basically it's a massive... hole, out there. And what happens is everything gets sucked into it, even light. That's why we can't see it, it just gets sucked in. (O'Neill)

Thank you (Teal'c)

Sure (O'Neill)

(Stargate SG1, Season One, 'ENIGMA')

Chapter 1

Introduction

In this chapter I introduce the subject of my studies, Cataclysmic variables (CVs), and give an overview of the main properties of CVs. In section 1.1 I introduce the standard models for CVs and their various sub-classes. In section 1.2 I present the standard description for the formation of CVs and introduce some of the features of the mass distribution of the stars relevant for my studies. Section 1.3 describes the evolution of CVs, detailing some of the important features seen in the observed sample, concentrating on the areas of greatest relevance to my subsequent studies.

1.1 Cataclysmic variables

CVs are a class of interacting binary stars in which the generally more massive (primary) star is a white dwarf, while the companion star (the secondary) is a normal star with a mass typically in the range $0.1-1.0M_{\odot}$. A white dwarf is an end stage of the evolution of a star with a mass of less than $\simeq 9\mathrm{M}_{\odot}$. The typical mass of a white dwarf is around $0.6\mathrm{M}_{\odot}$, though the mass may vary in the range $0.3\mathrm{M}_{\odot} \lesssim M \lesssim 1.4\mathrm{M}_{\odot}$. (See section 1.2.1). The stars orbit in such close proximity (typically within a few solar radii) that the secondary fills its Roche lobe (see section 1.1.1 on Roche geometry). Matter from the outer envelope of this star flows through the L_1 point and falls toward the primary. This material may

now take one of several routes depending upon the characteristics of the primary (see sections 1.1.2 - 1.1.4)

The vast majority of CVs are intrinsically very faint objects in the optical region of the spectrum, hence most of the currently known CVs lie at distances $50 \lesssim d \lesssim 300$ pc. In most cases the accretion luminosity of the system exceeds the intrinsic luminosity of the two stars, the spectrum is usually thus dominated by an essentially featureless blue continuum from the accretion disc. In addition the inferred mass transfer rates for CVs at any given period cover a range of values spanning one or two orders of magnitude (see Patterson (1984), Warner (1987), Warner (1995)). Thus about the only physical characteristic of CVs that can be measured directly with any certainty for most systems is the orbital period (see e.g. Ritter (1990)), the exceptions to this are double-lined eclipsing systems in which the masses of the stars may be reliably determined. As CVs evolve under mass and angular momentum loss the orbital period of the system changes with time (see section 3.1), thus any model for the evolution of CVs should aim to reproduce the main features of the observed orbital period distribution.

Over the past two decades, numerous studies have investigated the evolution of the secondaries in CVs with the aim of reproducing the observed orbital period distribution. The main features of this distribution are, (as can be seen from figure 1.1) the long period cut-off at around 12 hrs, the lack of systems in the 2-3 hr period range, the so called period gap, (The explanation for the period gap by the disrupted magnetic braking model [cf. Rappaport, Joss, and Verbunt (1983); Spruit and Ritter (1983), see section 1.3.2] is now widely accepted) and the sharp cut-off of the distribution at around 78 minutes (see e.g. King (1988) for a review). I ignore the very short period ($<$ 64.0min), helium rich AM CVn systems (Ulla (1994)). As the periods of these systems are so short and many of the stellar properties are greatly influenced by the metallicity of the star, the secondaries in AM CVn systems must be radically different from those for the hydrogen rich CVs. These differences guarantee a very different evolutionary path for this class of CVs. There have also been recent observations (see Thorstensen et al. (2002), Uemura et al. (2002), Wei et al. (2001)) of a dwarf nova system (1RXS J232953.9+062814) and (Ruiz, Rojo, Garay,

and Maza (2001)) of a nova-like double degenerate system (CE 315) with orbital periods at around 64 minutes, these systems, along with the dwarf nova V485 Cen with an orbital period of around 59 minutes, are also not taken into account.

Despite all the work on the subject, theoretical models have been unable to reproduce the

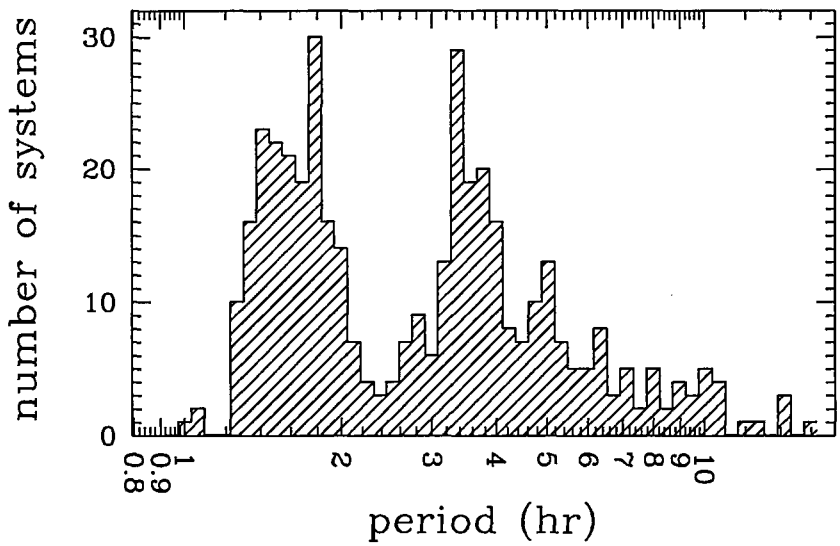

Figure 1.1: The observed orbital period distribution of CVs. (RKcat version 7.0, Ritter and Kolb (2003))

observed short period cut-off and the observed shape of the CV orbital period distribution of systems with orbital periods between the minium period and the lower edge of the period gap at around 2hr (see Kolb and Ritter (1992), Howell, Rappaport, and Politano (1997) and Chabrier and Baraffe (2000), also see section 1.3.3 below).

1.1.1 Roche geometry

In systems where two stars orbit each other about a common centre of mass, to understand the flow of material from one star to the other, it is useful to consider a non-inertial frame of reference co-rotating with the system about the centre of mass. Assuming that the two stars orbit in circular orbits about the centre of mass, (which in the case of

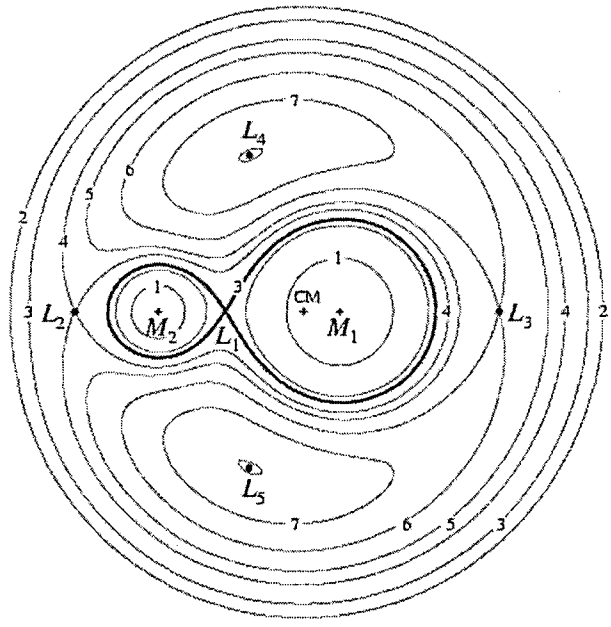

Figure 1.2: Roche equipotentials in the corotating orbital plane from; Frank, King, and Raine (2002). M_1, M_2 and CM are the centre of mass of the primary, secondary and the system respectively, while L_{1-5} are the stationary points in the potential

CVs is usually a good approximation as the timescale for circularization due to the tidal interactions is much shorter than the mass transfer timescale) and that the stars are point like masses (which is also a good approximation as the WD is small compared to its Roche radius and the secondary star is sufficiently centrally condensed) then within this frame the gravitational force and the centrifugal forces can be mapped as three dimensional equipotential surfaces surrounding the two stars. The section in the orbital plane in this rotating frame of reference is plotted in figure 1.2. The shape of the equipotentials are determined by the mass ratio $q = m_2/m_1$ (where m_1 and m_2 are the masses of the primary and secondary in *cgs* units respectively) and the orbital period. At large distances r from the centre of mass, CM, ($r \gg A$, where A is the orbital separation in *cm*) in the plane

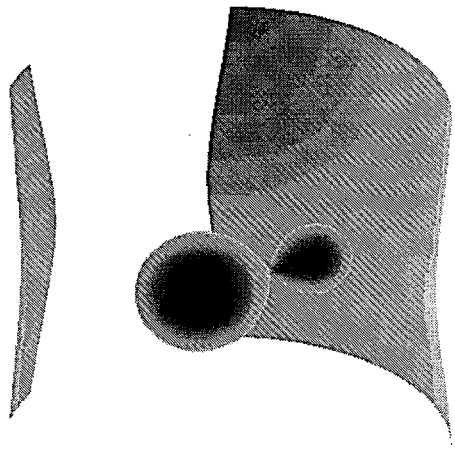

Figure 1.3: Roche equipotential surfaces with the same potential as the L_1 point labelled 3 in figure 1.2

the equipotentials can be seen to be circular (2), and the potential is the same as in the absence of any mass, i.e. it is purely centrifugal. Close to the centre of each star the potentials are once again circular (1). This is where the gravitational potential of the nearer star dominates. Moving out from the centre of the stars the equipotentials deviate more from circular. The last equipotential surrounding each star separately forms a figure of eight shape (shown in bold in figure 1.2). In 3-dimensions these lobes form a dumbbell shaped volume enclosed by an equipotential surface with the same potential, (see figure 1.3) known as the Roche lobes. The point at which the two lobes touch is called the inner Lagrangian point L_1. The two lobes can be thought of as two deep potential wells which interact via a saddle point at L_1. A test mass near the L_1 point would find it easier to cross from one Roche lobe to the other rather than travel up the potential gradient to escape from the system. There are two other saddle points, the L_2 and L_3 points, and two maxima, the L_4 and L_5 points, making up the five stationary points in the Roche potential.

The equation determining the shape of the equipotential surfaces is

$$\frac{U_{tot}}{Gm_1} = -\frac{1}{r_{t1}} - \frac{q}{r_{t2}} - \frac{r_t^2(1+q)}{2A}, \tag{1.1}$$

where U_{tot} is the total potential experienced by a test mass at any point in the system, r_{t1}, r_{t2} and r_t are the distance of the test mass from the primary, secondary and axis of rotation of the system respectively in cm, and G is the gravitational constant. Equation 1.1 is obtained as follows.

The gravitational potential about each star is given by

$$U_g = -\frac{Gm_\star}{r_\star}. \tag{1.2}$$

Here $r_\star$ is the distance to the test mass from the centre of the gravitating body of mass $m_\star$ in this case the star, both in cgs units. As the system is rotating, the stars orbit a common centre of mass and a centrifugal force is experienced by this mass. This is given as

$$F_c = m\omega^2 r_t, \tag{1.3}$$

where r_t is the perpendicular distance of the test mass from the axis of rotation of the system and ω is the orbital angular velocity, both in cgs units. From this the centrifugal potential is given as

$$U_c = -\frac{4\pi^2 r_t^2}{2P^2}, \tag{1.4}$$

where P is the orbital period of the system in seconds. Combining equations 1.2 and 1.4 with Kepler's third law gives equation 1.1.

Before continuing I state the following standard definitions.

1:- The circularization radius is

the radius at which material with the specific angular momentum of the L_1 point will orbit about the primary. Assuming that angular momentum is conserved this gives, in units of solar radius

$$R_{circ} = a(1+q)\left(\frac{b}{a}\right)^4, \tag{1.5}$$

where

a = the orbital separation of the system A in solar units.

b = the distance of the L_1 point from the centre of the primary in solar units.

As angular momentum is not strictly conserved this is only an approximation.

2:- The corotation radius is

the radius relative to the centre of mass of a body, in our case the primary, at which the Keplarian angular velocity for a particle in a circular orbit about the body is the same as the rotational angular speed of the body. This is given in units of solar radius as

$$R_{co} = \left(\frac{P_{spin}^2 G M_1}{4\pi^2}\right)^{\frac{1}{3}}, \tag{1.6}$$

where

P_{spin} = the spin period of the primary.

M_1 is the mass of the primary in solar units.

3:- The magnetospheric radius is

the radius at which the ram pressure of the in-falling material is equal to the magnetic pressure. Frank, King, and Raine (2002) approximate this in units of solar radius from the assumption that the white dwarf's magnetic feild is dipolar (see equation 1.7), the exact for of the approximation also depends on the accretion geometry (see sections 1.1.2-1.1.4 below),

$$R_{mag} = 1.62 \times 10^{-4} \dot{M}^{-\frac{2}{7}} M_1^{-\frac{1}{7}} B^{\frac{4}{7}} R_1^{\frac{12}{7}}, \tag{1.7}$$

where

$\dot{M}$ is the mass transfer rate through the L_1 point in $M_\odot$/yr.

B is the surface magnetic field strength of the white dwarf in Gauss.

R_1 is the radius of the white dwarf (R_{WD}) primary in solar radii, and is given by the analytical fit

$$R_{WD} \simeq 1.12 \times 10^{-2} \left(\left(\frac{M_c}{M_1}\right)^{\frac{2}{3}} - \left(\frac{M_1}{M_c}\right)^{\frac{2}{3}} \right)^{\frac{1}{2}}, \tag{1.8}$$

(Nauenberg (1972)) where $M_c \approx 1.44 M_\odot$ is the Chandrasekhar mass for a white dwarf.

I also define for this thesis the following units:

M_2 is the mass of the secondary in solar masses.

R_2 is the radius of the secondary in solar radii.

R_L is the Roche radius of the star under consideration in solar radii.

1.1.2 CVs with accretion discs

(see Frank, King, and Raine (2002)) If the primary has no magnetic field, or only a weak magnetic field ($B \lesssim 10^4 G$), the transferred material will fall toward the primary un-hindered. Due to the orbital angular momentum this material had on leaving the L_1 point, if unaffected by external forces, it would eventually orbit the primary at the circularization radius. Due to viscous forces (and tidal interactions with the secondary) the material then settles into a disc like structure (see figure 1.4). The material flowing

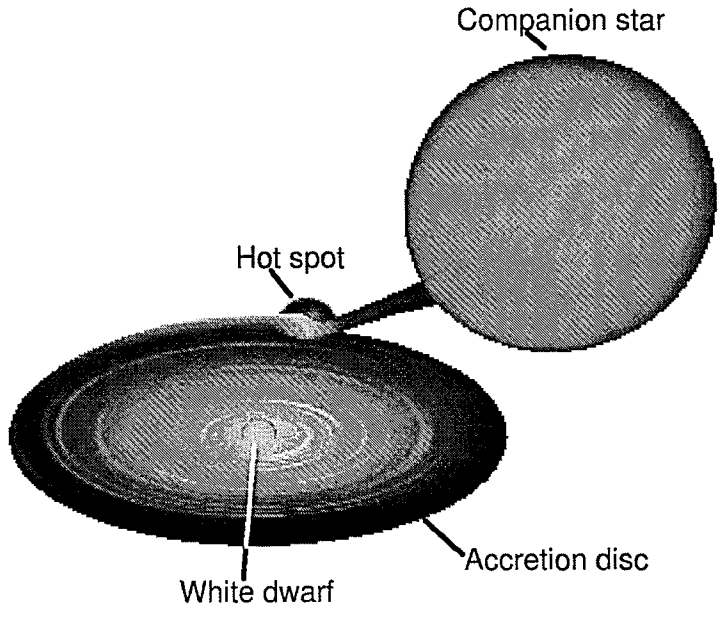

Figure 1.4: Representation of a system containing an accretion disc (reproduced with the kind permission of Dr. Dan Rolfe)

from the L_1 point and impacting the disc causes localized heating and forms an observable 'hot spot'. Material slowly spirals in through the disc structure to be accreted onto the primary. This hydrogen-rich material builds up on the surface of the primary to the point at which a thermonuclear runaway takes place, causing a nova outburst (see section 1.1.6 on classical novae, Starrfield (1989)).

1.1.3 CVs with an accretion stream

(see Frank, King, and Raine (2002)) If the primary has a high magnetic field ($B \gtrsim 10^4 G$) and a low spin angular velocity the transferred material will still form a disc if the magnetospheric radius is less than the circularization radius. In this instance, however, the disc formed will be truncated at the magnetospheric radius forming an intermediate polar (see figure 1.5).

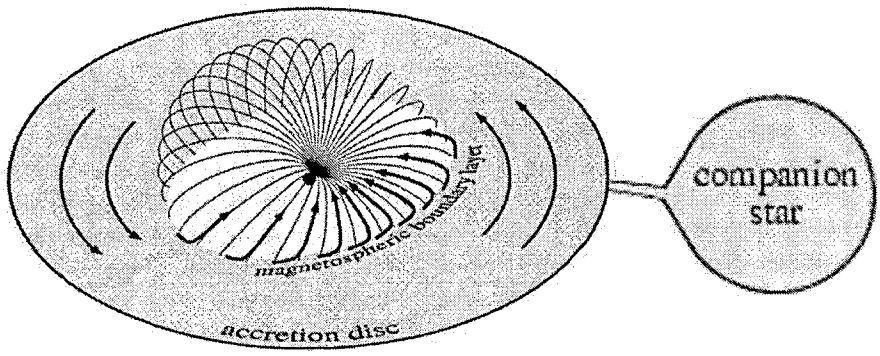

Figure 1.5: Representation of a system containing a slowly spinning moderately magnetic white dwarf, an intermediate polar (field lines shown assume a dipole magnetic field). (Frank, King, and Raine (2002))

If the magnetospheric radius is greater than the circularization radius, no disc will form. In either case on reaching the magnetospheric radius the material is threaded by the field lines and forced to co-rotate with the primary. The material then follows the field lines down to the primary's surface at its magnetic poles. If the field strength is high enough

hydrogen burning on the white dwarf produces a large flux of supersoft X-rays, these can drive strong winds from the heated face of the secondary and the accretion disc (see Chapter 6). The secondary in supersoft sources for a near main sequence star and a primary mass of around $0.7M_{\odot}$ should be in the range 1.3 - 2.5$M_{\odot}$. This would be consistent with an orbital period of around 1 day, therefore the existance of supersoft sources with periods at around 4 hours requires a different explanation for the initial thermal time-scale mass transfer epoch (see van Teeseling and King (1998)).

1.1.6 The CV menagerie

All these factors combine to produce a large variety of phenomena that are exhibited by these systems which has led to the introduction of several sub-classes as given below (also see Robinson (1976)).

Classical novae

The material transferred from the secondary to the primary can build up on the surface of the WD to the point where the temperature and pressure are sufficient to initiate nuclear burning of the hydrogen (Starrfield (1989)). As the WD is made from degenerate material, supported by electron degeneracy pressure, the pressure exerted by the material is virtually independent of the increasing temperature and hence a thermonuclear runaway is initiated as the energy released by nuclear burning increases the temperature which in turn increases the energy generation rate. The degeneracy is eventually lifted by this process and the outer layers of the WD can be blown off explosively. During this phase the energy released is so large as to raise the brightness of the system by as much as 12 magnitudes. Thus systems that were too faint to be observed previously are suddenly observable as new (Novae) stars. The recurrence time for such systems is dependent upon many factors such as the mass transfer rate and WD mass and is generally long, of the order of 10^4 yr, and may be much longer.

Dwarf novae

Dwarf novae also undergo regular outbursts where they exhibit increased luminosity. However this is only of around 2-5 magnitudes and they have a short recurrence time of

around a few weeks to a few months. The main mechanism proposed for the outbursts is thought to be an instability in the mass transfer process, this may be due to either of the two following models (see Frank, King, and Raine (2002))

- A thermal viscous instability in the accretion disc (Osaki (1996)). The temperature of a region of the disc reaches around 7000K there is a rapid change in the opacity as the hydrogen ionises, this gives two stable branches connected by an unstable branch leading to a limit cycle behavior of the disc which alternates between the two states (Meyer and Meyer-Hofmeister (1981)). The instability is triggered as some annulus in the disc exceeds the critical surface density and a heating wave then passes through part or all of the disc causing the outburst.

- The mass transfer rate from the companion star is variable due to dynamical instabilities in the envelope, this would mean that the outburst would correspond to a sudden burst of mass transfer from the secondary.

Nova-likes

Nova-likes include all CVs which show no major outbursts, though may exhibit minor fluctuations, which together with their spectroscopic and photometric properties resemble classical novae systems at minimum or dwarf novae in outburst. The magnetic systems discussed previously also fall into this catagory, in which little or no material forms a disc and in many cases little of the material passing the L_1 point is accreted by the WD hence systems would show no outbursts or have extremely long recurrence times.

1.1.7 Period distribution of subclasses

Figure 1.8 shows the period distributions of nova-like and dwarf nova systems. From this it can be seen that dwarf novae occur preferentially as short periods below the period gap. Nova-likes in contrast have a more even distribution and are found with similar frequency above and below the period gap. Some nova-like systems are also found at periods within the period gap whereas very few dwarf novae are found in this range (see chapter 7).

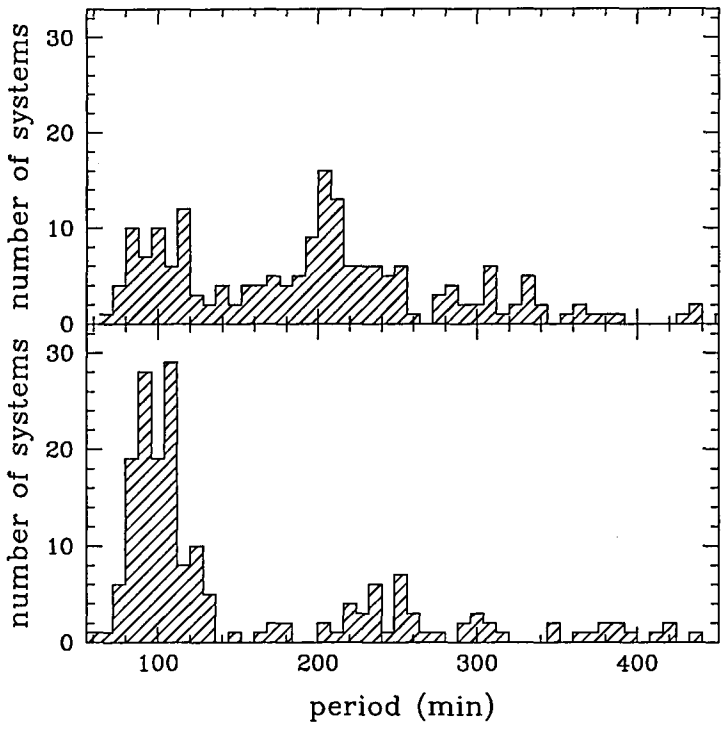

Figure 1.8: Distribution of Nova-like (Upper frame) and Dwarf Novae (Lower frame) (RKcat version 7.0, Ritter and Kolb (2003))

1.2 CV formation

Most CVs start life as a wide binary system consisting of two main sequence stars, one (the primary) with a mass of up to $9M_{\odot}$ and the other (the secondary) with a mass up to $\simeq 1.2\mathrm{M}_{\odot}$. The separation is such that the two stars initially evolve independently of each other (see figure 1.9 top frame). The separation of the system will evolve mainly due to wind losses from the more massive star, causing the stars to slowly spiral apart (see figure 1.9 1st and 2nd frames). Eventually the higher mass star evolves off the main sequence and if the orbital separation is sufficient (as in the case of figure 1.9) the star may pass through the red giant branch (RGB) phase of its life without filling its Roche lobe. The star will then enter the helium burning phase. At the end of the helium burning phase the star will once again experience an expansion of its envelope, on the asymptotic giant

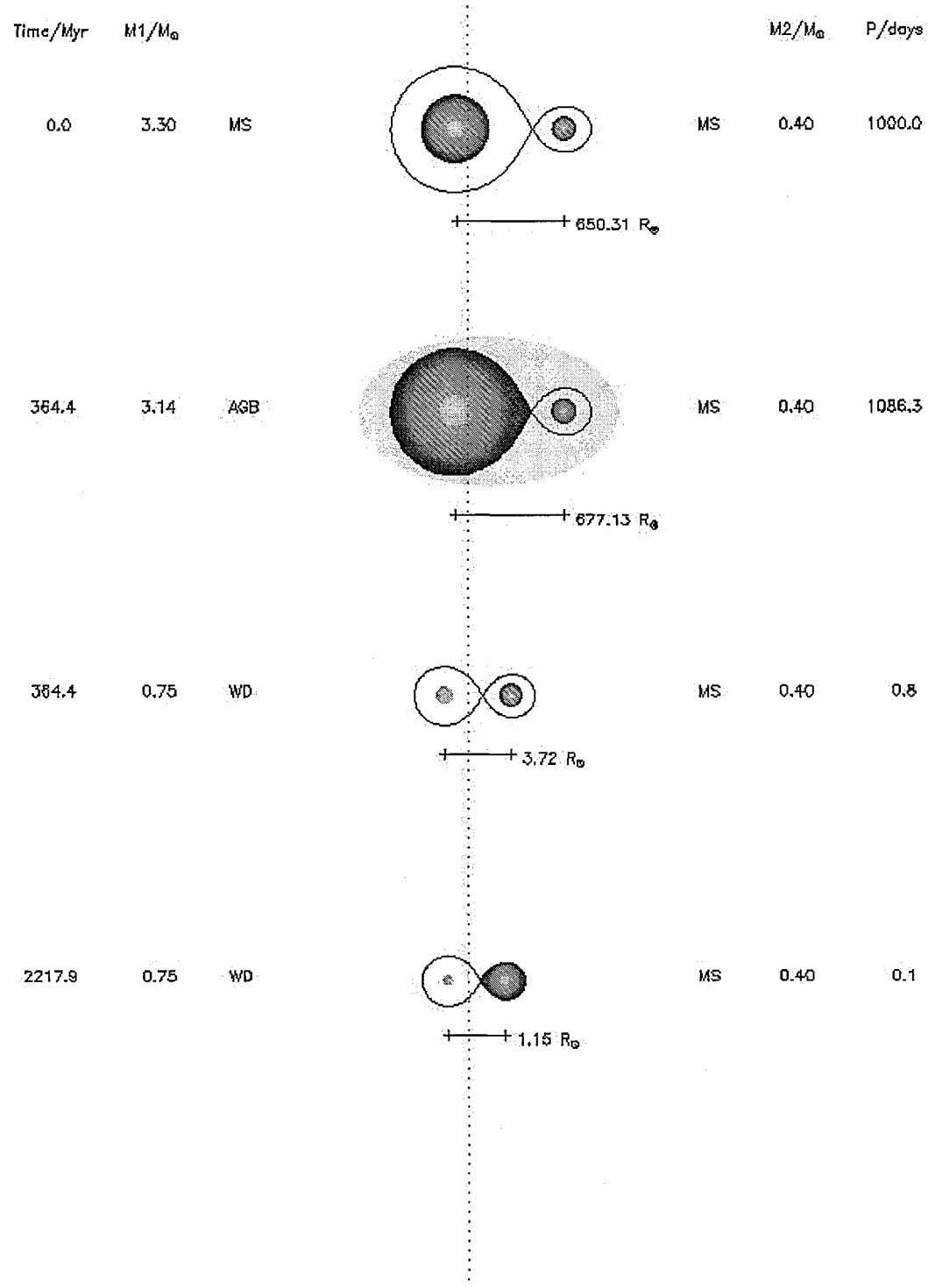

Figure 1.9: Schematic representation of the standard formation channel for CVs (reproduced with the kind permission of Dr Bart Willems (OU) 2002)

branch (AGB). If the separation at this point is sufficiently small the star will fill its Roche lobe and the lower mass main sequence star will be engulfed by the outer envelope of the giant (see figure 1.9 2nd frame). Thus the core of the giant and the main sequence star will orbit about each other inside the common envelope (CE) (see Taam and Sandquist (2000), Iben and Livio (1993), for reviews) and spiral together due to dynamical friction (also see section 1.2.1). The frictional forces transfer angular momentum from the orbit of the inner binary, consisting of the core of the more massive star and the lower mass star, to the envelope causing it to spin up and eventually be expelled from the system.

The result of this phase is dependent upon the initial separation of the system and the initial masses of the stars, as can be seen from the simple expression based on energy arguments that is used in population synthesis models (see e.g. Kolb and de Kool (1993),)

$$\frac{G(m_c + m_{env})m_{env}}{\lambda r_g} = \alpha_{CE}\left(\frac{Gm_c m_2}{2A_f} - \frac{G(m_c + m_{env})m_2}{2A_i}\right), \tag{1.9}$$

where α_{CE} is the fraction of the released orbital energy that is used to unbind the envelope and is of the order unity, A_i and A_f are the initial and final separation respectively, m_c and m_{env} are the masses of the core and envelope of the giant respectively. r_g is the Roche-lobe radius of the giant at first contact and m_2 the mass of the secondary (all units are in *cgs*). The parameter λ takes into account the structure of the giant and relates to the thermal energy and gravitational binding energy of the envelope (see Han, Podsiadlowski, and Eggleton (1995) for details, also see de Kool (1990)). Typical values for λ are around $0.2 - 0.8$ for intermediate mass giants (Dewi and Tauris (2000)) and generally smaller for higher mass stars (Dewi and Tauris (2001)). If the initial separation or the product $\lambda\alpha_{CE}$ are too small then the system will merge. If the initial separation or the product $\lambda\alpha_{CE}$ are too large then the systems final separation will be so large that a CV will not form within the age of the universe.

Generally the white dwarf, main sequence pair that emerge from the common envelope are close but still detached (figure 1.9 3rd frame). The following evolution into contact (figure 1.9 lower frame) is due to the loss of orbital angular momentum by gravitational

radiation, given by

$$\left.\frac{\dot{J}}{J}\right|_{GR} = -\frac{32}{5}\frac{G^3}{c^5}\frac{m_1 m_2 m}{A^4}, \tag{1.10}$$

where J is the total orbital angular momentum of the system, m_1 is the mass of the remnant core of the more massive star (the white dwarf), and $m = m_1 + m_2$ (Landau and Lifschitz (1958)) for accelerating distributions of mass, or by some other mechanism such as magnetic stellar wind braking

$$\frac{dJ_{MB}}{dt} = -0.5 \times 10^{-28} f^{-2} k^2 m_2 r_2^4 \omega^3, \tag{1.11}$$

where ω is the angular velocity of the star, f is a dimensionless parameter of order unity and k^2 is a structural constant from the radius of gyration of the star giving the moment of inertia of the star (e.g. Verbunt and Zwaan (1981), Rappaport, Joss, and Verbunt (1983)).

$$I = k^2 m_2 r_2^2 \tag{1.12}$$

1.2.1 Primary mass distribution

There have been a few studies of the theoretical distribution of the masses of white dwarfs in binary systems (see de Kool (1992)), in which the influence of the lower mass main sequence star on the evolution of the primary are taken into account (see below). This distribution is obviously also affected by the distribution of masses for main sequence stars, that are the progenitors of the white dwarf.

From figure 1.10 it can be seen that the mass distribution for the white dwarf primaries in CVs predicted by de Kool (1992), and others, should be split into two distinct regions. This is a feature due to the presence of the binary partner in the system. Initially the two main sequence stars that will form the CV orbit at such large separation that they evolve independently of each other. The more massive of the two burns all its fuel and ascends the giant branch. If the orbital separation is such that the secondary is engulfed by the outer layers of the expanding star before the onset of core helium burning, the effect is to eject the envelope (see section 1.2) leaving a low mass ($\lesssim 0.45 M_\odot$) helium white dwarf. If, however, the separation is such that the more massive star reaches the

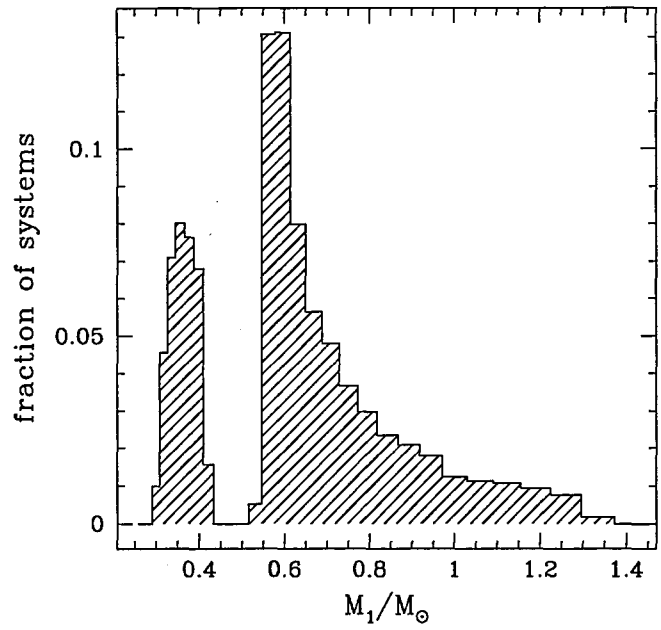

Figure 1.10: White dwarf mass distribution de Kool (1992)

helium burning phase without a CE phase, the mass of the core increases due to helium burning. This may leave an intermediate mass ($\gtrsim 0.55 M_\odot$) carbon/oxygen white dwarf. The mass gap between the helium and carbon/oxygen white dwarfs is due to the core mass increase from hydrogen shell burning during core helium burning. It is also possible for the primary to evolve fully through core carbon/oxygen burning and not be disrupted by a supernova (setting the upper limit for a white dwarf at around $1.4 M_\odot$) resulting in massive O/Ne/Mg white dwarfs. The minimum mass for a O/Ne/Mg white dwarf is unclear but is likely around $1.2 M_\odot$ (see e.g. Nomoto (1984)). The effects of the primary mass spectrum on the orbital period distribution are considered in section 3.4.2

1.2.2 Secondary mass distribution

The initial distribution of secondary masses in binaries is not well understood, though as CVs are interacting binaries the distribution will be affected by the binary effects. Starting

from the orbital angular momentum of the system

$$J = M_1 M_2 \left(\frac{Ga}{M}\right)^{1/2}, \tag{1.13}$$

and the Roche radius relation

$$R_2 \simeq 0.462 \left(\frac{M_2}{M}\right)^{1/3} a, \tag{1.14}$$

(Paczyński (1971)), in systems where the secondary approximates to the lower main sequence, logarithmic differentiation of equations 1.13 and 1.14 along with the assumption that mass transfer is conservative ($\dot{M} = 0$), and $\dot{R}_2/R_2 = \dot{M}_2/M_2$ the equation

$$\frac{(-\dot{M}_2)}{M_2} = \frac{-\dot{J}/J}{4/3 - M_2/M_1}, \tag{1.15}$$

is obtained (King (1988)) which limits stable mass transfer (also see Ritter (1988), Ritter (1996)) to systems where $M_2/M_1 \leq 4/3$. As the star may expand on mass loss this imposes even tighter restrictions on $M_2/M_1 < q_{crit} \simeq 1$. This limits the mass of the donor star to less than that of the primary and hence the mass of the donor is dependent upon the primary mass distribution. Systems which form as binaries where the secondary is more massive than the white dwarf may experience an episode of thermal timescale mass transfer. Most population models (see Hurley, Tout, and Pols (2002), Politano (1996), de Kool (1992)) tend to generate a peak in the mass distribution at around $M_2 \simeq 0.4 M_\odot$. Other than this the initial secondary mass distribution is roughly flat in log M_2; here M_2 is the initial mass of the secondary before the onset of mass transfer. The effects of the initial secondary mass spectrum on the orbital period distribution is considered section 3.4.4

1.3 The evolution of CVs

1.3.1 The long period cut-off

From figure 1.1 it can be seen that very few CV systems are found with periods greater than 12 hrs. As I show in section 1.2.2, for mass transfer stability it is required that $q < 1$. As the maximum mass of a white dwarf is the Chandrasekhar limit at around $1.44 M_\odot$,

this translates into $M_2 \lesssim 1.4 M_\odot$. Using Kepler's third law along with the approximation for the orbital separation

$$a = \frac{R_L}{0.462} \left(\frac{M}{M_2} \right)^{1/3}, \tag{1.16}$$

(Paczyński (1971)), where $M = M_1 + M_2$, this gives a maximum period of around 12.75 hrs.

1.3.2 The period gap

As can be seen from figure 1.1 there is a pronounced lack of systems with orbital periods between around 2 and 3 hours, this period range is referred to as the period gap. The standard explanation for the period gap is as follows.

The radial evolution of the secondary is governed by two competing effects. Mass transfer perturbs thermal equilibrium and expands the star (for stars with convective envelopes as considered here) typically on the mass loss time scale,

$$T_M = \frac{M_2}{|\dot{M}_2|}. \tag{1.17}$$

Thermal relaxation re-establishes thermal equilibrium and contracts the star back to its equilibrium radius on the Kelvin-Helmholtz (thermal) time scale

$$T_{KH} = \frac{GM_2^2}{R_2 L_2}, \tag{1.18}$$

where L_2 is the luminosity of the secondary. Systems with orbital periods longer than the upper edge of the period gap ($P \gtrsim 3$hr) have secondary masses $\gtrsim 0.3 M_\odot$. Systems here are subject to both gravitational radiation and magnetic braking. Main sequence secondaries with masses $0.3 M_\odot \lesssim M_2 \lesssim 1.5 M_\odot$ have convective envelopes and radiative cores. It is believed that convection is an essential ingredient of the dynamo process which produces the magnetic field of stars (van Ballegooijen (1982b), van Ballegooijen (1982a) and Spruit and van Ballegooijen (1982)), and that the radiative core anchors the field lines to produce a mainly dipolar field. The magnetic field is effectively forced to co-rotate with the star out to large distances thus, charged particles, such as in a stellar wind from the star, will effectively be forced to co-rotate out to large distances. This in turn exerts a large

spin-down torque on the secondary. This extracts angular momentum from the spin of the secondary which, by tidal interactions with the primary, is in turn extracted from the orbit of the system. This is commonly referred to as magnetic braking (see Rappaport, Joss, and Verbunt (1983), Verbunt and Zwaan (1981) and Mestel and Spruit (1987)).

For systems before the period bounce the combination of these sinks of angular momentum have the effect of reducing the orbital separation of the system. This causes the secondary to fill its Roche lobe and transfer mass at an increased rate, over that expected for gravitational radiation alone, causing the star to be out of thermal equilibrium ($T_m < T_{KH}$) and oversize for its mass.

When the mass of the secondary star falls to around $0.3M_\odot$ it becomes fully convective (Copeland, Jensen, and Jorgensen (1970)), the radiative core is lost, the magnetic field is no longer anchored and loses its dipole structure. The exact mass at which this occurs is dependent on how far out of thermal equilibrium the star is. For mass transferring systems above the gap with $\dot{M} \simeq 10^{-9} M_\odot\ yr_{-1}$ this reduces the mass to around $0.2M_\odot$. At this point magnetic braking becomes inefficient and the rate of angular momentum loss reduces discontinuously. The secondary, which has been held at an artificial over-size due to the high mass loss rate produced by the high rate of loss of orbital angular momentum, now detaches from its Roche lobe and shrinks to restore thermal equilibrium (see figure 1.11). Mass transfer stops. The orbital separation continues to shrink due to gravitational radiation until the point is reached where it has reduced sufficiently for the secondary to once again fill its Roche lobe. Mass transfer now recommences at a reduced rate driven by gravitational radiation alone.

1.3.3 The minimum period problem

The minimum period in CVs has long been identified as a 'period bounce' of CVs in which the derivative of the orbital period changes from negative to positive (see Paczynski and Sienkiewicz (1981), Rappaport, Joss, and Webbink (1982), D'Antona and Mazzitelli (1982)). As CVs evolve in period toward the minimum period there is a gradual change in the structure of the mass losing secondary star. Electron degeneracy increases and begins

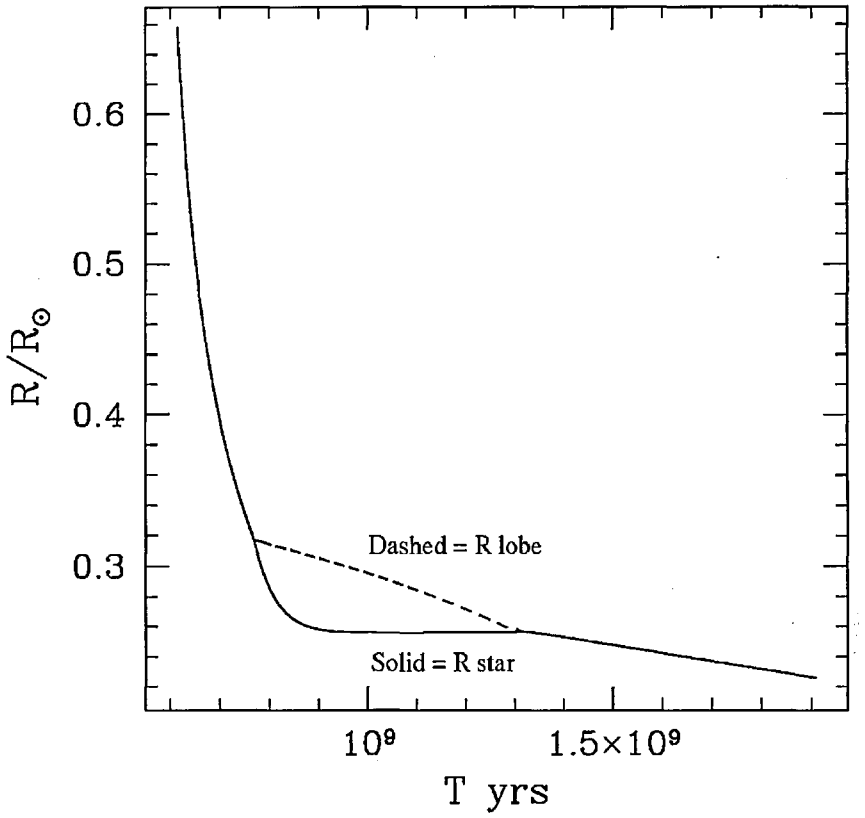

Figure 1.11: The radius evolution of the secondary star in a CV passing through the period gap. The solid curve represents the radius of the star, the dashed line the Roche radius of the star. The period gap corresponds to the time where the Roche radius is greater than that of the star

to dominate (the star) at around $0.1M_{\odot}$. Also at around this point nuclear burning in the core of the star effectively ceases. From this point the radius of the secondary does not decrease as rapidly as previously with mass loss, thus eventually the mean density of the star will reduce, whereas previously it was increasing.

From Kepler's third law

$$P^2 \propto \frac{a^3}{M}, \tag{1.19}$$

and to a good approximation

$$a \propto R_L \left(\frac{M}{M_2}\right)^{\frac{1}{3}} \tag{1.20}$$

(Paczyński (1971)). Thus in our case with

$$R_2 \simeq R_L, \tag{1.21}$$

the orbital period of the system is given as

$$P \propto \frac{R_2^{1.5}}{M_2^{0.5}}. \tag{1.22}$$

Now for non-degenerate stars $M_2 \propto R_2$, so P decreases as M_2. For degenerate stars R_2 decreases less rapidly with mass loss. Hence, as the secondaries density decreases, the orbital period increases, so $\dot{P}$ changes from negative to positive (see figure 1.12 middle frame). The actual period at which P_{min} occurs is dependent upon the ratio $\tau = T_{KH}/T_M$. If τ is small the period P_{min} at which systems bounce is short. Thus the minimum period is determined by both the orbital angular momentum loss rate and the internal structure of the donor. Paczynski (1981) was the first to point out that in systems subject to gravitational wave radiation alone this minimum period should be at around 80 minutes.

Various models with different input physics have been use to try to reproduce the observed minimum period (see Kolb and Ritter (1992); Howell, Rappaport, and Politano (1997)). Even with the most up to date input physics used for very low mass stars and brown dwarfs (see e.g. Chabrier and Baraffe (2000)) the calculated value for the minimum period P_{min} is still consistently too short for all these models at around 65 minutes.

As P_{min} can be increased by increasing τ and hence by decreasing T_M, which is dependent upon the angular momentum loss rate, various additional angular momentum loss mechanisms have been put forward. Some of these are in the form of a 'Consequential Angular Momentum Loss' (CAML) mechanism (see Webbink (1985) in the book 'Interacting Binary Stars', Pringle and Wade (1985); also see section 2.2). Numerical experiments show that an additional angular momentum loss rate of around three times that of gravitational radiation is required to reproduce the observed value for the minimum period (Kolb and Baraffe (1999)). An alternative to this was proposed by Nelson, Chau, and Rosenblum (1985) in which the corrections for the rotation and tidal deformation of the one-dimensional model of the donor star (Chan and Chau (1979)) were modelled. This was found to increase the minimum period by around 10%. More recent work (Kolb and

Baraffe (1999)) with more up to date stellar models obtained a much smaller increase of around 1 minute using the same corrections for rotation and deformation. Rezzolla, Uryū,

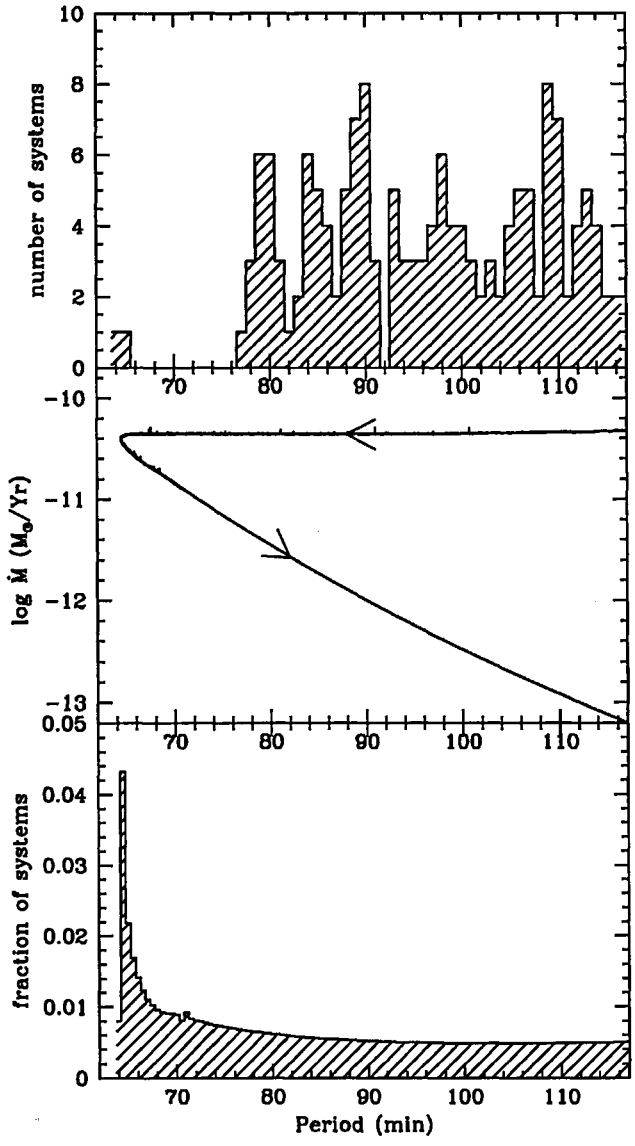

Figure 1.12: Upper frame: The observed period distribution of CVs with periods less than 116 minutes. Middle frame: Calculated evolutionary track in the orbital period versus mass transfer rate ($\dot{M}$) plane. Lower frame: Period distribution expected from evolutionary track in middle frame.

and Yoshida (2001) constructed three dimensional hydrostatic models of binaries using a polytropic equation of state to determine the effects of an extended mass distribution rather than the point mass assumed for the donor in the standard Roche model. The volume equivalent radius, orbital angular momentum and gravitational angular momentum loss rates were found to agree to within 1-2%. Renvoizé, Baraffe, Kolb, and Ritter (2002) also used three dimensional smooth particle hydrodynamic (SPH) simulations assuming a polytropic equation of state and found that the radius of the donor was larger than that for the same star in isolation. This increase was found to be around 6% for a fully convective star near the minimum period, though this is reduced by the inclusion of thermal effects (Renvoizé, Baraffe, Kolb, and Ritter (2002)). Thus, none of the improvement in the input physics used in the evolutionary simulations nor any single mechanism has yet been able to raise the theoretically predicted period bounce to that of the observed minimum period. I investigate additional mechanisms and reasonable combinations of these to try to reproduce the period bounce at around the observed minimum period. I also investigate what influence a reasonable spread of parameters, for each mechanism and combination of mechanisms, has on the smoothing out of the predicted period spike and carry out statistical tests to give a probability that I may reject each model as that underlying the observed distribution of CVs below the period gap.

1.3.4 Circumbinary discs

As some of the material passing through the L_1 point may be ejected from the system either by magnetic propellers, disc winds or other mechanisms it may be possible for some of this material to form a disc surrounding the binary system as shown in figure 1.13 (see Spruit and Taam (2001), Taam and Spruit (2001), Dubus, Taam, and Spruit (2002)). This material will then interact tidally with the binary system to extract orbital angular momentum and hence influence the evolution of the CV. Possible influences are to increase the mass transfer rate and hence raise the minimum period, or lead to the total dissolution of the secondary before the period bounce.

Over recent years there have been observational hints at the existence of material

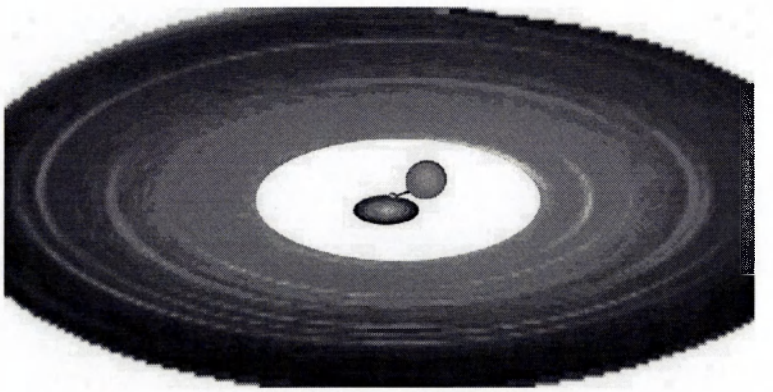

Figure 1.13: Representation of a CV with a circumbinary disc

surrounding interacting binary systems. This being in the form of absorption lines of NV, CIV and HeII for AMCVn (HZ 29) (Solheim and Sion (1994)), emission lines in the forbidden 'coronal-like' transitions of FeX, OV and NV from QR And (Kuduz, Reinsch, Beuermann, and Kube (2002)), and the detection of a high column density of material along the line of sight to BY Cam (see Mouchet et al. (2003)), all are suggestive of material surrounding these systems. More details on circumbinary discs can be found in chapters 4 and 5.

1.4 Thesis preview

This thesis is organized as follows: In chapter (2) I introduce the stellar evolution code used for all the work in this thesis. The code is used to investigate what the effects of Consequential angular momentum loss (CAML) and the structure of the secondary have on the expected value of the minimum period. The results of these investigations are carried over into chapter (3), where the evolutionary tracks from these and other parameters are used to construct synthetic period distributions. These distributions are compared with that for the observed systems and a probability that the observed distribution is drawn from each of the models is determined. Large parts of chapters 2 and 3 can be found in the publication Barker and Kolb (2003). In chapter (4) I give a brief introduction to

the structure and formation of circumbinary discs and review some of the recent work in this area. This sets the scene for chapter (5), where I give an overview of the model I use to investigate the effect of a circumbinary disc on systems below the period gap. The investigation looks at the influence of various circumbinary disc parameters along with the effects of CAML. This once again uses the full binary evolution code. In chapter (6) I give an overview of some of the work into irradiation driven winds and investigate the effects of an irradiation driven wind from the secondary on the orbital period evolution of CVs below the period gap. Once again focusing on the effect on the minimum period with additional effects introduced by feedback from the wind. In chapter (7) I diverge slightly from the minimum period to investigate the difference between the observed distributions of magnetic and non-magnetic CVs covering the full period range from 1.3 to 13 hours. I use a statistical analysis of the cumulative distributions of the two distributions to highlight the apparent lack of a period gap in the distribution of magnetic systems. In chapter (8) I summarize the results and present my conclusions, along with some possible directions for future research into this subject.

Chapter 2

Raising the theoretical period bounce to the observed minimum period

In section 1.3.3 it can be seen that the theoretical minimum period of around 65 minutes is in conflict with the observed minimum period (see figure 1.1) of around 78 minutes. In this section I investigate possible mechanisms to increase the theoretical minimum period and reduce the mismatch. To do this I use the full stellar code as detailed below with the addition of new routines to include additional angular momentum losses and structural changes in the secondary.

2.1 Mazzitelli's stellar evolution code

The stellar structure code I use is Mazzitelli's stellar evolution code (see Mazzitelli and Dantona (1986), (Mazzitelli (1989)). The code uses a generalized Newton-Raphson iteration (the Henyey scheme, see Henyey, Forbes, and Gould (1964)) to simultaneously solve the four differential equations describing the stellar interior:

1. Equation of hydrostatic equilibrium

$$\frac{dP_r}{dr} = -\frac{Gm_r\rho}{r^2}. \tag{2.1}$$

2. Equation of mass conservation

$$\frac{dM}{dr} = 4\pi r^2 \rho. \tag{2.2}$$

3. Equation of energy production

$$\frac{dL}{dr} = 4\pi r^2 \rho \varepsilon. \tag{2.3}$$

4. Equations of energy transport

$$\frac{dT}{dr} = -\frac{3\kappa\rho L}{16\pi a_r c r^2 T^3} \quad \text{(radiative equilibrium)}, \tag{2.4}$$

$$\left.\frac{dT}{dr}\right|_{ad} = \frac{(\Gamma_2 - 1)T}{\Gamma_2 P_r}\frac{dP_r}{dr} \quad \text{(adiabatic convection)}. \tag{2.5}$$

equation 2.5 is used whenever

$$-\frac{dT}{dr} > -\left.\frac{dT}{dr}\right|_{ad} \tag{2.6}$$

where

r = radius

P_r = pressure due to material within r

G = gravitational constant

m_r = mass of material within r of the centre of the star

ρ = density at r

L = luminosity at r (rate of energy flow across sphere at radius r)

ε = energy release per unit mass per unit time

T = temperature at r

κ = opacity at r

a_r = radiation density constant.

Γ_2 = second adiabatic exponent.

see Cox (2000)

In this the star is assumed to be spherically symmetric and thus only a 1-dimensional representation is considered (the one dimension being radial distance from the centre). The radius is split into small cells (between $\sim$ 600 and $\sim$ 3000), with a smaller width to

the cells at the boundaries of the convective zones and in the surface layers. The zoning for the cells is redistributed at the end of each time step, to prevent the relative values of the five structural quantities (radius, luminosity, pressure, temperature, and mass) between adjacent cells exceeding a maximum value. The length of the time step is also determined from the logarithmic derivatives of the structural quanitities and the restriction that the quantities need to converge within three iterations otherwise the time step is reduced. The code includes the correct treatment for the gravitational energy release up to the photosphere along with the equation of state, which includes all the effects which become important for low-mass and very low-mass stars (such as degeneracy, Coulomb corrections, pressure ionization, molecular ionization).

The Mazzitelli code was adapted by Kolb and Ritter (1992) to model binary systems, in which the secondary star is evolved using the Mazzitelli stellar structure code and the primary is assumed to be a point like mass. Routines were added to deal with the mass transfer from the secondary to the primary.

Input Physics

For the models in this study the secondaries use an initial solar composition ($X = 0.70$, $Y = 0.02$), pre OPAL opacities (Rogers, Swenson, and Iglesias (1996)) for three grey atmospheres, the equation of state is an improved version of that by Magni and Mazzitelli (1979), the mixing length theory of convection with the ratio of mixing length to pressure scale height is set at 1.4, and no overshooting.

Features of a typical evolutionary track

Figure 2.1 shows the typical evolution of a short period CV, generated by the binary code, in the "period - mass transfer rate ($P - \dot{M}$)" plane. On the right of the figure it can be seen that systems coming into contact below the period gap (also true for systems coming into contact at the upper edge and within the period gap), in which the secondaries are almost fully convective, experience a short initial phase of high mass transfer rate and increasing orbital period (The 'turn on flag'). This is as at the point where the secondary

has just filled its Roche lobe and is still in thermal equilibrium. As the secondary is, or is almost, fully convective it has an adiabatic mass-radius exponent

$$\zeta_{ad} = \frac{\mathrm{dln}R}{\mathrm{dln}M_2} \simeq -\frac{1}{3}. \tag{2.7}$$

(see section 2.2, equations 2.20 - 2.22) The star is initially is close to thermal equilibrium for a main sequence star with $\zeta_{eff} \simeq -1/3$. The star thus initially reacts adiabatically, but with continued mass loss ζ_{eff} increases and eventually saturates close to a new equilibrium value of around 1. This gives the characteristic flag shaped turn on, as orbital period increases for $\zeta_{eff} < +1/3$ and decreases for $\zeta_{eff} > +1/3$ (see Ritter and Kolb (1992), D'Antona, Mazzitelli, and Ritter (1989) for a review).

Also the evolutionary track shows a number of smaller spikes in the mass transfer rate.

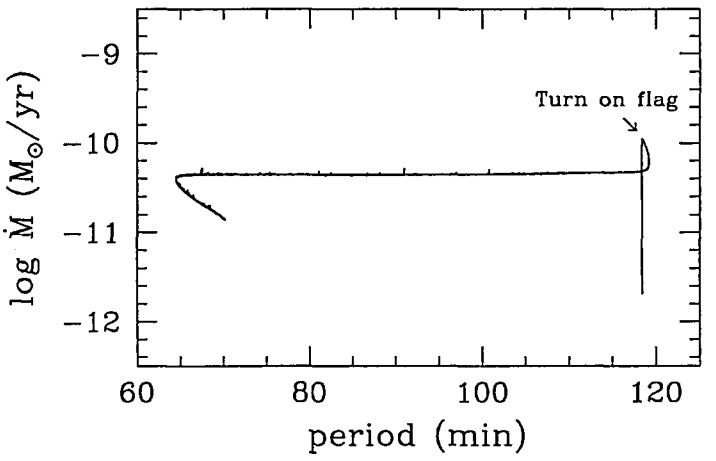

Figure 2.1: The typical evolution for a short period CV, generated by the binary code, in the "period - mass transfer rate" plane (initial masses $M_1 = 0.6M_\odot$, $M_2 = 0.2M_\odot$)

This is due to numerical noise some of which is caused by the use of tables to interpolation/extrapolation from to obtain values for opacities and the equation of state.

2.2 CAML description

As detailed in section 1.3.3 the period at which systems bounce is dependent upon the angular momentum loss rate: increasing the angular momentum loss rate increases the minimum period. I thus investigate consequential angular momentum loss (CAML) as an additional form of orbital angular momentum loss, in which the rate of loss is proportional to and a direct consequence of the rate of mass transfer in the system. My CAML prescription largely follows the derivation of King and Kolb (1995). With the addition of this CAML the orbital angular momentum loss rate $\dot{J}$ of a CV must be written as the sum of two terms,

$$\dot{J} = \dot{J}_{sys} + \dot{J}_{CAML}, \tag{2.8}$$

where $\dot{J}_{sys}$ denotes the "systemic" angular momentum losses, e.g. gravitational radiation and magnetic braking, which are independent of the mass transfer rate. While $\dot{J}_{CAML}$ is an explicit function of the mass transfer rate. I have

$$\frac{\partial \dot{J}_{sys}}{\partial \dot{M}_2} = 0, \tag{2.9}$$

and

$$\dot{J}_{CAML} \to 0 \qquad \text{as} \qquad \dot{M}_2 \to 0, \tag{2.10}$$

where $\dot{M}_2$ is the mass loss rate of the secondary through the L_1 point. The orbital angular momentum of the binary is given by

$$J = M_1 M_2 \left(\frac{Ga}{M}\right)^{\frac{1}{2}}, \tag{2.11}$$

where the orbits are assumed to be circular. Logarithmic differentiation of this gives

$$\frac{\dot{J}}{J} = \frac{\dot{M}_1}{M_1} + \frac{\dot{M}_2}{M_2} + \frac{\dot{a}}{2a} - \frac{\dot{M}}{2M}. \tag{2.12}$$

Hence with equation 2.8 I obtain

$$\frac{\dot{J}_{sys}}{J} + \frac{\dot{J}_{CAML}}{J} = \frac{\dot{M}_1}{M_1} + \frac{\dot{M}_2}{M_2} + \frac{\dot{a}}{2a} - \frac{\dot{M}}{2M}. \tag{2.13}$$

I define α as the total fraction of mass lost from the secondary that leaves the system (see figure 2.2). That is

$$\dot{M} = \alpha \dot{M}_2 \quad \text{with} \quad \alpha \geq 0. \tag{2.14}$$

From this I get the rate of change of mass of the primary as

$$\dot{M}_1 = (\alpha - 1)\dot{M}_2. \tag{2.15}$$

The angular momentum loss rate associated with the CAML may be written as

$$\dot{J}_{CAML} = \nu \frac{\dot{M}_2}{M_2} J, \tag{2.16}$$

where in general ν may also be a function of $\dot{M}_2$. From equation 2.10 it can be seen that it is required that $\nu \dot{M}_2 \to 0$ as $\dot{M}_2 \to 0$. The term $\dot{a}/a$ can be eliminated from equation 2.13 by using the relation

$$R_L \simeq 0.462 \left(\frac{M_2}{M}\right)^{\frac{1}{3}} a \tag{2.17}$$

(Paczyński (1971)) which is sufficiently accurate for $q = M_2/M_1 \lesssim 0.8$. Logarithmic differentiation and rearranging for $\dot{a}/a$ gives

$$\frac{\dot{a}}{a} = \frac{\dot{R}_L}{R_L} - \frac{\dot{M}_2}{3M_2} + \frac{\dot{M}}{3M}. \tag{2.18}$$

If I assume stationary mass transfer (that is $\ddot{M} = 0$) it is required that

$$\frac{\dot{R}_L}{R_L} = \frac{\dot{R}_2}{R_2}. \tag{2.19}$$

To determine R_2 I introduce the expression for the adiabatic mass-radius exponent ζ_{ad}

$$\zeta_{ad} = \frac{M_2}{R_2} \left(\frac{\partial R_2}{\partial M_2}\right)\Big|_{s(M_2)=const}, \tag{2.20}$$

which determines the change of R_2 with the change in stellar mass provided the entropy profile within the star remains fixed. If the nuclear evolution of the secondary is neglected equation 2.20 may be used to decompose the radius change of the secondary under mass loss into the adiabatic response and the contribution from thermal relaxation.

$$\frac{\dot{R}_2}{R_2} = \zeta_{ad} \frac{\dot{M}_2}{M_2} + \frac{1}{R_2} \left(\frac{\partial R_2}{\partial t}\right)_{th} \tag{2.21}$$

(see e.g. Ritter (1988)). The relaxation term $(\partial R_2/\partial t)_{th}$ only changes on a thermal time-scale, thus the effective mass-radius exponent ζ, can be defined as

$$\frac{\dot{R}_2}{R_2} = \zeta \frac{\dot{M}_2}{M_2}, \tag{2.22}$$

which offers a convenient way of expressing $\dot{R}_2$ in terms of $\dot{M}_2$. If the mass loss turns on from a star in thermal equilibrium [i.e. where $(\partial R/\partial t)_{th} = 0$] then initially $\zeta = \zeta_{ad}$; a new equilibrium value $\zeta \simeq \zeta_{th}$ with $\partial R/\partial t_{th} \neq 0$ is established on a thermal timescale (see e.g. D'Antona, Mazzitelli, and Ritter (1989)).

Using equations (2.8)-(2.16), (2.18) and (2.22) I obtain

$$0 = \frac{\dot{R}_L}{R_L} - \frac{\dot{R}_2}{R_2} = 2\left(\frac{\dot{J}_{sys}}{J} - D\frac{\dot{M}_2}{M_2}\right), \tag{2.23}$$

where

$$D = D_\zeta(\alpha, \nu) = \left(\frac{5}{6} + \frac{\zeta}{2}\right) - q + \alpha\left(q - \frac{q}{3(1+q)}\right) - \nu. \tag{2.24}$$

Rearranging equation 2.23 gives the expression for the steady-state mass transfer

$$\frac{\dot{M}_2}{M_2} = 2\frac{\dot{J}_{sys}}{JD} \tag{2.25}$$

To determine ν I consider the general case in which the CAML mechanism, along with nova mass ejections, causes a fraction of the transferred mass to leave the system. This fraction may be greater than unity as the primary may lose more mass during a nova outburst than was accreted since the last outburst.

I employ a generic prescription of the effect of a CAML mechanism, thus avoiding the need to specify its physical nature. Possible CAML mechanisms include a magnetic propeller, i.e. a system containing a rapidly spinning magnetic WD where some of the transferred material gains angular momentum from the WD spin by interaction with the WD's magnetic field (see e.g. Wynn, King, and Horne (1997); section 1.1.4), and an accretion disc wind (see e.g. Livio and Pringle (1994)).

The angular momentum is assumed to be lost via mass loss that is axis-symmetrical with respect to an axis A fixed at the WD centre but perpendicular to the orbital plane. The total orbital angular momentum loss rate due to CAML can then be written as

$$\dot{J}_{CAML} = \dot{J}_b + \dot{J}_1 + \dot{J}_{wind}, \tag{2.26}$$

where $\dot{J}_b$ is the CAML rate with respect to the centre of the WD, $\dot{J}_1$ accounts for the change to the centre of mass frame and $\dot{J}_{wind}$ is the averaged rate of angular momentum lost to the system due to nova mass ejections (see below).

A mass packet with mass m_b leaving the secondary through the L_1 point has angular momentum relative to the primary of

$$\Delta J_b = b^2 \omega m_b, \tag{2.27}$$

where b is the distance of the L_1 point to the centre of the primary and ω is the orbital angular velocity. If the mass packet is ejected from the system symmetrically with respect to axis A I have

$$\Delta J_1 = \frac{M_2 J}{M_1 M} m_b. \tag{2.28}$$

to account for the transition from the co-rotating frame (about the primary) to the inertial frame (about the centre of mass). I assume further that a fraction β (see figure 2.2) of the transferred mass leaves the system with some fraction f of the angular momentum it had on leaving the L_1 point.

This gives

$$\dot{J}_b = \beta f b^2 \omega \dot{M}_2, \qquad \text{for} \qquad 0 \leq \beta \leq \alpha. \tag{2.29}$$

and

$$\dot{J}_1 = \frac{\beta M_2 J \dot{M}_2}{M_1 M} \tag{2.30}$$

I also consider mass that is lost from the system via nova mass ejections which, over the long term, can be considered as an isotropic wind from the primary (see e.g. Kolb et al. (2001)). This material will carry away the specific orbital angular momentum of the primary and will account for the fraction $(\alpha - \beta)$ of the mass loss (see figure 2.2), giving

$$\dot{J}_{wind} = (\alpha - \beta) \frac{M_2 J \dot{M}_2}{M_1 M}. \tag{2.31}$$

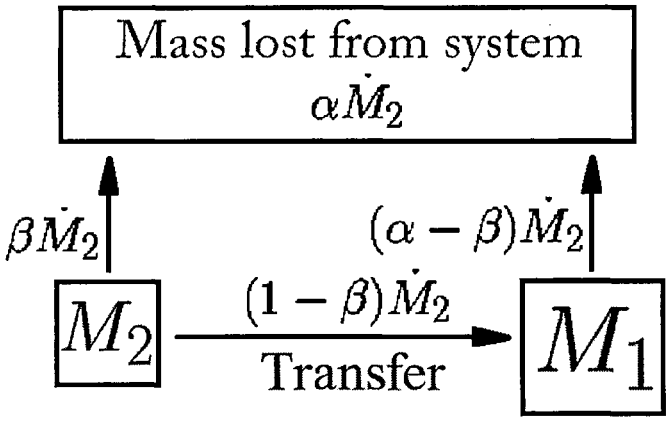

Figure 2.2: Mass flow diagram, defining the parameters α and β. $(1-\beta)$ is the fraction of transferred mass being accreted or forming a disc. β is the fraction of the mass passing through the L_1 point that is ejected from the system and responsible for CAML. $(\alpha-\beta)$ is the fraction of the transferred mass that is lost to the system via nova outbursts.

Substituting (2.29), (2.30) and (2.31) into equation (2.26) thus obtaining

$$\dot{J}_{CAML} = \eta b^2 \omega \dot{M}_2 + \frac{\alpha M_2 J \dot{M}_2}{M_1 M}, \tag{2.32}$$

where I define $\eta = \beta f$ as the CAML efficiency. For comparison with King, Frank, Kolb, and Ritter (1997) equating this to equation 2.16 I obtain

$$\nu = \eta(1+q)\left(\frac{b}{a}\right)^2 + \frac{\alpha q^2}{(1+q)}. \tag{2.33}$$

2.3 Approximate expression for b/a

There are quite a few good approximations for the value of b/a each is accurate over a limited range of values of q. I thus felt this was worth further investigation to find expressions that have the minimum error over the range of interest for this study. The

three standard approximations are,

$$\frac{b}{a} \simeq 0.500 - 0.227 \ln q \quad \text{for} \quad 0.1 \leq q \leq 10, \tag{2.34}$$

$$\frac{b}{a} \simeq (1.0015 + q^{0.4056})^{-1} \quad \text{for} \quad 0.04 \leq q \leq 1, \tag{2.35}$$

$$\frac{b}{a} \simeq 1 - \varphi + \frac{\varphi^2}{3} + \frac{\varphi^3}{9}; \quad \varphi = \frac{q}{3+3q} \quad \text{for} \quad q \leq 0.1, \tag{2.36}$$

taken from Plavec and Kratochvil (1964), Silber (1992) and Kopal (1959) respectively. Each of the approximations is quoted to within 1% of the true value over the given ranges of q. Each equation was tested against the true value for b/a as shown in figure 2.3 which

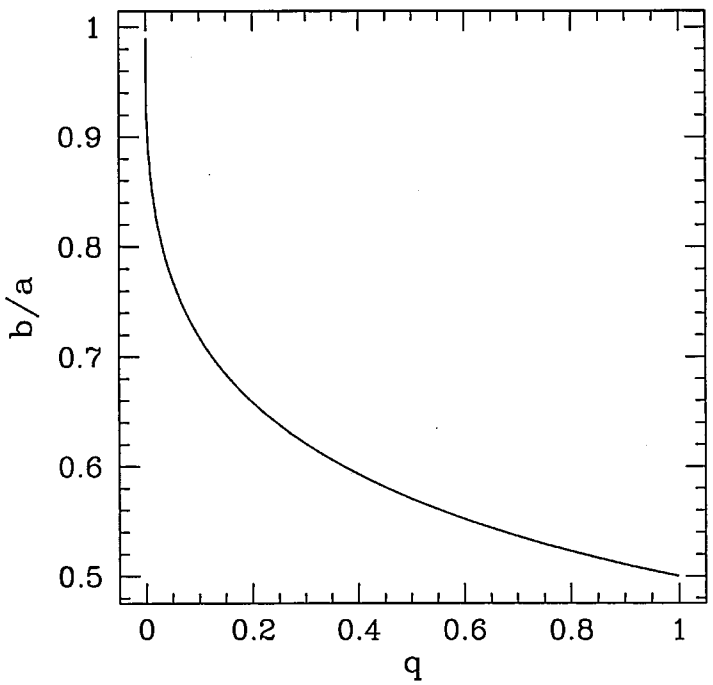

Figure 2.3: b/a as a function of q.

were obtained analytically from the Roche potential (see equation 1.1) as follows. As all the points of interest lie on a projected line joining the centres of the primary and secondary I may use this as my coordinate axis. Setting the origin of the coordinate

system to coincide with the centre of the primary I get the following relations.

$$R_{t1} = |X|, \tag{2.37}$$

$$R_{t2} = |X - a|, \tag{2.38}$$

$$R_t = |X - \mu a|, \tag{2.39}$$

where μa is the distance from the centre of the primary to the centre of mass and is given by

$$\mu a = \frac{qa}{(1+q)}. \tag{2.40}$$

Substituting all of the above relations (2.37) to (2.40) along with Kepler's law into (1.1), with some rearrangement I obtain

$$\frac{Ua}{GM_1} = -\frac{1}{|X_a|} - \frac{q}{|X_a - 1|} - \frac{X_a^2}{2}(1+q) + X_a q - \frac{q^2}{2(1+q)}. \tag{2.41}$$

where X_a is the distance from the centre of the primary to the point in question (in this case b/a).

To find the points at which this is a maximum we need to find the points at which the derivative of (2.41) equates to zero. The first thing to notice in differentiating this is that the function is discontinuous at the points $X_a = 0$ and $X_a = 1$ thus we have the following conditions on the derivative

$$\left(\frac{1}{|X_a|}\right)' = \begin{cases} \frac{1}{X_a^2} & \text{if } X_a < 0 \\ -\frac{1}{X_a^2} & \text{if } X_a > 0 \end{cases}$$

and

$$\left(\frac{1}{|X_a - 1|}\right)' = \begin{cases} \frac{1}{(X_a-1)^2} & \text{if } X_a < 1 \\ -\frac{1}{(X_a-1)^2} & \text{if } X_a > 1\ . \end{cases}$$

There are thus three possible cases:

1. for $X_a < 0$ corresponding to the L_3 point

$$0 = -\frac{1}{X_a^2} - \frac{q}{(X_a - 1)^2} - X_a - X_a q + q; \tag{2.42}$$

2. for $0 < X_a < 1$ corresponding to the L_1 point

$$0 = \frac{1}{X_a^2} - \frac{q}{(X_a - 1)^2} - X_a - X_a q + q; \tag{2.43}$$

3. for $X_a > 1$ corresponding to the L_2 point

$$0 = \frac{1}{X_a^2} + \frac{q}{(X_a - 1)^2} - X_a - X_a q + q. \tag{2.44}$$

The main equation of interest is that for the L_1 point, so with some rearrangement of (2.43) I obtain

$$q = \frac{X_a - \frac{1}{X_a^2}}{1 - X_a - \frac{1}{(X_a - 1)^2}}, \tag{2.45}$$

From this equation values of q were obtained for various values of $X_a = b/a$, these values of q were then substituted into each of the equations 2.34 to 2.36 to give the calculated value of b/a. These values of b/a were then compared with the true values to calculate the percentage error. Figure 2.4 shows the actual percentage error calculated for each approximation, all of which can be seen to be within the quoted accuracy. The range of

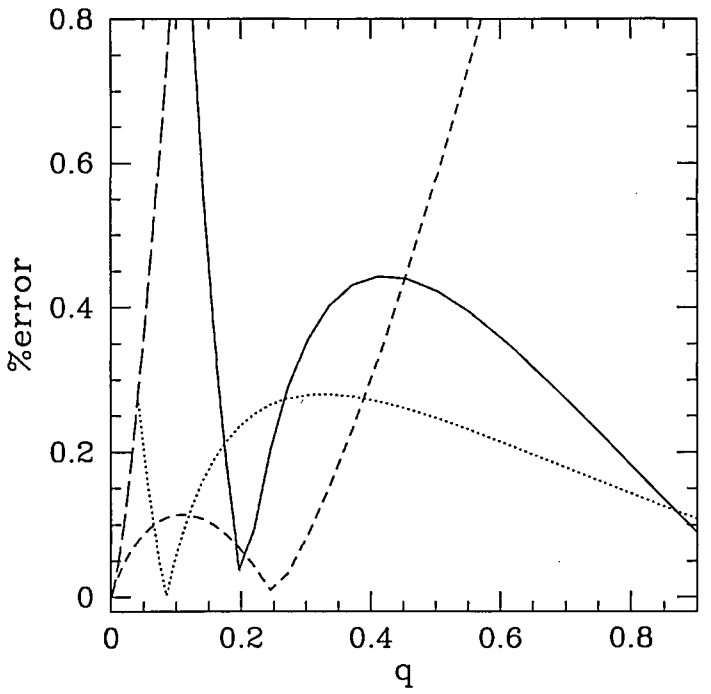

Figure 2.4: Percentage errors in b/a for, solid line (Plavec and Kratochvil (1964)), dotted line (Silber (1992)) long dashed line (Kopal (1959)) and short dashed line equation 2.46.

greatest interest to me is for the values of $0 \leq q \lesssim 0.4$. Equations (2.35) and (2.36) best cover this range with a change between them at $q = 0.05$. It was found that an adaptation of the equation by Kopal (1959) as below produced an error of less than 1% over this full range (see figure 2.4)

$$\frac{b}{a} \approx 1 - \varphi + \frac{\varphi^2}{3} - \frac{5\varphi^4}{12}, \quad \text{with} \quad \varphi^3 = \frac{q}{3+3q}. \tag{2.46}$$

This is the equation that was used in most of the following models though at a later date a lookup table was generated and a linear interpolation routine written to try to improve the accuracy, though the difference was found to be minimal over the quoted range of interest.

2.4 Results of numerical experiments

In this subsection I present calculations of the long-term evolution of CVs as they approach and evolve beyond the period minimum. The systems are subject to various CAML efficiencies (see section 2.4.1) or various rotational and tidal deformations (see section 2.4.2). I also comment on the possibility that the observed minimum period is an age selection effect (see section 2.4.3). In these I use the assumption that the donor star has solar chemical composition (X = 0.70, Z = 0.02) at the onset of mass transfer. These evolutionary sequences are used as the basis for generating some of the theoretical CV period distributions I present in Chapter 3.

2.4.1 Consequential angular momentum loss (CAML).

I calculated the evolution of individual systems that are subject to CAML according to equations 2.10 and 2.33. For this I use a constant WD mass of $M_1 = 0.6M_\odot$, (consistent with the expected peak in the primary mass distribution see section 1.2.1), and an initial donor mass $M_2 = 0.2M_\odot$ (consistent with the lower edge of the period gap). The range of CAML efficiencies was taken to be $0 \leq \eta \leq 0.95$ as shown in figure 2.5.

The systems initially evolve from longer periods toward the period bounce (right to left) at almost constant mass transfer rate. The minimum period increases with increasing

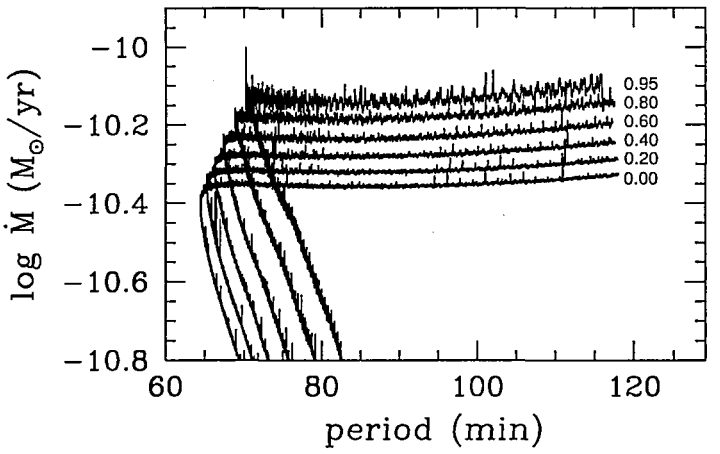

Figure 2.5: The increase in mass transfer rate and corresponding increase in minimum period for increasing CAML efficiency (from 0 to 0.95 as indicated).

CAML efficiency (see figure 2.5 and table 2.1) to a maximum of around 70 min for $\eta = 0.95$. The increase in numerical noise that can be seen in figure 2.5 as $\eta \to 1$ is due to increasing instability in the mass transfer. For higher CAML or higher initial secondary mass the systems may experience thermal time-scale mass transfer (see figure 2.7). Some of the noise is also due to the numerical nature of the code, this was minimized by trying various time step lenghts from aroud 100yrs to 10^7yrs, little bifference was found in the noise for time steps less than around 10^5yrs thus values between 10^4 and 10^5 were used for minimum computational time with good resolution.

Table 2.1: Increase in minimum period, in minutes, due to increase in CAML efficiency η

η	0.0	0.2	0.4	0.6	0.8	0.95
P_{min}	64.5	65.2	66.0	67.2	68.6	70.1

Mass transfer stability requires that there is an upper limit on the CAML efficiency. An obvious upper limit is 1, where all the angular momentum of the transferred material is ejected from the system. Although the ejected material may carry more angular momentum than was transferred (as in the case of a propeller system where additional angular momentum is taken from the spin of the WD) this does not affect the net loss of orbital angular momentum.

The maximum CAML efficiency still compatible with mass transfer stability could be smaller than unity. For stability the parameter D which enters the expression for steady-state mass transfer (see equation 2.25) must be positive

$$D > 0, \tag{2.47}$$

(e.g. King, Frank, Kolb, and Ritter (1997)); this defines an upper limit on η.

A plot of D against q for an initially marginally stable system ($M_1 = 0.7M_\odot$, $M_2(init) = 0.2M_\odot$ and $\eta = 1.0$) is given in figure 2.6. The system initially exhibits cycles of high mass transfer rate $\dot{M}_2 > 10^{-9}M_\odot/yr$ (D close to 0) and very low mass transfer rate $\dot{M}_2 \to 0$. The high states are short lived, on the order of 2×10^6 years (see figure 2.7). The system finally stabilizes with $D \approx 0.65$. At around P_{min} ($q \simeq 0.15$) D starts to decrease further but always remains positive, settling at a value around 0.3.

2.4.2 Structure of the secondary

The tidal deformation of the secondary may have an effect on the period minimum. Calculations by Renvoizé et al. (2002), [see also Kolb (2002)] using 3–dimensional SPH models suggest that the secondary is deformed in the non-spherical Roche lobe such that its volume–equivalent radius is around 1.06 times that of the same star in isolation.

I mimic this effect in the 1-dimensional stellar structure code by multiplying the calculated radius by a deformation factor λ before the mass transfer rate is determined from the difference between the radius and the Roche lobe radius via

$$-\dot{M}_2 = \dot{M}_0 \exp\left(-\frac{R_L - R_2}{H_p}\right), \tag{2.48}$$

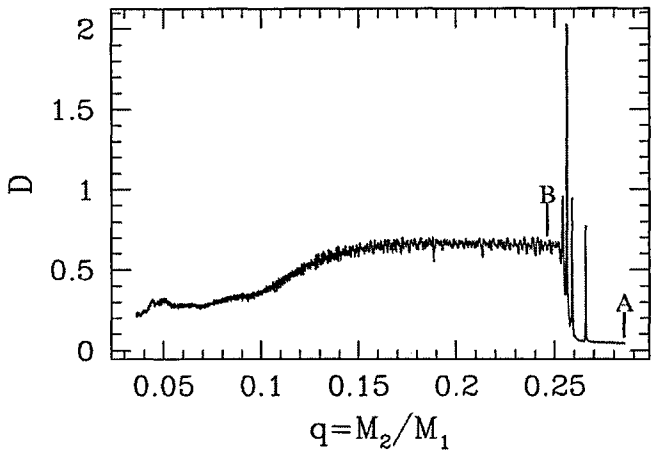

Figure 2.6: Evolution of the stability factor D with mass ratio q for an initially marginally stable system, ($M_1 = 0.7M_\odot$, $M_2 = 0.2M_\odot$, $\eta = 1.0$).

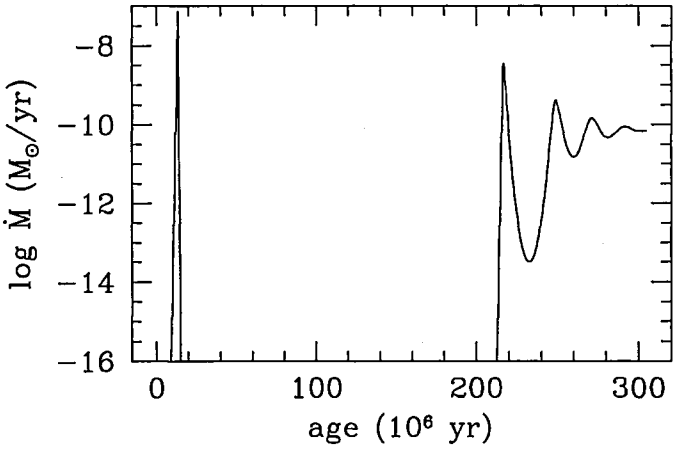

Figure 2.7: Mass transfer rate cycles for the initially marginally stable system shown in figure 2.6 over the range $B \leq q \leq A$.

where $\dot{M}_0 \simeq 10^{-8} M_\odot yr^{-1}$ is the mass transfer rate of a binary in which the secondary just fills its Roche potential and H_p is the photospheric pressure scale height of the secondary

(see e.g. Ritter (1988)).

Figure 2.8 shows the effect on the minimum period and mass transfer rate for systems with various deformation factors λ, ranging from 1 (no deformation) to 1.24. The mass transfer rate is seen to decrease with increasing deformation. This can be understood from the functional dependence on orbital period and donor mass in the usual quadrupole formula for the angular momentum loss rate due to gravitational radiation (Landau and Lifschitz (1958), see equation 1.10). Although the quadrupole formula is strictly valid only if both components are point masses, Rezzolla, Uryū, and Yoshida (2001) found that the GR rate obtained, using a full 3-dimensional representation of the donor star, differs from the point–mass approximation by less than a few percent.

It can be seen from figure 2.8 that with the deformation factor 1.06 the minimum period increases from around 65 min to around 69 min. A deformation factor of around 1.18 was required to raise the minimum period to the observed value of ~ 77 min. This is somewhat larger than the intuitive expectation, from Kepler's law and Roche geometry.

$$\text{increase in radius} \approx \left(\frac{\text{new period}}{\text{old period}}\right)^{\frac{2}{3}} = \left(\frac{77}{65}\right)^{\frac{2}{3}} = 1.12 \tag{2.49}$$

In my calculations I consider the simple case in which only geometrical deformation effects are taken into account. Renvoizé, Baraffe, Kolb, and Ritter (2002) consider the additional thermal effects in which the inflation of the secondary, due to tidal and rotational forces, increases the surface area of the secondary. This increase in surface area will affect the surface luminosity of the secondary and hence its thermal properties. Renvoizé et al. (2002) derive a rough estimate for the thermal relaxation effects, and find that there is a reduction in the bounce period P_{min}, possibly by around 2% compared to the case with purely geometrical effects.

One possible physical mechanism that could cause a deformation factor above the value of 1.06 is magnetic pressure inside the star, as suggested by D'Antona (2001)).

As can be seen from figure 2.8 as the bloating factor λ is increased, the orbital separation and hence the period at which the standard $0.2M_{\odot}$ secondary (assuming that the systems had pre period gap mass transfer) comes into contact increases. This would fill the period

gap with systems unless some other mechanism can reduce the mass of the secondary to offset this increase. One possible solution to this is that the bloating factor is a function of

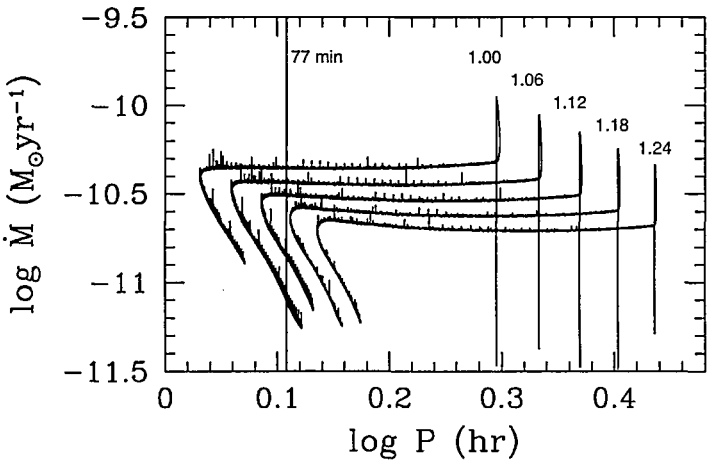

Figure 2.8: Evolutionary track of a system with $M_1 = 0.6M_\odot$ and $M_2(init) = 0.2M_\odot$ for various deformation factors (as indicated).

the secondary's mass and increases to a value of around 1.18 at the period bounce. This was modeled using the following prescription

$$\lambda = 1.0 \qquad \text{for } M_2 > 0.2M_\odot, \tag{2.50}$$

and

$$\lambda = 1.4(0.2 - M_2) + 1.0 \qquad \text{for } M_2 \leq 0.2M_\odot. \tag{2.51}$$

This gives an increasing bloating factor from 1.0 at $M_2 = 0.2M_\odot$ to 1.18 at $M_2 = 0.07M_\odot$, which for a $0.6M_\odot$ primary gives the evolutionary track as seen in figure 2.9. This shows a turn on period of around 2 hrs, consistent with a λ of 1.0, the mass transfer rate decreases with decreasing period and increasing λ, as expected from figure 2.8, before reaching the period bounce at around 77.8 minutes consistent with a λ of 1.18 in figure 2.8.

I note that Patterson (2000) claims to find observational evidence for "bloated" secondaries in short period CVs. On the basis of donor mass estimates from the observed

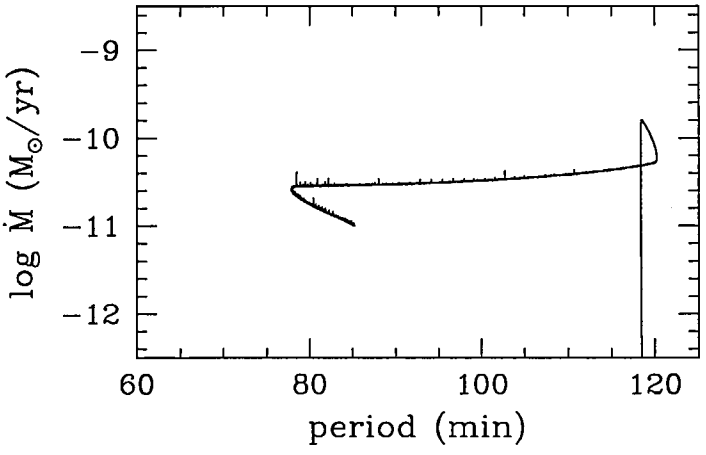

Figure 2.9: Evolutionary track of a system with $M_1 = 0.6M_\odot$ and $M_2(init) = 0.2M_\odot$ for the increasing bloating factor as given by equation 2.51.

superhump excess period he finds that the donors have 15 – 30% larger radii than predicted from 1 dimensional, non–deformed stellar models if gravitational radiation is the only angular momentum sink. Even if true, this observation cannot distinguish between an intrinsic deformation of the donor star or the non-equilibrium caused by orbital AM losses in excess of the GR rate.

2.4.3 Age limit hypothesis

It has been suggested that the currently observed short-period cut-off is not the true minimum period but purely an age effect (e.g. King and Schenker (2002)). This would arise if systems that we currently observe have not had sufficient time to evolve to the true period bounce, as illustrated in figure 2.10.

Here systems at the currently observed short-period cut-off of around 77 minutes will continue to evolve to shorter periods for around another 8×10^8 years before reaching the period bounce (if $\dot{J}_{sys} = \dot{J}_{GR}$, $\lambda = 1.0$). This hypothesis would also remove the problem with the expected spike at the minimum period (see section 3.4.1), though this would lead us to expect that there should be many pre-CV systems in the form of white dwarf, main

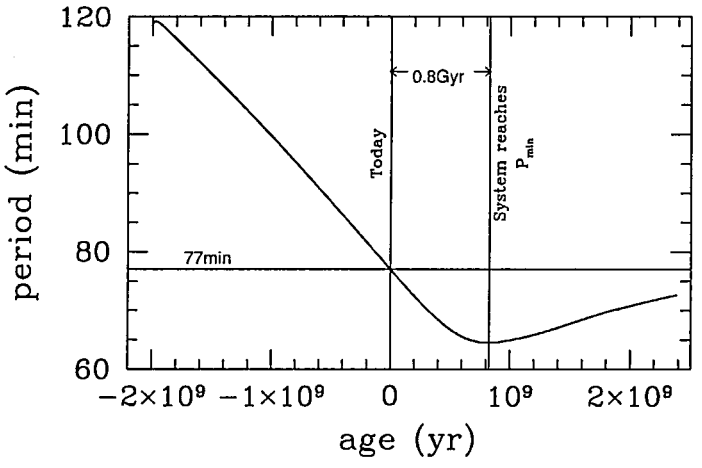

Figure 2.10: The age limit hypothesis. A system with current orbital period of 77 minutes will continue to evolve to the true period bounce at around 66 minutes for the next 8×10^8 years.

sequence binary systems with orbital periods in excess of 12 hrs. Only around 30 such systems have yet been found and all of these (except one) are thought to be young, that is they have just left their CE phase, systems and should start mass transfer at below 4 hrs (Schreiber and Gänsicke (2003)). Though this situation should improve with the increasing number of WD systems found through the Sloan digital sky survey for white dwarfs (see Gänsicke, Euchner, and Jordan (2002)).

2.5 Conclusions

As can be seen from section 2.4 even with a large CAML efficiency ($\eta = 0.95$) the minimum period is only raised by around 8% to 70 minutes. Larger CAML efficiencies are unable to raise the minimum period further as these would only be short lived events powered by extracting angular momentum from the spin of the primary. Large CAML efficiencies can induce large amplitude mass transfer cycles (see figure 2.7). These mass transfer cycles, along with the variation in mass transfer rate for differing CAML efficiencies, could help

to explain the range of mass transfer rates observed in systems at a given orbital period (see section 1.1).

The tidal and rotational deformation factor λ (see section 2.4.2) is able to raise the minimum period to that observed though only for a deformation factor of around $\lambda = 1.18$, well above the predicted deformation of 1.06 (Renvoizé, Baraffe, Kolb, and Ritter (2002)), though this is consistent with observational evedence from Patterson (2000). A deformation factor of 1.06 raises the expected minimum period by around 8% to around 69 - 70 minutes. Also as the deformation factor is increased the more the standard systems would be expected to fill up the period gap (see section 2.4.2). The possibility that there is a range of deformation factors once again gives a spread of mass loss rate for a given period.

If I combine the effect of the maximum CAML $\eta = 0.95$ and the predicted deformation $\gamma = 1.06$ it is possible to raise the expected minimum period to around 76 minutes, roughly the observed minimum period. This would restrict systems to be very efficient mass ejectors and all donor stars to have the same structure.

Chapter 3

Comparison of model period distributions with the observed period distributions

The orbital period distribution of CVs below the period gap (figure 1.12 upper frame), displays a rather featureless continuum. If all CVs were to follow the same evolutionary path, as in figure 1.12 (middle frame), and if sufficient time has elapsed for systems to be expected at all phases of evolution, then the period distribution should be similar to that of figure 1.12 (lower frame). If I assume that the observed minimum period is the true point for the period bounce, this would give a distribution similar to that of figure 3.1 (bottom left frame). This distribution shows a pronounced feature around the minimum period 'a period spike'. Clearly this feature is not seen in the observed distribution, I address this problem in this chapter. I present the calculated period distributions for model populations with various assumptions about evolutionary parameters (see section 3.4 for details) to try to smooth out this spike. These models were then tested statistically against the observed distribution to give a measure of the goodness of fit.

3.1 Method for generating parent populations

As systems evolve after the minimum period a point is reached (typically when $\dot{M}$ falls below $10^{-11} M_{\odot} yr^{-1}$) where numerical fluctuations in $\dot{M}$ become so large that the Henyey

scheme no longer converges (see figure 3.1 top left frame). The stellar code uses tables to interpolate/extrapolate the opacities and equation of state for each iteration, and in this region the extrapolations become very uncertain. To extend the tracks I used a semi-analytical method as follows.

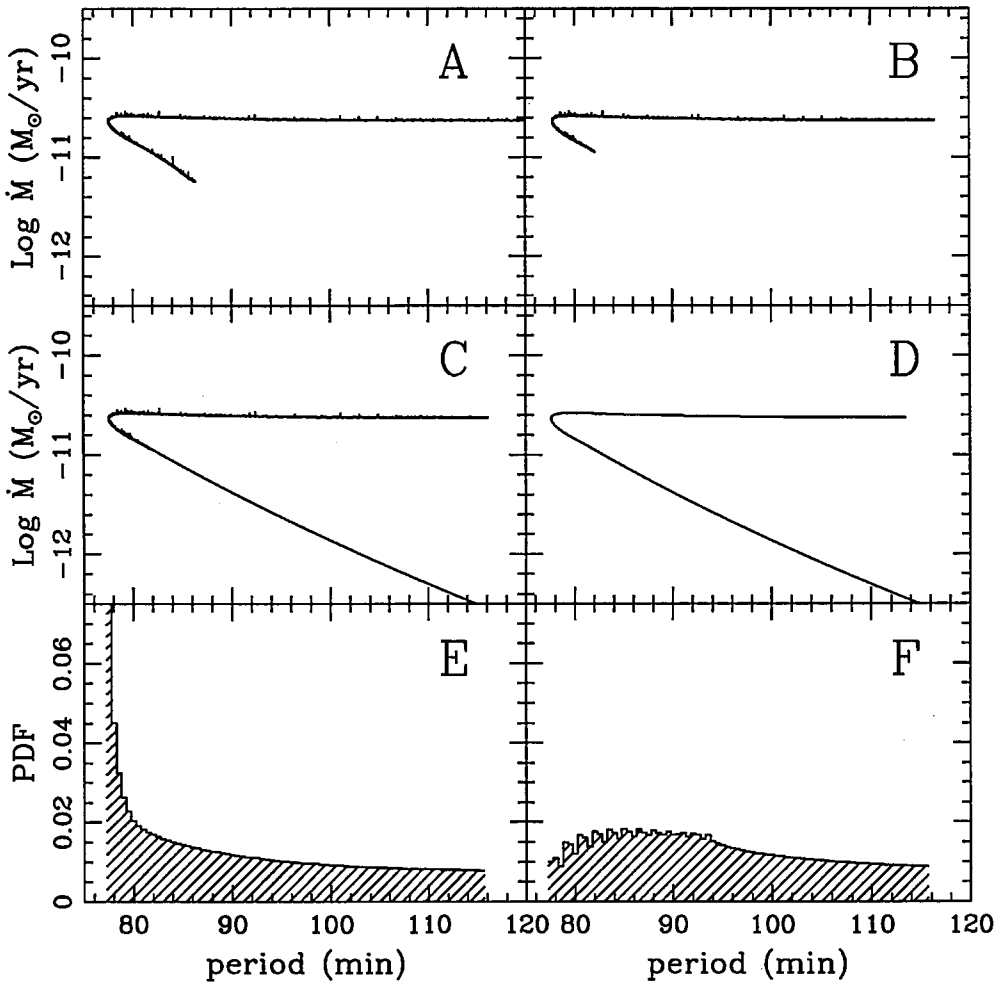

Figure 3.1: Steps in generating a parent distribution. 1: (frame A) the raw data. 2: (frame B) the cut data. 3: (frame C) the extended data. 4: (frame D) the smoothed data. 5: (frame E) the probability distribution function (PDF) from the smoothed data. 6: (frame F) the full parent distribution from the summing of many PDFs.

The tracks were terminated at a value of $\log \dot{M}_2 = \log \dot{M}_2(\mathrm{Pturn}) - 0.3$, where $\dot{M}_2(\mathrm{Pturn})$

is the mass transfer rate at the minimum period for the track (see figure 3.1 top right frame). The radius of the star for the final part of the track is approximated by

$$R_2 = R_0 M_2^{\zeta}, \tag{3.1}$$

where the parameters R_0 and ζ are constant. The values of R_0 and ζ were determined from the final few data points for each track. ζ takes a typical value of around 0.15 for systems beyond the period bounce. To generate the extension to the track I then calculated P from the Roche lobe condition (see equation 2.17), and $\dot{M}_2$ by assuming stationarity as in equation 2.19 (see figure 3.1, middle left frame for an example of an extended track).

The extended track is now smoothed to remove the numerical noise from it. This is done by using a rolling average method. Data is read for a given number of points (nominally 200), a typical data set would have in excess of 100,000 data points, the mass transfer rate and the period are averaged over this range and saved along with the mean age. The start for reading in the data set is advanced by one data point and the process repeated. This produces a track as in figure 3.1 (middle right frame).

The chances of detecting a system within a given period range is proportional to the time taken for the system to evolve through this range, hence the discovery probability

$$Prob \propto \frac{1}{\dot{P}}. \tag{3.2}$$

As pointed out by Ritter and Burkert (1986) it is more likely that brighter systems, hence systems with a higher mass transfer rate $\dot{M}$, will be observed than those with a lower mass transfer rate, the chances of observation of a system is weighted by assuming

$$\frac{\dot{M}^{\gamma}}{\dot{P}}, \qquad \gamma \geq 0.0, \tag{3.3}$$

for the discovery probability. The selection factor γ depends on the distribution of CVs within the volume of space in question and their brightness in the waveband used for observing them. For an isotropic distribution of sources the expected values of γ are 3/2 for a bolometric magnitude limited sample and 1 for a visual magnitude limited sample of accretion disc systems (see Kolb (1995), also see Dünhuber (1993), Dünhuber and Ritter (1993)). The track is then split into sections, above the period bounce, below the period

bounce and turn on flag (see section 2.1) as appropriate. The period space for each section is then split into 0.5 minute bins on a regular grid to cover the whole area of interest. For each 0.5 minute bin the average mass transfer rate $\dot{M}_{ave}$ is calculated and the probability of finding a system in a given bin is given by

$$X = |T_1 - T_2|\dot{M}_{ave}^{\gamma}/0.5, \tag{3.4}$$

where T_1, T_2 are the maximum and minimum ages of the system in a given bin. The corresponding period bins from each of the sections are summed and the resultant normalized to give the overall probability of finding a system within a given bin, giving a probability distribution function (PDF) similar to that shown in figure 3.1 (lower left frame), for a single set of the evolutionary parameters. For each investigation I generated typically 20-40 evolutionary tracks covering the range of evolutionary parameters under investigation, these were all binned by the same method. The corresponding period bins for each distribution are then summed and normalized to produce the final parent distribution similar to that shown in figure 3.1 (lower right frame).

3.2 Statistical tests

To make a comparison of the various model parent distributions with the observed distribution, I require a statistical test to quantify the differences. In this section I introduce the tests I used, and in some cases rejected, to perform this task.

3.2.1 The K-S test

The K-S (Kolmogorov-Smirnov) test uses the maximal value of the absolute difference D between the cumulative distribution functions of the observed $S_N(x)$ and theoretical $P(x)$ distributions (see figure 3.2)

$$D = max|S_N(x) - P(x)|, \tag{3.5}$$

where the cumulative distribution function in our case is given by

$$C(x) = \frac{\text{Number of systems with period less than P}}{\text{N (total number of systems in sample)}} \tag{3.6}$$

as a measure of the significance that the two distributions are not drawn from the same distribution.

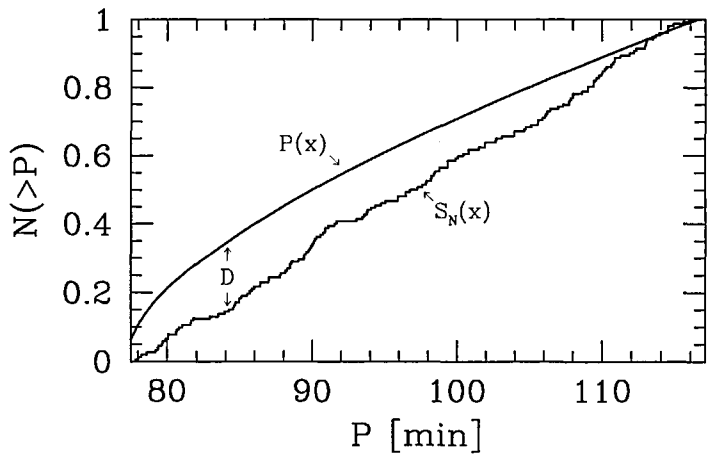

Figure 3.2: Cumulative distributions for observed period distribution of CVs ($S_N(x)$) and theoretical period distributions as shown in figure 3.1 ($P(x)$) used in a K-S test.

In the case of the cumalative distribution of systems the K-S test is insensitive to the differences between the parent distributions. The greatest difference in the cumulative distribution functions of the observed and modelled distributions occur at the lower boundary of the cumulative distributions functions, (see figure 3.2 for example of observed against theoretical distribution) i.e. in the least sensitive region for the K-S test (Press, Teukolsky, Vetterling, and Flannery (1992)). I thus decided to use the following modified χ^2 test.

3.2.2 The modified χ^2 test

See Press, Teukolsky, Vetterling, and Flannery (1992) for a description of the standard χ^2 test. For each parent distribution 10000 model samples each containing 134 systems[1]

[1]134 was the number of observed CVs in the range $77 \leq P(min) \leq 116$; Ritter and Kolb (1998), internal update June 2001. As of Feb 2003 the number of systems in this period range is now 160 (RKcat version 7.0, Ritter and Kolb (2003)); although this does alter the values given by the χ^2 test, the trends and hence

were generated. Each sample was tested against the model parent distribution using a standard χ^2 test, with 1, 2 and 4 minute bins. This range bridges the need for good resolution and significance of the χ^2 test which requires a minimum number of CVs per bin. The observed period distribution was tested against the model parent distribution also, giving the reduced χ^2 value χ^2_{obs}. The fraction f of generated samples with a reduced χ^2 value less than χ^2_{obs} was used as a measure of the significance level of rejecting the hypothesis that the observed distribution is drawn from the parent distribution. In the following I quote the rejection probability $P_r = f$.

3.2.3 The F-test

The F-test (Press, Teukolsky, Vetterling, and Flannery (1992)) uses the F statistic which is the ratio of the theoretical variances (σ^2_{obs}) of the observed sample, and (σ^2_{theo}) of the model sample generated from a theoretical period distribution containing the same number of systems as the observed sample. The F statistic is given as

$$F = \frac{\sigma_x^2}{\sigma_y^2} \tag{3.7}$$

where the theoretical variance σ_x^2 is taken as the variance σ^2_{obs} or σ^2_{theo} which has the greatest value, σ_y^2 is the remaining variance with the least value. The standard variances are given by

$$\sigma^2 = \sum_{i=0}^{N} (x_i - \mu)^2/(N-1) \tag{3.8}$$

in which μ is the average value of the distribution under consideration (in this case the average orbital period), consisting of N data points (the number of systems in the sample) and x_i is the value of the random variable (in this case the orbital period of a given system) at the data point i. Large values $F >> 1$ indicate a very significant difference in the two distributions. The value of F is compared to a standard distribution for F to give a probability (Prob) that the two distributions are drawn from the same underlying distribution (small values of Prob indicate large differences). The F-test was used as a test of the modified χ^2 test and to check that the general results were consistent.

the results remain unchanged.

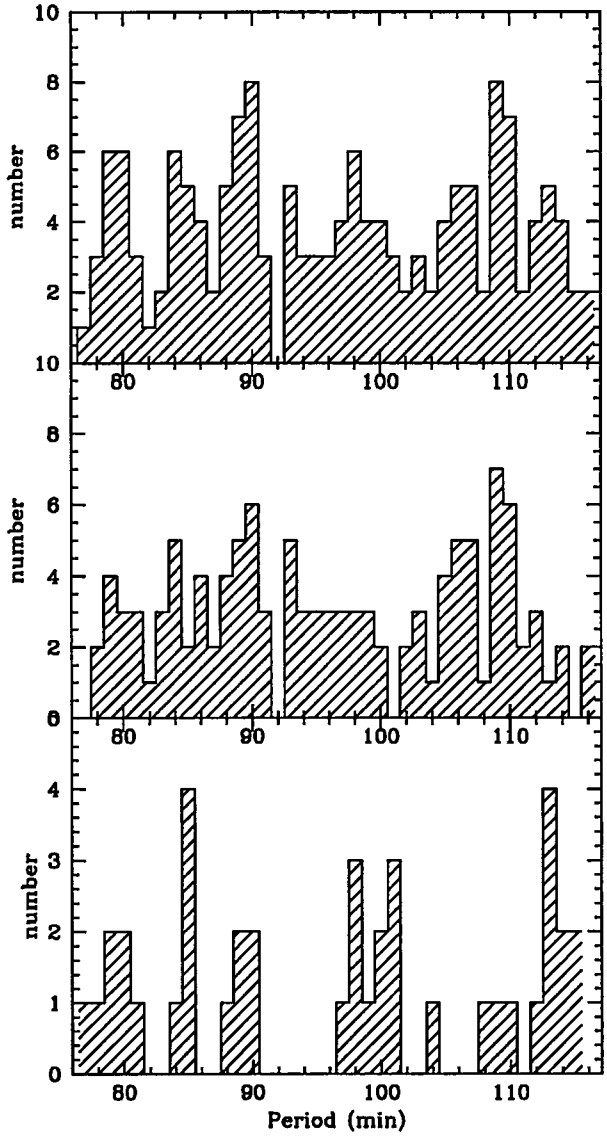

Figure 3.3: Observed orbital period distribution for $76 \leq P(min) \leq 116$. Upper frame: all CVs; Middle frame: non-magnetic CVs; Lower frame: magnetic CVs. Data from RKcat version 7.0, Ritter and Kolb (2003).

3.3 Magnetic and non-magnetic CVs

Kolb and Baraffe (1999) noted that the observed distribution of non-magnetic CVs (figure 3.3, middle frame), and the observed distribution of magnetic CVs (figure 3.3, lower

frame) show no significant difference below the period gap. To test and quantify this I compared these distributions for $P \leq 116$ min, and obtained a reduced χ^2 probability of 0.12. Hence on the basis of this it cannot rule out that the distributions are drawn from the same underlying parent distribution. This is borne out by the results of comparing both distributions with a parent distribution that is flat in P (see also Table 3.1 below, entries F and G) which give similar rejection probabilities ($P_r = 0.71$ and $P_r = 0.78$, respectively), (Also see section 7.3). In the following I therefore test models against the combined magnetic and non-magnetic distribution of observed systems.

The lack of any distinct features in the combined observed period distribution (figure 3.3, upper frame) does indeed suggest an essentially flat distribution for the underlying parent distribution. The flat distribution gives $P_r = 0.55$ (for the 1 minute bin width, see Table 3.1), I use this value as a benchmark for the models discussed below.

3.4 Parent populations

I define a standard set of assumptions for a simple parent population models as follows:

(1) The primary mass in all systems is $0.6M_{\odot}$. This is the value around which the majority of WDs in CVs are expected to form (see e.g. de Kool (1992)).

(2) All systems form as CVs at orbital periods greater than 2 hours. This is consistent with the secondary stars in CVs being somewhat evolved (see Baraffe and Kolb (2000)).

(3) The flux of systems through the period gap is constant. That is, sufficient time has elapsed since the formation of the Galaxy for a steady state to have been reached, so that the number of systems arriving at the lower edge of the period gap is just balanced by the number of new systems forming at orbital periods greater than two hours.

(4) The CAML efficiency is set to 0.

(5) The systemic AM loss rate is $\dot{J}_{sys} = 3\dot{J}_{GR}$.

(6) The deformation factor is $\lambda = 1.06$.

Assumptions (5) and (6) are used together to set the modelled P_{min} equal to the observed $P_{min} = 77$min, thus enabling us to test the statistical significance of the period spike.

Table 3.1: Results of the χ^2 tests on the the observed distribution with the following parent distribution models.

	1 min binning		2 min binning		4 min binning	
Distribution	χ^2_{obs}	P_r	χ^2_{obs}	P_r	χ^2_{obs}	P_r
A	1.00	0.55	0.73	0.21	0.74	0.32
B	1.08	0.66	0.84	0.33	0.74	0.33
C1	1.25	0.83	1.25	0.75	1.89	0.95
C3	1.07	0.61	0.89	0.38	1.15	0.67
D1	1.38	0.92	1.42	0.89	1.99	0.96
D3	1.12	0.69	0.91	0.44	0.94	0.53
E1	1.21	0.79	1.26	0.78	1.50	0.85
E3	1.05	0.58	0.94	0.45	0.81	0.36
F	1.11	0.71	1.34	0.85	1.51	0.88
G	1.16	0.78	1.09	0.64	1.27	0.75

KEY

A: Flat distribution versus complete observed sample.

B: Age limit versus complete observed sample.

C1: CAML versus complete observed sample, $\gamma = 1$.

C3: CAML versus complete observed sample, $\gamma = 3$.

D1: M1 versus complete observed sample, $\gamma = 1$.

D3: M1 versus complete observed sample, $\gamma = 3$.

E1: CAML plus M1 versus complete observed sample, $\gamma = 1$.

E3: CAML plus M1 versus complete observed sample, $\gamma = 3$.

F: Flat distribution versus magnetic CVs only.

G: Flat distribution versus non-magnetic CVs only.

A model population subject to these standard assumptions can be rejected with the probability $P_r > 1 - 10^{-4}$.

In the following discussion of various population models any differences of individual models from this standard set of assumptions is quoted at the start of each section.

3.4.1 Age limit hypothesis

Relaxing assumptions (5) and (6) and using the definition of the age limit model from section 2.4.3, I obtain $P_r = 0.66$ for the period distribution generated from the single evolutionary track corresponding to figure 2.10, cut at 77 minutes, (for a 1 minute binning, table 3.1, model B), quite close to the value for a flat distribution. In this period region $\dot{M} \simeq const$ (see figure 1.12, middle frame). As $\dot{P}$ scales roughly as $\dot{M}$, the discovery probability is roughly constant if $\gamma = 1$. A period distribution based on the age limit hypothesis is shown in figure 3.4. The overall distribution is insensitive to variations in the evolutionary parameters, e.g. CAML efficiency, M_1, etc. For systems before the period bounce variations in the evolutionary parameters have a similar effect on systems at all periods, (see figure 2.5) hence the age limit model is largely unaffected by these paramters.

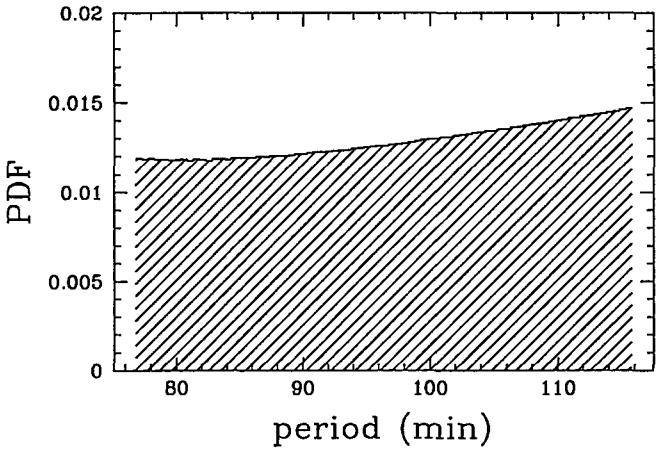

Figure 3.4: Period distribution for a population based on the age limit model; $\gamma = 1.0$.

The same flat distribution would be obtained if some mechanism would cause systems to 'die' (e.g. become too faint to be detected) before reaching the period bounce. Meyer and Meyer-Hofmeister (1999a) speculate that AM Her stars become propeller systems before the period bounce, and so are no longer observed as CVs as their accretion luminosity would be very low. For non-magnetic disc-accreting CVs Meyer and Meyer-Hofmeister (1999b) speculated that, as the secondaries become degenerate, the magnetic activity of the secondary reduces rapidly to zero. The disc would then be fed by non-magnetic material, thus reducing the viscosity of the disc plasma and vastly increasing the recurrence time.

3.4.2 CAML efficiency and primary mass spectrum

I now abandon assumption (4) and allow systems to occur with equal probability with any value of the CAML efficiency in the range $0.0 \leq \eta \leq 0.95$. This produces the period distribution in figure 3.5 (upper frame) for $\gamma = 1$. A spike is still present, though now broadened, and peaked at around 87 minutes. The PDF then falls with increasing period. This parent distribution gives P_r=0.83 (1 minute binning, see Table 1, model C1), somewhat larger than that for the flat distribution.

The result of varying γ is summarised in Table 3.2. At $\gamma = 3$ the rejection probability reaches a minimum value $P_r = 0.61$. This corresponds to the parent distribution shown in figure 3.5 (lower frame). The broadened peak at around 87 minutes is almost the same as for $\gamma = 1$, but at longer P the PDF increases again, i.e. there is a minimum at around 95 min. This is caused by a corresponding minimum of $\dot{M}$ along the tracks of figure 2.5.

Table 3.2: χ^2 test on CAML parent distribution versus complete observed sample for various γ

γ	1	2	3	4	6
χ^2_{obs}	1.25	1.17	1.07	1.11	1.15
P_r	0.83	0.75	0.61	0.66	0.96

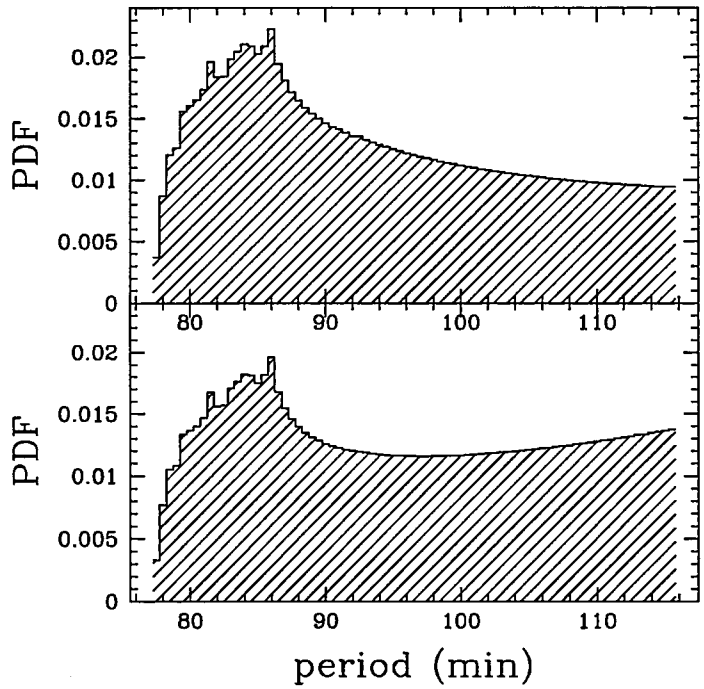

Figure 3.5: Period distribution for a population based on a CAML spectrum ($0 \leq \eta \leq 0.95$). Upper frame: $\gamma = 1.0$. Lower frame: $\gamma = 3.0$.

So far I have assumed that all CVs in the population have the same WD mass. Observations (e.g. Ritter and Kolb (2003)) and population synthesis (e.g. de Kool 1992, also see section 1.2.1) show that a spread of WD masses is likely. To investigate the effect this has on the shape of the PDF near P_{min} I reinstate assumption (4) and abandon assumption (1) and adopt the WD mass spectrum calculated by de Kool (1992).

The corresponding full parent distributions for $\gamma = 1$ and $\gamma = 3$ give $P_r = 0.92$ and $P_r = 0.69$, respectively, for a 1 minute binning (see Table 3.1 for full results). These values are slightly higher (worse) than for the CAML efficiency spectrum population with fixed WD mass.

If I combine the effect of the primary mass distribution and the CAML efficiency spectrum, i.e. abandon assumptions (4) and (1), I obtain the parent distributions shown in figure 3.6. The PDF for $\gamma = 1$ (upper frame) gives $P_r = 0.79$ and exhibits a broad peak

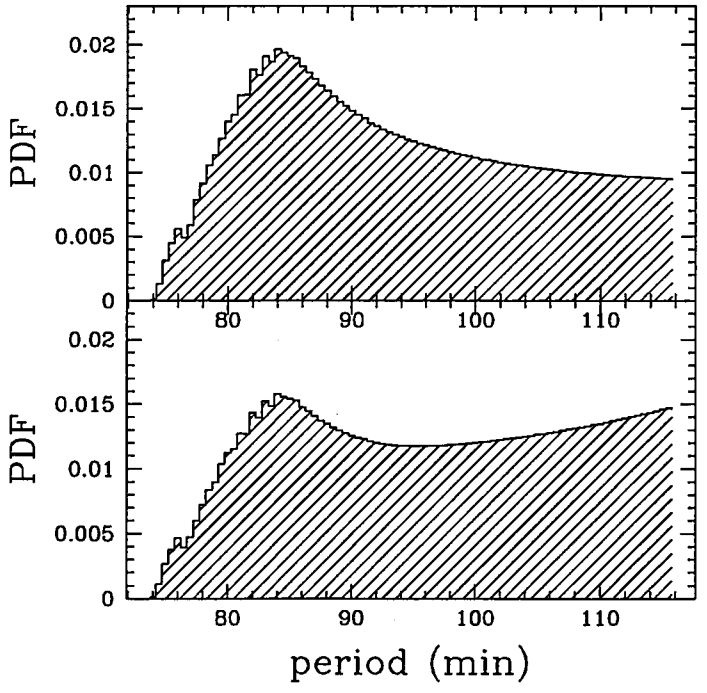

Figure 3.6: Period distribution for a population based on a primary mass spectrum (de Kool 1992) and CAML efficiency spectrum ($0 \leq \eta \leq 0.95$). Upper frame: $\gamma = 1$. Lower frame: $\gamma = 3$.

with a maximum at around 85 minutes, followed by a gradual decrease with increasing period. The PDF for $\gamma = 3$ figure 3.6 (lower frame) gives $P_r = 0.58$ and also shows a similar, though somewhat sharper, broad peak as for the case with constant WD mass. The values of Pr are lower (better) than either of the previous models alone (see Table 3.1 for full results). With $\gamma = 3$ the rejection probability approachs a value similar to that of a flat distribution (0.55).

3.4.3 Deformation factor spectrum

Here I abandon assumptions (5) and (6) and assume instead that the secondary stars are subject to various deformation factors λ (as described previously in section 2.4.2). A minimum value of $\lambda = 1.18$ is used to set P_{min} equal to the observed $P_{min} = 77min.$

Each value of λ between 1.18 and a maximum value λ_{max} was given equal weighting. The rejection probability for different values of λ_{max} are given in Table 3.3, it can be seen that there is a minimum in rejection probability ($P_r = 0.89$) at $\lambda_{max} \simeq 1.35$. The parent distribution generated for this range of deformation factor ($1.18 \leq \lambda \leq 1.35$) is shown in figure 3.7 and exhibits a gradually increasing PDF with increasing period to a peak at around 90 minutes, and then a gradual decrease to longer periods.

Table 3.3: χ^2 test for the model based on a deformation factor spectrum (versus complete observed sample, for $\gamma = 1.0$)

λ_{max}	1.31	1.33	1.35	1.37	1.39
χ^2_{obs}	1.39	1.35	1.30	1.38	1.45
P_r	0.93	0.92	0.89	0.93	0.96

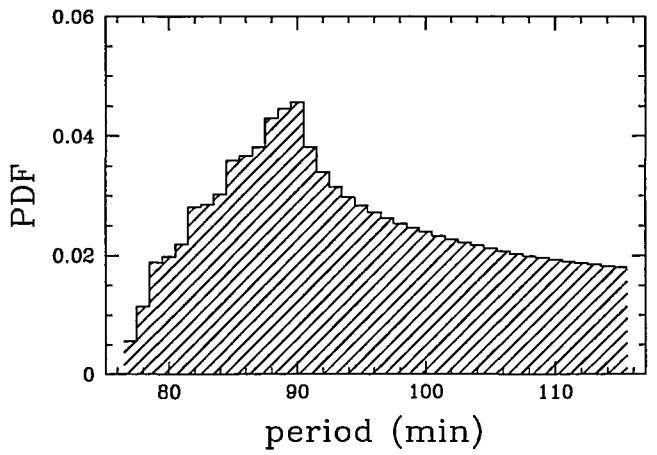

Figure 3.7: Period distribution for a population based on a deformation factor spectrum.

3.4.4 Initial secondary mass spectrum

I now abandon assumption (2) that all systems form with orbital periods greater than 2 hours and consider the other extreme: all CVs form with orbital periods of less than 2 hours. Specifically, I assume that all CVs form with donor masses in the range $0.13M_{\odot} \leq M_2 \leq 0.17M_{\odot}$ (this sets $P_{max} = 116$ min), and that any M_2 is equally likely. From this I obtain a parent distribution as in figure 3.8. The PDF exhibits a sharp spike at the minimum period (here 78 minutes) and then a gradual decline with increasing period. The corresponding χ^2 test results are given in Table 3.4. I conclude that if I were to include any secondary mass spectrum in the previous models I would effectively weight the PDF with a ramp function, similar to the one seen in figure 3.8, in which above an orbital period of around 95 minutes the PDF appears to decrease linearly with increasing period. This would only increase the rejection probability.

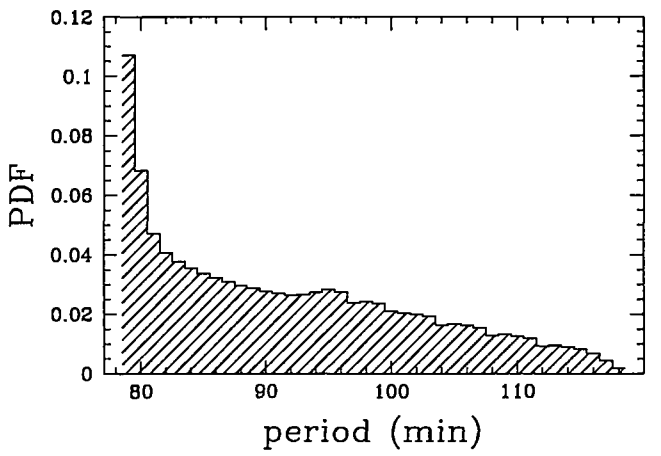

Figure 3.8: Period distribution for a population based on an initial secondary mass spectrum. Note the linear decrease in PDF for systems with periods greater than 100 minutes.

Table 3.4: χ^2 test for the model based on a secondary mass spectrum ($0.13M_\odot \leq M_2 \leq 0.17M_\odot$) (versus complete observed sample, for $\gamma = 1$)

binning (min)	χ^2_{obs}	rejection probability
1	3.0878	$> 1 - 10^{-4}$
2	4.3233	$> 1 - 10^{-4}$

3.4.5 A contrived weighting?

King, Schenker, and Hameury (2002) constructed a (nearly) flat period distribution by superimposing individual idealized PDFs with different bounce periods P_b according to a suitably tailored weighting. For the double box-shaped idealised PDFs modelled on the PDF shown in my figure 1.12 (lower frame) the required weighting is $n(P_b) = \exp[-0.124(P_b - P_0)]$ (P_0 is the observed minimum period). This weighting function effectively mirrors the shape of the sharply peaked individual PDFs. King et al. (2002) found that the range $78 \leq P_{min} \leq 93$ is sufficient to wash out the period spike. It is clear that this procedure involves a certain degree of fine-tuning for $n(P_b)$ if the shape of the input PDF is given. Such a fine-tuning must surprise as the two functions involved presumably represent two very different physical effects.

I applied the weighting $n(P_b)$ quoted in King et al. (2002) to my non-idealized model PDFs that involve the CAML efficiency and the deformation factor as a means to vary P_b. The weighting produced a marginally worse fit ($P_r = 0.84$ versus $P_r = 0.83$; 1 minute binning) for the CAML PDFs compared to the parent population based on the flat CAML efficiency spectrum I discussed earlier. In part this is due to the fact that the upper limit on η does not allow a big enough range of P_b. In the case of the deformation factor PDFs the fit marginally improved ($P_r = 0.84$ versus $P_r = 0.89$; 1 minute binning, $1.18 \leq \lambda \leq 1.35$). It is possible to optimise the fit by adding systems with deformation factors up to 1.42, and by using the weighting $n(P_b) = \exp[-0.07(P_b - P_0)]$, but this still gives the fairly large

value $P_r = 0.83$ (see also figure 3.9). However, such a parent population is inconsistent with the observed distribution for longer periods. As can be seen from figure 2.8 systems that are subject to larger deformation factors would evolve into the period gap, hence the gap would be populated in this model.

For completeness I show in figure 3.10 the result of the superposition suggested by King et al. (2002) if realistic rather than idealised PDFs are used. This model assumes additional systemic AM losses ($5 - 11 \times \dot{J}_{GR}$; no CAML, no deformation factor, $\gamma = 1$) as the control parameter for varying P_b, and the weighting as in King et al. The pronounced feature just above 2 hrs orbital period is the result of the adiabatic reaction of the donor stars at turn-on of mass transfer (see e.g. Ritter and Kolb (1992)). Such a feature is absent in the observed distribution. This pronounced feature is not generated in the other

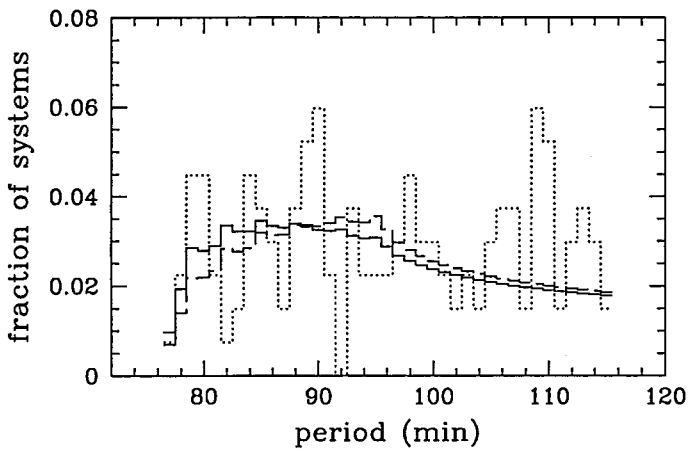

Figure 3.9: Period distributions based on a deformation factor spectrum with $1.18 \leq \lambda \leq 1.42$ and $n(P) = \exp[-0.124(P_b - P_0)]$ (solid line), $n(P) = \exp[-0.07(P_b - P_0)]$ (dashed line). The observed distribution (dotted line) is shown for comparison.

models in this chapter. Most of the models produce a spread of period at which systems

start mass transfer hence reducing the effect of the turn on flag (for an example of this see figure 3.8). The models are also cut at 116 minutes for comparison with the observed distribution.

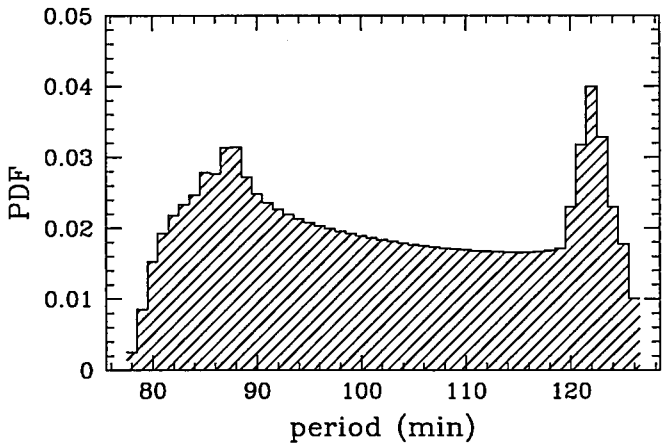

Figure 3.10: Period distributions based on a spread of systemic AM losses $5 - 11 \times \dot{J}_{GR}$ and $n(P) = exp[-0.124(P_b - P_O]$

3.5 Conclusions

In this investigation all the parent models, with the exception of the age limit model (see section 3.4.1), retain a pronounced feature due to an accumulation of systems near to the period bounce. I employ a modified χ^2 test to measure the 'goodness of fit' for each parent distribution against the observed sample. None of the synthesized model populations fits quite as well as the distribution which is simply flat in orbital period, the flat parent distribution having a rejection probability of 0.55. The age limit model however comes quite close as expected as this has an almost flat distribution in orbital period. In the other parent distributions only if the brighter systems carry a far greater weighting than expected in a simple magnitude limited sample (selection factor $\propto \dot{M}^{\gamma}$ with $\gamma \simeq 3$ rather

than $\simeq 1$, see equation 3.3) are similar values for P_τ achieved. However, most of our models with $\gamma = 1$ cannot be rejected unambiguously on the basis of this test.

Models designed to 'wash out' the period spike by introducing a large spread of the CAML efficiency (section 3.4.2) do generally better than population models based on donor stars that are subject to a large spread of intrinsic deformation factors (section 3.4.3). For all models the rejection probability decreases if the full WD mass spectrum is taken into account, as this introduces an additional spread in the bounce period. Model populations where all CVs form at long orbital periods (chiefly above the period gap) give a much better fit than models that include newborn CVs with small donor mass (section 3.4.4). Adding these systems to the population introduces a general increase of the orbital period distribution towards short periods, thus making the period spike more pronounced. This suggests that most CVs are likely to have formed at long periods and evolved through the period gap to become short-period CVs. This is consistent with independent evidence that CV secondary stars are somewhat evolved (Baraffe and Kolb (2000); Schenker et al. (2002); Thorstensen et al. (2002)).

Recently, King, Schenker, and Hameury (2002) constructed a flat orbital period distribution by superimposing idealised PDFs that describe subpopulations of CVs with a fixed initial donor mass and initial WD mass, but different bounce periods. This superposition required a strongly declining number of systems with increasing bounce periods. I repeated this experiment with a realistic PDF (section 3.4.5), but failed to obtain a markedly improved fit.

Chapter 4

An introduction to circumbinary discs

A circumbinary disc is a disc in which gaseous material, which in the case of CVs has flowed out of the binary system, orbits at some distance from the central binary beyond the Lagrangian points (see section 1.3.4). Circumbinary discs may start life as the remnants of the common envelope phase of the pre CVs life. Alternatively, a circumbinary disc may form from material that is ejected from the binary system, either from a wind from the primary star, secondary star or accretion disc or, in the case of magnetic systems, from a magnetic propeller (see section1.1.4). This material will leave the central binary with a range of specific orbital angular momenta, and some fraction of the material will form a circumbinary disc at some distance from the central binary. Observational evidence is discussed in section 1.3.4. This material can interact with the binary via tidal interactions and remove angular momentum from the orbit of the central stars hence influencing the evolution of the system. The circumbinary disc should evolve in much the same way as the standard accretion disc though the material will be forced to flow out rather than in through the disc, due to the differing boundary conditions. It should thus be possible to describe the mechanisms controlling the disc structure as for the standard model.

4.1 Disc physics

The derivation of the equations which determine the structure and evolution of discs, usually applied to accretion discs, is dealt with in several standard textbooks and review papers (e.g. Frank, King, and Raine (2002), Pringle (1981)). Rather than repeating this derivation, I shall highlight some of the important aspects.

The main requirement for the formation of a disc is the presence of gas or dust moving around a central body (in the case of a CV accretion disc this is the WD primary) with large angular momentum. In a CV accretion disc the gas/dust and angular momentum are mainly supplied from the material leaving the L_1 point. This material has approximately the specific angular momentum of the L_1 point considered in the white dwarf frame of reference.

The disc is assumed to be Keplerian, that is the material moves in circular orbits with Keplerian speed (v_ϕ) about the central object,

$$v_\phi = v_{Kep}(R) = \left(\frac{GM}{R}\right)^{1/2} \tag{4.1}$$

and the vertical scale height of the disc H is given by demanding hydrostatic equilibrium between gravity and gas pressure (see Frank, King, and Raine (2002)). As a consequence of which, for a thin disc, H is required to be small compared to the radial extent of the disc giving

$$\frac{H}{R} = \frac{c_s}{v_\phi} \ll 1, \tag{4.2}$$

where c_s is the local sound speed. As the sound speed in hydrogen gas is only around 10 km/s in a hot disc $T \sim 10^4$K and around 1.6 km/s for a cool circumbinary disc $T \sim 100$K, even at $200R_\odot$, from a binary with total mass of $0.8M_\odot$ the Keplerian speed is around $5 - 20 \times c_s$ for hot and cool discs respectively. As the disc is more likely to be cool at the outer edge it can be seen that the Keplerian velocity is highly supersonic and hence the thin disc approximation should still be valid here.

In a Keplerian disc the material closer to the central object moves with greater velocity than that further away, this causes a differential rotation of the disc (see figure 4.1). The disc material interacts viscously due to, e.g., the interaction of the chaotic thermal motion

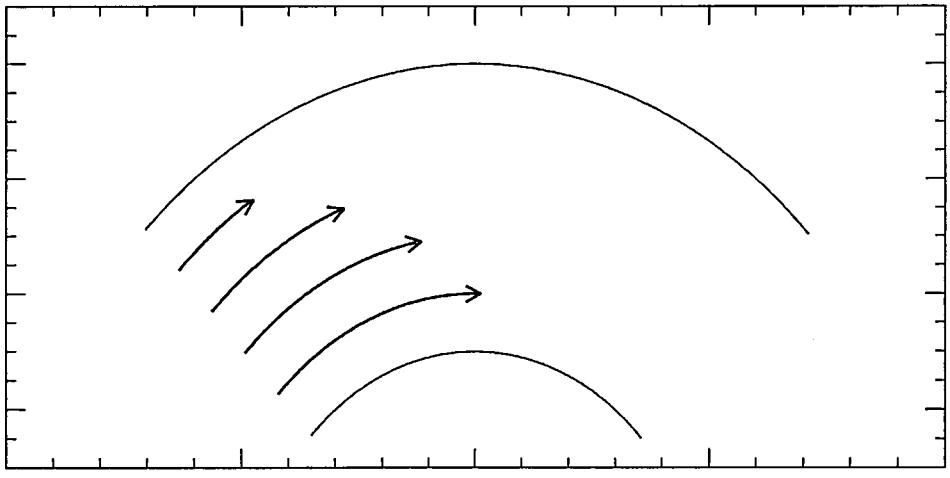

Figure 4.1: Schematic representation of the velocity varying in the disc with distance from central object

of particles and turbulent motion of the fluid elements with the differential rotation of the disc. The effect of the viscosity is to slow down the faster moving material and speed up the slower moving material. In the following I use cylindrical coordinates (R, ϕ, z) where R is the radial distance in the mid plane from the rotation axis (in our case the centre of mass of the binary), ϕ is the azimuth angle and z is the height above the disc mid-plane. As mass and density variations in the vertical structure of the disc happen on the dynamical timescale which is short compared to the viscous timescale on which the radial variations occur, a vertically integrated quantity of the surface mass density Σ (the mass of the column per unit surface area of the disc), where

$$\Sigma(R) = \int_{-\infty}^{+\infty} \rho(R, z) dz, \tag{4.3}$$

is used to describe the disc properties. The disc is assumed to be axisymmetric.

The fundamental conservation laws for the conservation of mass and angular momentum can be written in terms of Σ and R as

$$R\frac{\partial \Sigma}{\partial t} + \frac{\partial}{\partial R}(R\Sigma v_R) = 0, \tag{4.4}$$

and

$$R\frac{\partial}{\partial t}(\Sigma R^2\omega) + \frac{\partial}{\partial R}(R\Sigma\nu R^2\omega) = \frac{1}{2\pi}\frac{\partial G}{\partial R}, \tag{4.5}$$

(Pringle (1981)). With the Keplerian value for ω and the equation for viscous torque

$$G(R,t) = 2\pi R\nu\Sigma R^2\frac{d\omega}{dR}, \tag{4.6}$$

where ω is the angular velocity at the point in the disc and ν is the viscosity of the material at the given radius. The radial drift velocity v_R of the disc material may be eliminated giving

$$\frac{\partial\Sigma}{\partial t} = \frac{3}{R}\frac{\partial}{\partial R}\left(R^{\frac{1}{2}}\frac{\partial}{\partial R}[\nu\Sigma R^{\frac{1}{2}}]\right). \tag{4.7}$$

This has the characteristic form of a diffusion equation.

Generally ν can be a function of the local disc conditions i.e. the temperature, density and radius, thus equation 4.7 would be a nonlinear diffusion equation for Σ. Hence except under certain special conditions (e.g. if ν is considered to vary only as a power of the radius) the equation must be solved by numerical methods. With the addition of the appropriate boundary conditions a set of equations describing the structure of the disc can be found.

4.2 Previous studies of Circumbinary discs in CVs

In this section I review some of the recent work mainly by Taam, Spruit and Dubus, on circumbinary discs in CVs, in which they develop a simple model for the disc and see how the inclusion of a circumbinary disc affects the evolution of CVs. I build on this work in chapter 5 to produce my own model for a circumbinary disc using the full binary evolution code as previously to model the inner binary system. I use this model to determine the effect that the disc parameters have on the mass transfer rates and the period at which systems bounce.

Section 4.2.1 describes Spruit and Taam's initial simplified model for a circumbinary disc, high-lighting the assumptions made and the effects the model has on the evolution of the CV systems. Section 4.2.2 shows how Taam and Spruit build on the results of the first

model high-lighting the improvements in the viscosity prescription used for the disc model and the effect this has on the CV evolution. In section 4.2.3 I describe how Dubus, Taam and Spruit use a much more detailed model which accounts for the vertical structure of the disc and the influence this has on the systems. Section 4.2.4 gives a brief overview of the latest paper by Taam, Sandquist and Dubus in which a systematic investigation of CV evolution with a circumbinary disc is presented.

4.2.1 Circumbinary discs and cataclysmic variable evolution

Spruit and Taam (2001) make the standard note, that in models for CVs with only gravitational radiation and magnetic braking as the angular momentum loss mechanisms, the mass transfer rates depend on the timescale of these angular momentum loss mechanisms and the mass of the secondary with little dependence on the characteristics of the primary. Thus there is a strong relation between mass transfer rate and the orbital period. Observational estimates of the mass transfer rates for CVs do not appear to have this one to one correspondence (Patterson (1984), Warner (1987), Sproats, Howell, and Mason (1996), also see section 1.1). There appears to be a spread of mass transfer rates of over an order of magnitude for a given orbital period. This is further aggravated by the three short period super softsources found at the upper edge of the period gap (also see section 1.1.5), J0439.8-6809 (Schmidtke and Cowley (1996)), J0537.7-7304 (Orio, della Valle, Massone, and Oegelman (1997)) and 0035.4-7230 (Crampton, Hutchings, Cowley, and Schmidtke (1997)) where the mass transfer rate is believed to be around $10^{-7}M_{\odot}$ per year, well above the expected rates at the upper edge of the period gap of around $10^{-9}M_{\odot}$ per year.

Spruit & Tamm propose that the solution to the problems is in the additional angular momentum loss that can be obtained from a circumbinary disc, which could cause mass transfer rates, for CVs above the period gap, well above the rates for magnetic braking and gravitational radiation. The additional angular momentum is proposed to be removed from the binary by tidal torques (see Lin and Papaloizou (1979), Eggleton and Pringle (1985), Pringle (1991)). Spruit and Taam (2001) approximate the interaction of the binary with

the disc as taking part at the inner edge of the disc, this is a reasonable first approximation as the mass in the disc is concentrated toward the inner edge and regions far from the binary will only interact weakly. The angular momentum loss rate due to this idealized interaction is given by

$$\dot{J} = 3\pi \left(\frac{r_i}{a}\right)^{\frac{1}{2}} \omega a^2 \nu_i \Sigma_i, \tag{4.8}$$

where ν_i and Σ_i are the viscosity and surface mass density at the inner edge of the disc respectively and ω is the orbital frequency of the binary. The equation assumes that the vertical and axial structure of the disc are of little importance, though variations in either of these may affect the possition of the inner edge of the disc and hence its interaction with the binary system.

The model they propose assumes conservative mass transfer and that a fraction δ of the transferred mass is fed into the circumbinary disc. The mass input rate for the disc is then given as

$$\dot{M}_e = -\delta \dot{M}_2. \tag{4.9}$$

The fraction δ is assumed to be sufficiently small $\delta \ll 1$ so as to approximate the assumption of conservative mass transfer. This is a significant simplification as even though only a tiny fraction of the transfered mass $\delta \sim 0.001$ is passed to the disc, any mechanism such as a disc or secondary wind that expelled mass from the system, would be expected to lose mass in all directions. An exception to this would be in the case of a magnetic propeller system where most of the mass may be ejected in the orbital plane. In the case of a disc wind the mass loss could even be in the direction perpendicular to the orbital plane, thus any mass transferred to the disc is likely to be only a fraction of the total mass lost to the system.

The fraction δ is fixed with time and is assumed to enter the disc, at the inner edge, with the specific angular momentum of the inner edge of the disc. The mass input into the disc is, however, likely to be spread over a large area of the disc, though the exact distribution of this will be determined by the mechanism by which mass is expelled. The viscosity ν in the disc is taken to be a function of radial distance r from the centre of

mass, given as

$$\nu = \nu_i \left(\frac{r}{r_i}\right)^n, \tag{4.10}$$

where $n \geq 0$ is a parameter determining how rapidly the viscosity varies with radius. This takes no account of the changes in density and temperature which may have an effect on the viscosity. From equation 4.7 for the viscous evolution of a disc they obtain the standard diffusion equation

$$\partial_\tau y = x^{2n-2} \partial_{xx} y, \tag{4.11}$$

by the use of the variables

$$x = \left(\frac{r}{r_i}\right)^{\frac{1}{2}}, \quad y = 3\pi x \nu \Sigma, \quad \tau = \frac{t}{t_{vi}}, \tag{4.12}$$

where t_{vi} is the viscous timescale at the inner edge of the disc. They assume that, at large distances (the outer edge of the disc), the function $y \to 0$ and the mass input rate forms the boundary condition at the inner edge of the disc,

$$(\partial_x y)_i = -\dot{M}_e. \tag{4.13}$$

The ratio of the radius at the inner edge of the disc to the orbital separation is quite insensitive to the mass ratio and is of the order $r_{in}/a \sim 1.7$ (see Artymowicz and Lubow (1994)).

From these model parameters Spruit and Taam propose that the column densities in the circumbinary disc may build to greater than $\Sigma \sim 10^3 - 10^4$ g cm^{-2}, with disc masses of over $10^{-6} M_\odot$. At these surface densities the angular momentum loss from the system due to the circumbinary disc is similar to that due to standard magnetic braking and hence will have a significant influence, and for higher Σ will dominate, the evolution of the system. This high angular momentum loss will cause the secondary to become further out of thermal equilibrium, compared to the standard model, and the system to have a period bounce at much longer periods (possibly even above the period gap). It is also possible that this could cause the total disruption of the secondary within quite a short time. The large spread of mass transfer rates seen in the observed CV population could thus be explained by the fact that, as systems at any period could be at various times after their

formation, they would also have circumbinary discs at various stages of formation. This would lead to a large spread of angular momentum loss rates from the disc interaction and hence a large spread of mass loss rate. The additional angular momentum loss due to the disc could also account for the high mass loss rate required to drive the short period ($P \simeq 3$ hrs) supersoft sources. Spruit and Taam further propose that magnetic CVs should not form circumbinary discs as they have either small or no accretion discs within the system, though why this should prevent material from the winds of the primary or secondary along with material propelled from the system from forming a circumbinary disc is to be questioned.

Spruit and Taam also discuss a couple of problems with the proposed model. A nova outburst (in which as much as $10^{-4}M_{\odot}$ of material may be expelled from the system) may be sufficient to disrupt the circumbinary disc completely, though this in turn could add to the large spread of mass transfer rate as observed at a given orbital period. The effect on the period gap could be significant. Systems that have only small or no circumbinary discs would follow the normal evolution and form a gap, whereas systems with significantly increased mass transfer would follow a different evolution and may even bounce at periods above 3 hr.

With the low densities of the circumbinary discs these structures would have very low luminosity compared to the bright background of the accretion disc. This would make them very difficult to detect for most CVs, though it may be possible to detect them in the near infrared dust emission region of the spectrum (see section1.3.4).

4.2.2 The evolution of CV binary systems with circumbinary discs

In this paper Taam and Spruit (2001) build on their previous paper (Spruit and Taam (2001), as discussed above) and give a more detailed account of the numerical models used for both the evolution of the binary system and viscous evolution of the circumbinary disc. Taam and Spruit use a modified version of the stellar evolution code developed by Eggleton (1971), Eggleton (1972) to model the evolution of the binary, though the mass transfer is once again assumed to be conservative.

Taam and Spruit use a more sophisticated model of the way in heat lost and hence the temperature of a region in the disc is partially determined by the opacity at that point. As the viscosity of the region is assumed to be dependent upon the temperature of the region the viscosity is thus dependent upon the opacity. The opacity of the disc also varies with the temperature, and at a temperature of around 10^4K hydrogen ionizes producing a sudden change in the opacity. Taam and Spruit (2001) assume a cool disc, so that there is little change in temperature, and use the opacities for dust grains from Bell and Lin (1994) and Bell, Cassen, Klahr, and Henning (1997). Figure 4.2 shows the variation of viscosity ν for the circumbinary disc as a function of the surface mass density Σ, at a radius of 10^{11} cm from a binary with a total mass of $1M_{\odot}$. The viscosity can be seen to take the form of an S curve, with a negative slope in between X and Y in this region there is no stable solution for the disc viscosity. To avoid the problems with thermal instabilities in the disc due to a limit cycle in the viscosity within this region Taam and Spruit (2001) adopt a monotonic dependence (shown as a dot-dashed line in figure 4.2) of the viscosity on the surface mass density above the upper turning point on the lower stable branch X.

As the viscous evolution (typically around 200 yrs) of the disc takes place on a much shorter timescale than the secular evolution (typically around 10^8 yrs) of the binary each time step in the integration of the orbital evolution of the binary is subdivided into smaller time steps for the disc integration to try to keep the relative change of the surface mass density at any point in the disc below a fixed value (typically 0.05) to improve accuracy. The diffusion equation is solved implicitly using a Crank-Nicholson scheme and the viscosity is calculated explicitly between the time steps. The spatial coordinate

$$x = r^{\frac{1}{2}}, \tag{4.14}$$

is used as this simplifies the diffusion equation (equation 4.7) to

$$\partial_t \Sigma = \frac{3}{4x^3} \partial_{xx}(x\nu\Sigma). \tag{4.15}$$

The disc is then evolved on a equidistant grid in x with the grid initially extending to around 1.5 times the radius for the outer edge of the disc. As the disc spreads toward the edge of the grid, the grid is rescaled (doubled in geometrical size whilst holding the

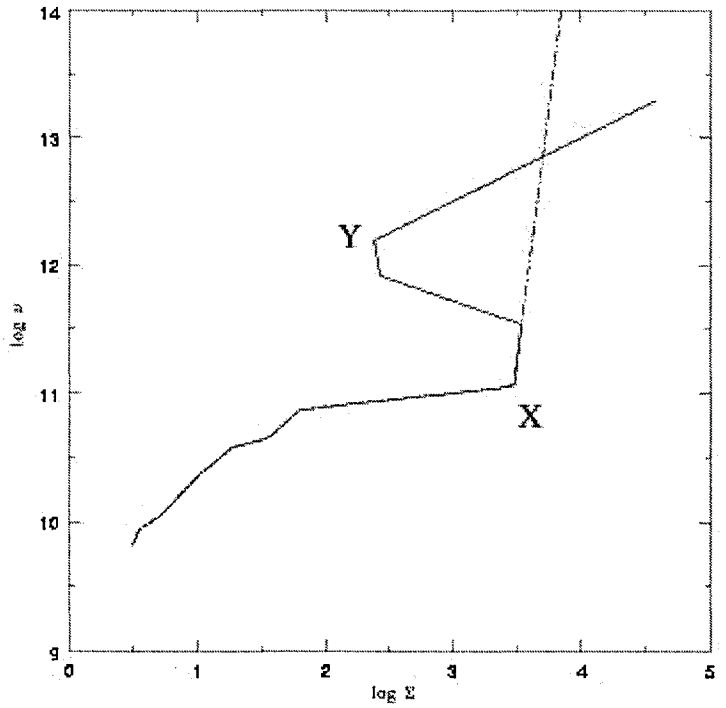

Figure 4.2: Variation of viscosity, ν, in the circumbinary disc as a function of Σ. The dot dash line corresponds to the form used by Taam and Spruit (2001) (for a radius of 10^{11} cm from the central binary of mass $1M_{\odot}$).

number of grid points fixed). The disc is set to have a minimum Σ of around 10^{-2} $g\ cm^{-1}$ to prevent numerical problems with the expressions for viscosity, and the mass flux into the disc is used to give the inner boundary condition,

$$\frac{\delta\Sigma}{\delta t} = -\delta\dot{M}_2. \tag{4.16}$$

The results of the numerical simulations by Taam and Spruit suggest that the evolution of the CV system is affected significantly, by the interaction with the circumbinary disc, once the fractional mass input rate δ is greater than around 0.01, this value is found to be much smaller in subsequent work (see below). For δ less than this they find that systems evolve via the standard magnetic braking path, toward shorter orbital periods, with elevated mass transfer rates. If δ is above around 0.015 systems have high mass transfer rates $\sim 10^{-7}M_{\odot}yr^{-1}$, similar to that for supersoft sources, and systems with main sequence

secondaries evolve to longer periods. The variation of the magnitude of the viscosity, via an α parameter (see Shakura and Sunyaev (1973)), was found to have a smaller influence on the evolution than variation of δ. A change of δ by a factor of 3 was approximately the same as a change of 10 in α. Thus the evolution is more sensitive to a change in the mass input rate to the disc than the viscosity of the disc.

Systems with material remaining from earlier stages of thermal timescale mass transfer could already have substantial circumbinary discs at the onset of mass transfer. This could lead to higher rates of mass transfer and in turn enhance winds from the disc and sustaining an elevated level of mass transfer. This could result in very high mass transfer rates $\sim 10^{-7} M_{\odot} yr^{-1}$ comparable to that for super soft sources, thus giving a mechanism to move from one class of CV to another.

The authors point to the period gap as a problem for some combinations of values of the free parameters. If the secondaries are sufficiently evolved then for $\delta \lesssim 0.01$ systems do not bounce above the period gap but evolve into it from the upper edge, consistent with Baraffe and Kolb (2000). For the short period systems if $\delta \gtrsim 0.015$ then systems will evolve to longer periods into the period gap from the lower edge.

In addition to the problems the authors point out, i.e. if all systems above the gap bounce at or before the upper edge of the gap then this subdivides CVs into two distinct populations. These being systems forming above the gap with initial $M_2 > 0.3 M_{\odot}$ and systems forming within and below the gap with initial $M_2 < 0.3 M_{\odot}$. If systems form with equal probability at all periods then assuming sufficient evolutionary time since the systems came into contact the observed distribution of systems below the upper edge of the gap would be expected to be one of the following depending upon the disc characteristics:

- for systems which generaly evolve to shorter periods the distribution should exhibit an increasing number of systems with decreasing period for $1.3 \lesssim P \lesssim 2.6$ hours.

- for systems which undergo an evolution which is fairly static in period a fairly flat distribution of systems over the whole period range including the period gap would be expected.

- for systems which generaly evolve to longer periods the distribution should exhibit an increasing number of systems with increasing period for $1.3 \lesssim P \lesssim 2.6$ hours, this would also lead to the expectation of large numbers of CVs within the period gap.

I thus see problems with resolving the lower edge of the period gap if systems above the gap bounce before or at the upper edge of the gap.

4.2.3 The structure and evolution of circumbinary discs in CV systems

In this paper by Dubus, Taam, and Spruit (2002) the one zone model (with the disc parameters being determined by radial distance from the binary alone) used in Spruit and Taam (2001) and Taam and Spruit (2001) is replaced by a more detailed model of the vertical structure of the circumbinary disc in which convection and departures from the local thermal equilibrium are taken into account. The optically thin regions above the disc photosphere were also taken into account and treated in the grey approximation. The opacities for the disc are once again taken from Bell and Lin (1994) with the contribution from iron-poor opacities for $T \lesssim 1500$ K where dust particles exist from Henning and Stognienko (1996). Both the inner and outer radii of the disc are allowed to vary with time, the inner edge once again being at $1.7a$, with the mass fed into the disc at its inner edge and assumed to have the specific angular momentum of the inner edge of the disc as before. The disc structure is solved in a fully implicit model on an adaptive grid (see Hameury et al. (1998)).

The main aim of the paper is to look into the evolution of the disc and not the binary system within the disc, they thus use a simplified model for the binary system. The angular momentum loss from magnetic braking is simplified and assumed to take place on a fixed timescale, while the expression used to calculate the angular momentum loss due to the disc is the same as in previous papers (see Spruit and Taam (2001), Taam and Spruit (2001)). They run the model for both non-evolving binary systems, where the angular momentum loss from the binary system is ignored and the inner radius and the mass input rate of the circumbinary disc are fixed, and evolving binary systems. For the non-evolving systems they find the results to be roughly similar to the results of Spruit

and Taam (2001).

In the models with evolving binary systems, for $\delta = 0.005$, $\alpha = 0.001$ and a magnetic braking timescale of $t_W = 2 \times 10^8$yr, they find that the circumbinary disc initially evolves as for the non-evolving binary systems. As the mass in the disc builds up, the torque from the circumbinary disc begins to dominate over the standard systemic angular momentum losses. This then leads to a runaway and the mass input rate to the disc climbs to over $10^{-9} M_\odot yr^{-1}$ (for a mass input fraction of $\delta = 0.005$ this requires a mass transfer rate of around 2×10^{-7}) causing the orbital period to increase and the complete disruption of the secondary on a short time scale. The variation of the parameters alters the timescale on which the circumbinary disc dominates. For small α and δ the timescale becomes so long as to have little influence on the evolution of the binary system, but for higher values of these parameters the timescale becomes short, $\lesssim 10^6$yr. They find that a variation of t_W has little influence on the evolution.

The column densities and temperatures of the circumbinary discs are found to be similar to those of circumstellar discs around young stars with Σ_i up to around $4 \times 10^4 gcm^{-1}$ giving temperatures at the inner edge of the disc in excess of 10^4K.

4.2.4 Cataclysmic variable evolution with circumbinary discs

In this paper (Taam, Sandquist, and Dubus (2003)) present the results of a systematic investigation into the evolution of cataclysmic variables with circumbinary discs, in which 200 models are used to cover $0.15 \leq M_2 \leq 1.2 M_\odot$, $0.3 \leq M_1 \leq 1.4 M_\odot$, $0.00001 \leq \delta \leq 0.001$ and $10^6 \leq J/\dot{J}_{MB} \leq 10^{10} yr$. Both the evolution of the binary, via a numerical model, and the circumbinary disc, from a simplified version of that used in Dubus et al. (2002), are taken into account in the models. The results once again show that fractional mass input rates into the circumbinary disc of $\delta \sim 10^{-4}$ are sufficient to promote significantly increased mass transfer rates, and that the mass transfer rate is more sensitive to a change in δ than a change in the magnetic braking time-scale $\tau_J = J/\dot{J}_{MB}$. Once again two populations of CV are discussed, those above the period gap requiring a higher mass fractional input rate into the disc for them to bounce at periods greater than the upper edge of the gap,

and those below the gap requiring a lower value to prevent them evolving into the gap from the lower edge.

Taam, Sandquist and Dubus find that a value of $\delta > 2\times10^{-4}$ is required to prevent long period systems with unevolved secondaries evolving into the gap, evolved donors require larger values still ($\delta > 10^{-3}$). For systems below the gap for $\delta \gtrsim 10^{-4}$ the authors find that the donor may be totally transferred within a Hubble time leaving lone white dwarfs. The effect of systems bouncing at a range of periods is once again quoted as a possible reason for the missing period spike at the observed minimum period.

Chapter 5

Modelling circumbinary discs and the CV minimum period

In this chapter I discuss the development of my model for a circumbinary disc along with some preliminary results (see sections 5.2 and 5.3). In section 5.4 I discuss a possible improvement to the disc model along with my first attempts at this and some of the problems associated with this new model. In section 5.5 I discuss the effects that circumbinary discs have on the expected period distribution and what restrictions the observed period distribution of CVs places on the disc parameters and systemic angular momentum loss mechanisms. This leads into section 5.6 where I discuss the reduced form of magnetic braking proposed by Andronov, Pinsonneault, and Sills (2003) and how this relates to the restrictions imposed by the observed population if circumbinary discs are to be accepted as the norm.

5.1 A numerical model for the diffusion equation

In this section I give an outline of the numerical method used to solve the standard diffusion equation (see equation 4.7) used in my disc model. The model used was a one dimensional approximation, that is the disc is assumed to be axi-symmetric and the thickness of the disc is ignored, hence the disc is considered to only vary in the radial direction. The radius was split into N zones of equal width, in the chosen coordinate system, and the initial

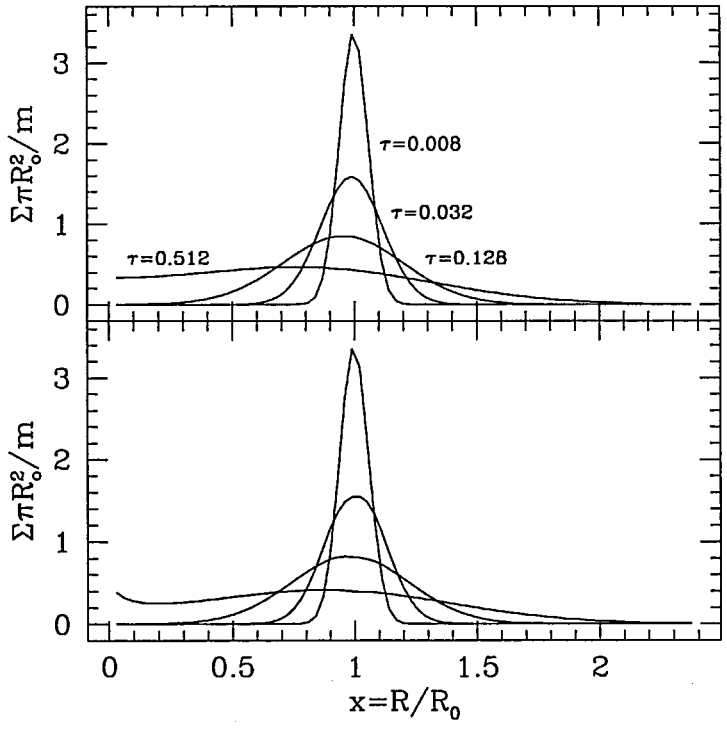

Figure 5.1: The evolution of a ring of matter of mass m at the initial radius R_0 according to the diffusion equation 4.7. Upper frame:- the analytical solution. Lower frame:- The numerical solution. The surface density function is shown as a function of the dimensionless radius $x = R/R_0$.

conditions for that of an empty disc applied.

The method chosen to solve the non-linear diffusion equation (4.7) is the Crank-Nicolson method. This is an implicit method in which the known conditions in the disc at time t are used to solve for the new conditions at time $t + \delta t$ via a series of simultaneous equations which are solved via Gauss's elimination method. The boundary conditions determine how material is gained and lost by the disc at its inner and outer edges.

5.2 Test of the numerical solution to the diffusion equation

In this section I describe the testing of my numerical solution for the disc model by using a comparison with that for the analytic solution for the standard accretion disc model in which the viscosity varies as a function of radius only. The upper frame in figure 5.1 shows the analytical solution to the diffusion equation (see Pringle (1981) and Frank, King, and Raine (2002)), the dimensionless time parameter τ is given as $12\nu t/R_0^2$ where R_0 is the initial radius of the ring of mass. The lower frame shows the application of the numerical model to the same system. The test run used as the initial condition the analytic solution for $\tau = 0.008$ shown in the upper frame of figure 5.1. The disc was then evolved using the diffusion equation (equation 4.7) with the spatial coordinate as from Taam and Spruit (2001) $x = r^{1/2}$. The viscosity is assumed to be constant both in time and spatial coordinates. This gives the diffusion equation as

$$\partial_t Y = \frac{3\nu}{4x^2}\partial_{xx} Y, \tag{5.1}$$

where

$$Y = x\nu\Sigma. \tag{5.2}$$

The inner boundary condition is set so that mass cannot flow through this point and hence builds up[1]. The outer boundary the condition is set so that mass flows away from this point and is lost to the system, these are given as

$$\left.\frac{\partial Y}{\partial x}\right|_{x=r_{inner}^{1/2}} = 0, \tag{5.3}$$

and

$$\left.\frac{\partial Y}{\partial x}\right|_{x=r_{outer}^{1/2}} = -Y, \tag{5.4}$$

respectively. The results of the numerical method are shown in lower frame of figure 5.1 and are plotted for the times corresponding to the values of τ in the upper frame. The numerical solution can be seen to reproduce the analytical solution reasonably well,

[1]It should be noted that the 1D approximation used in this model is quite sensitive to the form of the inner boundary condition, that is small changes in the boundary condition can lead to large changes in the disc structure

though does start to deviate slightly once the inner boundary at $x = 0$ is reached by the spreading material. Thus the numerical solution appears valid.

5.3 Numerical experiments

I developed the circumbinary disc model along the lines followed in Spruit and Taam (2001) and Taam and Spruit (2001), with the exception that the binary system was allowed to evolve and lose mass. The first circumbinary disc model I tried used a fixed grid with the inner edge set at the distance $R_i = 1.7a_i$ where a_i is the initial separation at the start of mass transfer. I use the angular momentum loss rate from Spruit and Taam (2001) as in equation 4.8 repeated below,

$$\dot{J} = 3\pi \left(\frac{r_i}{a}\right)^{\frac{1}{2}} \omega_0 a^2 \nu_i \Sigma_i,$$

where ω_0 is the orbital frequency of the binary. The inner boundary condition was set as

$$\frac{\partial Y_i}{\partial x} = -\delta \dot{M}_2, \tag{5.5}$$

where δ is defined as above (see section 4.2.1). This causes mass to only flow out through the disc from the input of angular momentum due to the tidal interaction with the binary. The outer boundary condition was set as

$$\frac{\partial Y_o}{\partial x} = -Y_o. \tag{5.6}$$

This sets the rate of change of mass at the outer edge of the disc to the total mass in the outer most bin, thus all mass arriving at the outer edge of the disc is lost to the system. The grid consisted of 19000 points and extended to around $360a$ from the binary system. This gives a disc which extends to around 2AU from the binary, sufficiently large for the low mass fluxes of around $5 \times 10^{-13} M_\odot yr^{-1}$ for $\delta \sim 0.01$ below the period gap[2]. If required the extent of the grid could be resized by a simple rescaling of the spatial coordinate, though this was not found to be necessary. Taam and Spruit (2001) used a

[2]see figure 2 of Dubus, Taam, and Spruit (2002) which shows that for the values of Σ in the regions discussed below the outer radius of the disc does not exceed 1AU from the binary

smaller number of grid points and increased the grid size as the disc reached the outer edge, keeping the number of grid points fixed. This results in some loss of accuracy at the inner regions of the disc. This first disc model was used to verify the stability of the numerical solution and give some preliminary indication of what influence the disc had on the evolution of the binary. Once this static disc model was giving consistent results the prescription for the inner edge of the disc was changed and allowed to evolve with the orbital separation of the binary, being held at $\sim 1.7a$ for all values of a. This was initially tried by having a moving grid, in which the inner edge of the disc was fixed at the first grid point and this grid point held at $1.7a$. The spatial coordinates of all the grid points along with the values of Σ at each grid point required recalculating as the inner edge of the grid evolved with the binary. This caused problems with the spatial coordinates and required interpolation for each point as the disc inner edge moved in and out relative to the binary system, this also increased the computational time.

The result was a grid which was fixed, with the inner point on the grid at the centre of mass of the system. The inner edge of the disc was allowed to evolve within this grid and kept at $\sim 1.7a$. The closest grid point to this [3] on the spacial coordinate system $x = R^{1/2}$ was set to be the inner boundary, the diffusion equation and boundary conditions were as previous. As the disc evolved within the grd the boundary conditioons at its inner edge were applied as follows: As the inner edge moved out the old inner edge grid point was assumed to be empty and the inner boundary condition applied to the new point. As the inner edge moved in the new grid point for the inner edge was assumed to have the same surface mass density as the old inner edge grid point and the inner boundary condition applied to the new point (this is reasonable as the inner edge of the disc should not have a sharp cut off). An alternative viscosity prescription was applied to the disc to try to improve the model, based on the viscosity prescription of Cannizzo and Reiff

[3] for systems below the gap the maximum deviation from the true inner radius is around $1.5 \times 10^8 cm$, which is approximately 0.2%. This maximum deviation occurs either just before the grid point changes in the case of an expanding inner radius or just after a grid point changes in the case of a contracting inner radius

(1992). Given as

$$\nu = \frac{2}{3}\frac{\alpha R_g T_{mid}}{\mu\omega^2}, \tag{5.7}$$

where α is the viscosity parameter, μ is the mean molecular weight, as the disc is assumed to be mainly atomic hydrogen, this was taken to be 1, R_g is the ideal gas constant, ω is the Keplerian angular velocity at the given point and T_{mid} is the mid-plane temperature at this point. The mid-plane temperature is given as

$$T_{mid} = \left(\frac{2^{a+5}}{9}\frac{\sigma}{\kappa_0}\right)^{-2/d}\left(\frac{\mu}{R}\right)^{(a-2)/d}\omega^{2(a+1)/d}\alpha^{2/d}\Sigma^{2(a+2)/d}. \tag{5.8}$$

(Cannizzo and Reiff (1992)) where $d = a - 2b + 6$, σ is Stephan's constant and κ_0, a and b are parameters in the assumed Kramers opacity law

$$\kappa = \kappa_0 \rho^a T^b, \tag{5.9}$$

where ρ is the density at the point in the disc. The appropriate values of a and b are dependent upon the temperature and density regimes and are obtained from various sources (see Cannizzo and Reiff (1992)). For my initial study of the disc I assume that for the low mass input rates below the CV period gap that the mid-plain temperature will be low $\lesssim 1200K$. In this region Cannizzo and Reiff (1992) use the opacities of Pollack, McKay, and Christofferson (1985), PMC in figure 5.2. The main features of the opacity in figure 5.2 are due to the varying absorbtion mechanisms. For temperatures $T \lesssim 10^3 K$ the absorbtion is mainly by molecular absorbtion, for $10^3 \lesssim T \lesssim 4 \times 10^3$ the absorbtion is mainly due to bound-bound transitions, for $4 \times 10^3 \lesssim T \lesssim 10^4$ the absorbtion is mainly due to bound-free transitions (ionization) and for temperatures above $T \simeq 10^4$ the absorbtion is increasingly due to free-free transitions. I adopt a simplified prescription for this region which gives a constant opacity $\kappa = 2.0 cm^2 g^{-1}$, hence $a = 0$, $b = 0$ and $\kappa_0 = 2.0 cm^2 g^{-1}$. Substituting into equation 5.8 I get

$$T_{mid} = \left(\frac{9}{2^4\sigma}\right)^{1/3} R^{1/3}\omega^{1/3}\alpha^{1/3}\Sigma^{2/3}. \tag{5.10}$$

Substituting for this in equation 5.7 I obtain

$$\nu = 0.55\alpha^{4/3}R^{4/3}\sigma^{-1/3}\omega^{-5/3}\Sigma^{2/3}. \tag{5.11}$$

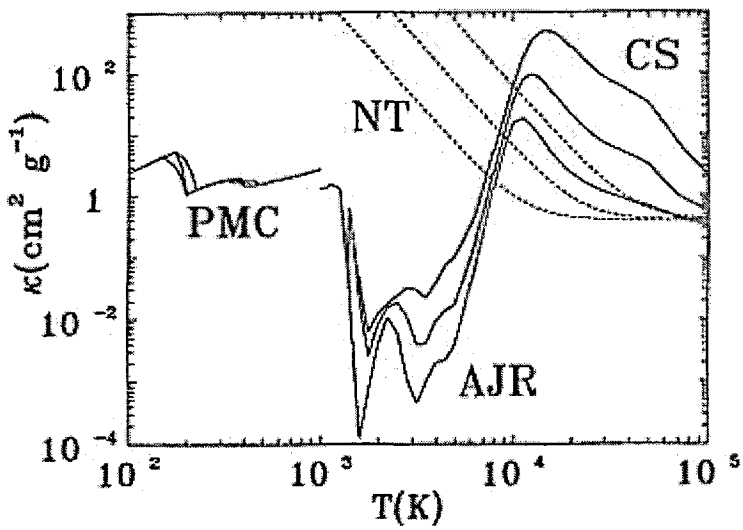

Figure 5.2: Opacity κ vs. temperature T(K) for three mid-plane densities of 10^{-9}, 10^{-8} and $10^{-7} g\ cm^3$ and are obtained from various sources and an analytical fit (NT) (for details see Cannizzo and Reiff (1992)).

With this description for the viscosity the binary system and circumbinary disc, with $M_1 = 0.6M_\odot$ and $M_2 = 0.2M_\odot$ (initially), was evolved for various values of α and δ. The results of this can be seen in figure 5.3 and table 5.1.

Figure 5.3 shows the mass transfer rate (left hand column) and associated surface mass density (right hand column) at the inner edge of the circumbinary disc. Most of the noise on the plots is numerical noise associated with the movement of the inner edge of the disc from one grid point to the next. For an increase in the viscosity parameter α from 0.0005 to 0.001 (top left - middle left frames) the mass transfer rate increases slightly, but the surface mass density at the inner edge of the disc decreases by a factor of around 1.3. (top right - middle right frames). If the mass input fraction to the disc is increased from 0.0005 to 0.001 (top left - bottom left frames) once again the mass transfer increases slightly but the surface mass density at the inner edge of the disc increases by around a factor of 1.4 (top right - bottom right frames). The relative change in mass transfer rate for a change in either δ or α appears to be dependent upon the initial values of the parameters. At

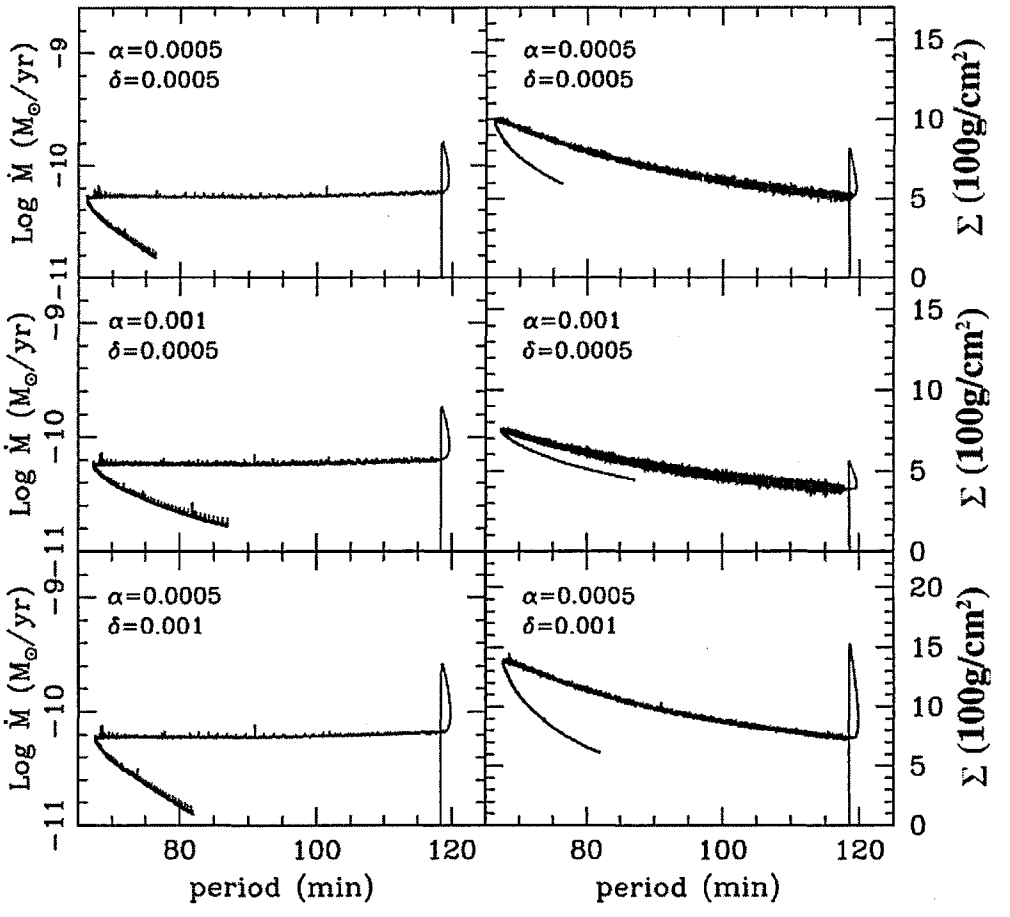

Figure 5.3: Evolutionary tracks for systems with various values of the viscosity parameter (α) and mass input fraction (δ). Left hand column shows orbital period in minutes against mass transfer rate in $Log(M_{\odot}/yr)$, Right hand column shows orbital period in minutes against the surface mass density at the inner edge of the circumbinary disc in $100g/cm^2$.

around 80 minutes a change in δ from 0.001 to 0.002, with $\alpha = 0.001$, gives a change in $\dot{M}$ around 2.4 times that for $\delta = 0.001$ and the change in α from 0.001 to 0.002, this is similar to that expected from Taam and Spruit (2001) of around 3. But for a change in the δ from 0.0005 to 0.001 with $\alpha = 0.0005$ gives only a 1.5 times greater increase in $\dot{M}$ than that due to the same change in α with $\delta = 0.0005$. It thus appears that there is not a one-one relation between either α and $\dot{M}$ or δ and $\dot{M}$, though the conclusion that the

evolution is more sensitive to a change in fractional mass input rate than to the viscosity still holds.

Table 5.1: Minimum period (in minutes) for different viscosity parameters (α) and mass input fractions (δ). N/A indicates systems which evolve to longer periods only.

	α			
δ	0.0005	0.001	0.002	0.005
0.0005	66.2	67.4	69.8	78.8
0.001	67.6	68.8	71.6	81.7
0.002	71.8	73.3	N/A	N/A

Table 5.1 shows the variation of the minimum period due to a change of the viscosity parameter α and the mass input fraction δ. As can be seen the observed minimum period of around 78 minutes is easily reproduced with quite small values $\delta \sim 0.0005$ and $\alpha \sim 0.005$. The entries (N/A) in the table correspond to systems in which there is no period bounce as the systems only evolve to longer periods. From table 5.1 the change in P_{min} can be seen to be more sensitive to a change in δ than α, as expected from the change in mass transfer rate due to these two parameters.

It was noted that if the angular momentum loss due to a circumbinary disc can be considered as a CAML there should be a one to one correspondence between the mass transfer rate and the product of the surface mass density Σ_i and viscosity ν_i at the inner edge of the disc. This can be seen from equation 2.16 where $\dot{M}_2 \propto \dot{J}_{CAML}/J$ and equation 4.8 where $\dot{J}/J \propto \Sigma_i \nu_i$. Figure 5.4

show the evolution of the product $\Sigma_i \nu_i$ at the inner edge of the circumbinary disc with mass transfer rate for various values of α and δ. It can be seen that, during the turn on of mass transfer, there is a non-linear relationship between $\Sigma_i \nu_i$ and $\dot{M}$. Once a steady

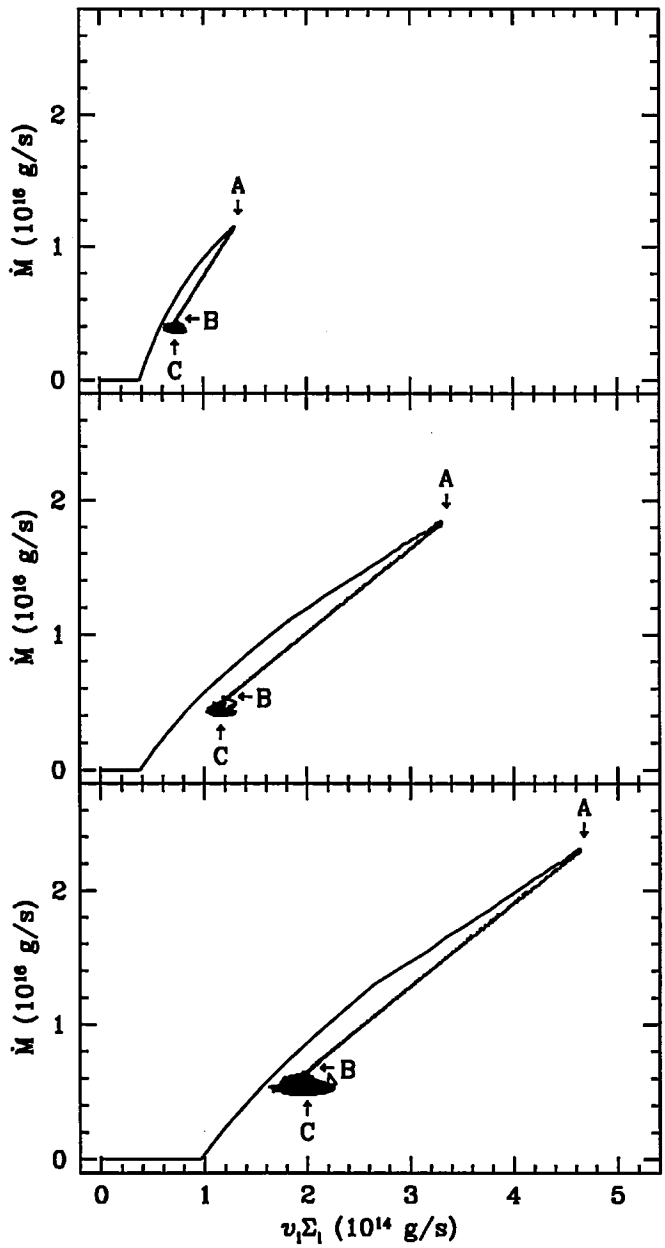

Figure 5.4: Mass transfer rate verses viscosity times surface mass density at the inner edge of the disc for: Top frame $\alpha = 0.001$ and $\delta = 0.0005$, Middle frame $\alpha = 0.001$ and $\delta = 0.001$, Bottom frame $\alpha = 0.002$ and $\delta = 0.001$.

state is reached there appears to be a linear relationship between $\Sigma_i \nu_i$ and $\dot{M}$ (the noise is once again due to the evolution of the inner edge of the disc). This linear relationship is

dependent upon both the disc parameters α and δ as can be seen from the change in slope between figures 5.4 (Top frame) and 5.4 (Middle frame) for a change in δ from 0.0005 to 0.001 and the change in position between figures 5.4 (Middle frame) and 5.4 (Bottom frame) for a change in α from 0.001 to 0.002.

Figure 5.5 shows the positions of points A, B and C in figure 5.4 relative to the turn

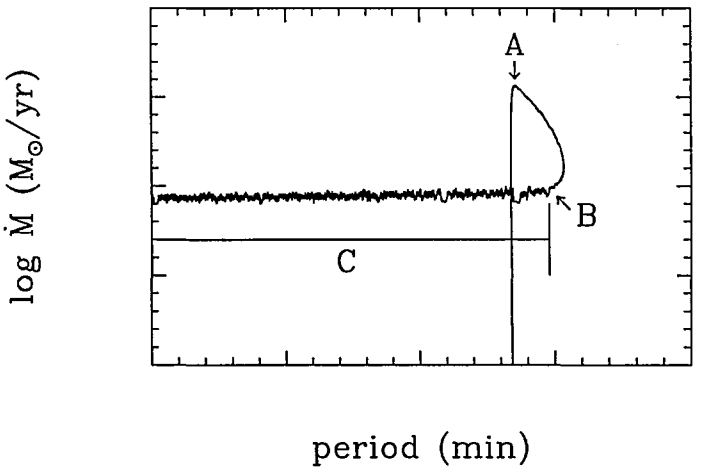

Figure 5.5: Diagram showing the positions of the points A, B and C in figure 5.4 relative to the turn on flag in the period / mass transfer plot.

on flag in the period / mass transfer plot. This shows the non-linear section between the turn on of mass transfer and point A is due to the filling of the disc where the change in ζ at the onset of mass transfer dominates the mass transfer rate which increases faster than the disc fills. Once the disc is full, and the mass transfer rate due to the changing $\zeta \rightarrow 1$ begins to fall, the linear relationship reveals itself between points A and B. This linear relationship holds in region C (see figure 5.6), with some numerical noise due to the movement of the inner edge of the disc, until the period bounce is reached at which point ζ undergoes further changes.

From the results of the numerical experiments and the assumption that the region

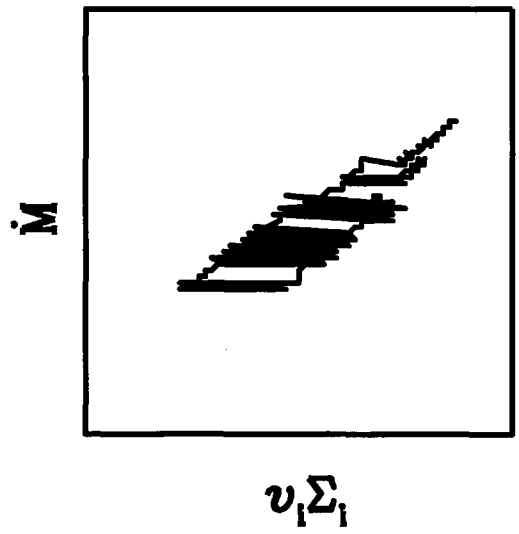

Figure 5.6: Close up of region C in figure 5.4 lower frame.

between A and B may be fitted with a linear approximation, for any given α and δ, the relationship of $\dot{M}$ to $\nu_i\Sigma_i$ was found for each model. The results of fitting each model with a linear equation were then combined to give the general equation for this linear region as,

$$\dot{M} \simeq \frac{2\pi\nu_i\Sigma_i - 4\times10^{17}\alpha - 1.6\times10^{14}}{100\delta} \quad M_\odot yr^{-1}. \tag{5.12}$$

There thus appears to be a one to one relationship between the mass transfer rate and mass flow rate $\Sigma_i\nu_i$ at the inner edge of the disc with the given opacity rule for a steady state system. This relation however fails if the fraction of the transferred mass δ exceeds around 0.002 or if α exceeds around 0.008 (assuming a value of 0.001 for the other parameter). With this a runaway system, in which the surface mass density at the inner edge of the disc increases, is rapidly produced. Obviously at this point the assumption that the opacity relation is constant fails ($T_{mid} > 1220K$) and a more realistic prescription is required. As this linear relationship also fails to pass through zero for $\Sigma_i\nu_i$ for $\dot{M} = 0$ the angular momentum loss mechanism cannot be considered as a CAML.

5.4 A possible improvement to the model

The first and most obvious improvement to the model is the prescription for the opacity. This requires extending it to cover the full range of mid-plane temperatures. A preliminary study of this, with an idealized version of the opacities shown in figure 5.2, was tried as shown in figure 5.7, in this the relation is assumed not to depend on the density i.e. $a = 0$, was applied to the model. This gives three regions with differing opacity relations,

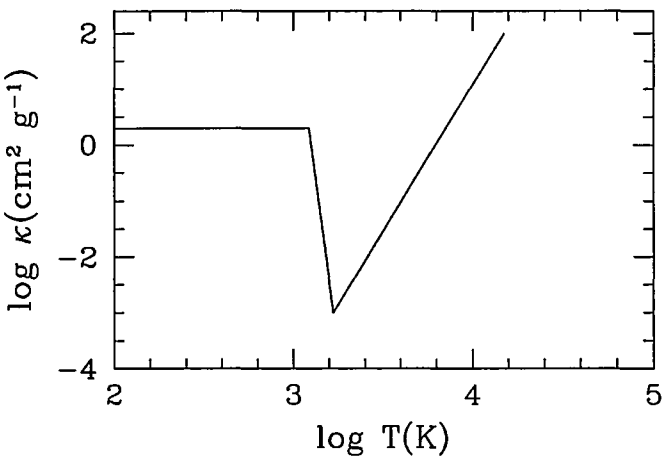

Figure 5.7: Idealized fit to the temperature/opacity relation shown in figure 5.2.

for $T \leq 1220$K the opacity is the same as previously with $\kappa_o = 2cm^2g^{-1}$, $b = 0$, for 1220K$< T_{mid} \leq$ 1675K $\kappa_o = 3.112 \times 10^{74}cm^2g^{-1}$, $b = -24.039$ and for 1675K$< T_{mid}$ $\kappa_o = 1.185 \times 10^{-20}cm^2g^{-1}$, $b = 5.25$. The model initially appeared to work well following the previous model, as expected, for the low surface mass density ($T_{mid} <$ 1220K) regions, however problems arose at the point where the opacity prescription changed at a mid-plane temperature of 1220K. The model exhibited a limit cycle behaviour as the opacity flipped between one region and the other, this in turn causes the surface mass density at the inner edge of the disc to oscillate between high and low values. One possible solution would be to reduce the time steps for the disc model, but this was calculated from the changes in

surface mass density to require around 20000 iterations of the disc for each time step of the stellar code around this region, this is far to time consuming. Thus a solution which blends the two regions via a smooth function is required (unfortunately this is beyond the scope of this thesis), the same will also be required at the change in opacity relation at 1675K.

5.5 The effects of circumbinary discs on the expected population

Any additional form of angular momentum loss mechanism will have an effect on the overall observed distribution of CVs. Thus, if the material in circumbinary discs comes as a by-product of mass transfer, systems would be expected to start forming such discs at the onset of mass transfer. This would have a large influence on the numbers of CVs we would expect to see at any given period at the current epoch. Work in progress by Willems, Kolb, Sandquist, Taam, and Dubus (2003) looks into whether the period gap can be explained by the inclusion of circumbinary discs, without having to appeal to disrupted magnetic braking. Using the output of a population synthesis model (BiSEPs see Willems and Kolb (2002)), with a common-envelope efficiency of 1.0 and a binding-energy parameter of 0.5, a zero age distribution of CVs was produced using the initial mass function of Willems and Kolb (2002). This zero age population was then subject to evolution with various circumbinary disc mass input rates δ and magnetic braking rates.

The upper frame in figure 5.8 shows the observed distribution of CVs binned in 15 minute bins for comparison with the generated models. Of the generated models the one shown in lower frame of figure 5.8 shows the greatest similarity to the observed distribution, the distributions are normalized to each other for comparison. In this case the mass transfer is assumed to be nonconservative, that is the mass of the white dwarf primary is fixed, the magnetic braking is assumed to have a characteristic time scale of 10 Gyr, and the fractional mass input rates into the CB disc are $\delta = 0.0003$ for a donor mass of greater than $0.35M_{\odot}$ and $\delta = 0.00001$ for a donor mass less than $0.35\mathrm{M}_{\odot}$. The differing mass input fraction above and below $M_2 = 0.35M_{\odot}$ is used to prevent systems evolving

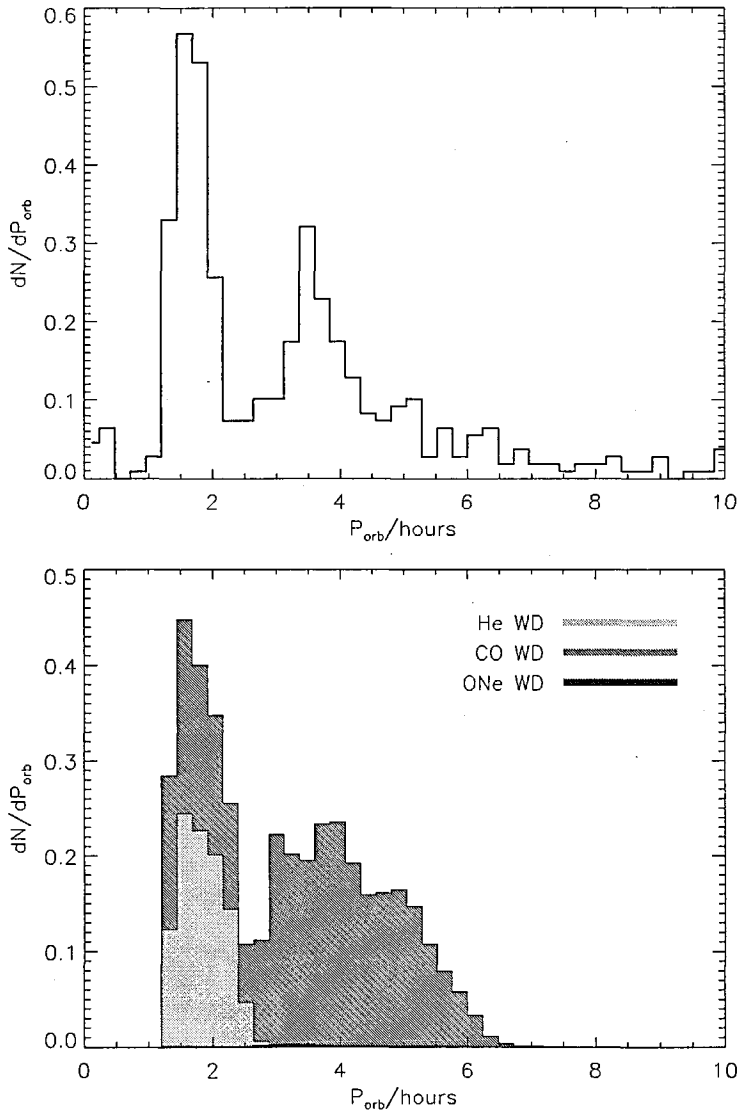

Figure 5.8: Upper frame: the observed distribution of CVs. Lower frame: the simulated distribution of CVs. from Willems, Kolb, Sandquist, Taam, and Dubus (2003).

into the gap from shorter periods.

5.6 Alternative magnetic braking prescription

Work by Willems, Kolb, Sandquist, Taam, and Dubus (2003) shows that the effects of circumbinary discs can be used to replace the standard prescription for disrupted magnetic

braking and reasonably reproduce the period gap in the distribution of CVs, though an alternative form of reduced magnetic braking is thus required. One possible alternative has been proposed by Andronov, Pinsonneault, and Sills (2003) in which the angular momentum loss rates used so far for CVs are shown to be inconsistent with the results as measured from open cluster data. Above the period gap the angular momentum loss rate due to 'standard' magnetic braking and gravitational radiation is around 2 orders of magnitude greater than that which Andronov et al. deduce from their observations. The observed data is also suggestive that there is little or no change in the angular momentum loss rate at the point where the star becomes fully convective. This reduced angular momentum loss rate on its own would increase the evolutionary timescale for CVs such that it would be comparable to the Hubble time, hence systems may not yet have had sufficient time to reach the true minimum period (see section 2.4.3 on the age limit hypothesis).

The angular momentum loss prescription Andronov, Pinsonnealt and Sills used is the same as that of Sills, Pinsonneault, and Terndrup (2000) given by

$$\left(\frac{dJ}{dt}\right)_{wind} = -K_W\sqrt{\frac{r}{m}}\begin{cases}\omega^3 & \text{for } \omega \leq \omega_{crit}\\ \omega\omega_{crit}^2 & \text{for } \omega > \omega_{crit}\end{cases} \tag{5.13}$$

where ω_{crit} is the critical angular frequency at which the angular momentum loss rate saturates and $K_W = 2.7 \times 10^{47}\ g\ cm\ s$ is a calibration constant to reproduce the solar rotation rate for the age of the sun. The value of ω_{crit} is taken to be inversely proportional to the convective overturn timescale in the star τ (see e.g. Kim and Demarque (1996)),

$$\omega_{crit} = \omega_{crit\odot}\frac{\tau_\odot}{\tau}, \tag{5.14}$$

where $\omega_{crit\odot}$ is taken to be 10 $\omega_\odot$ and the convective overturn timescales for masses $M \geq 0.5M_\odot$ were linearly interpolated from the results of Kim and Demarque (1996) and linearly extrapolated from this for masses $M < 0.5M_\odot$. The resulting angular momentum loss rate for differing, zero age main sequence, secondary masses (the primary is fixed at $0.62\mathrm{M}_\odot$) is shown in figure 5.9

In this figure the SPT model includes both gravitational radiation and the new prescription for magnetic braking. The angular momentum loss rate suggested by Rappaport

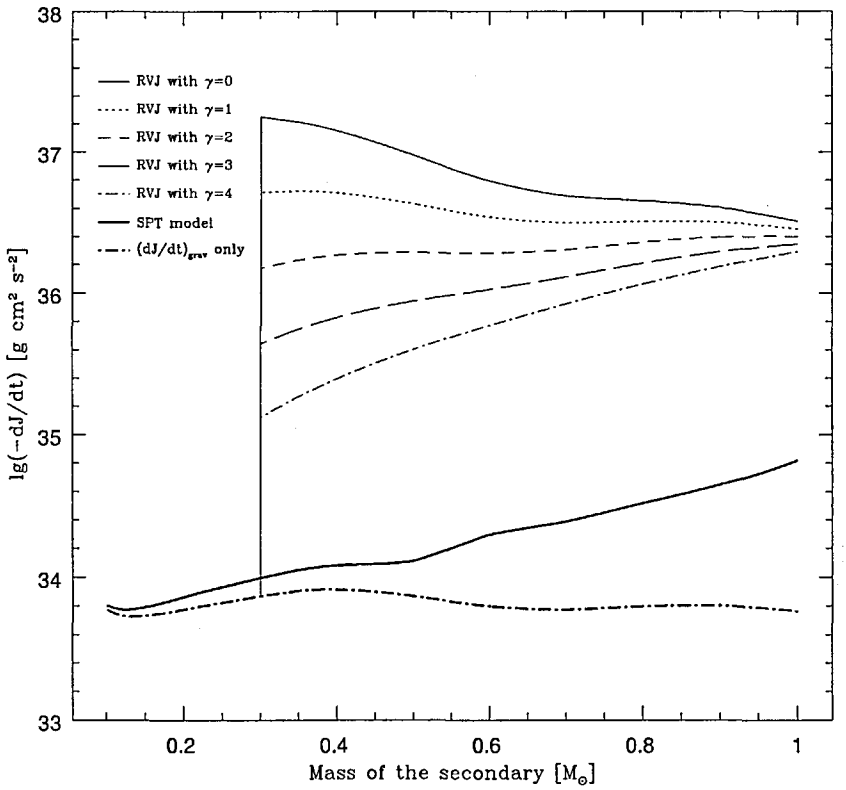

Figure 5.9: Angular momentum loss rates for a CV with a $0.62M_{\odot}$ white dwarf primary. The lines RVJ represent the Rappaport et al. (1983) disrupted magnetic braking model; the heavy solid line is the Sills et al. (2000) prescription and the heavy dot dashed line is for gravitational radiation alone.

et al. (1983) is

$$\left(\frac{dJ}{dt}\right)_{mb} \approx -3.8 \times 10^{-30} m_2 R_{\odot}^4 \left(\frac{r_2}{R_{\odot}}\right)^{\gamma} \omega^3 \text{ dyn cm}, \tag{5.15}$$

where all units are in cgs. If this is compared with the angular momentum loss rate for gravitational radiation alone (see figure 5.10) it can be seen that the effect of the magnetic braking is vastly reduced.

The prescription by Andronov et al. (2003) falls roughly into the region between angular momentum loss timescales of 10 Gyr and 100 Gyr (the latter being equivalent to virtually

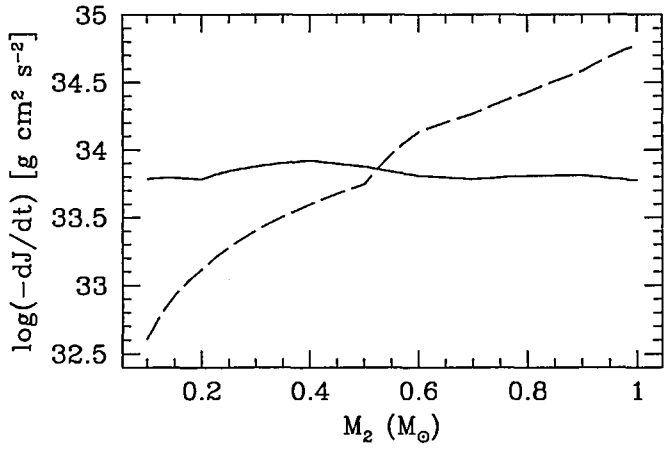

Figure 5.10: Angular momentum loss rates for a system with a $0.62M_{\odot}$ primary. Solid line: gravitational radiation alone, dashed line: reduced magnetic braking from Sills, Pinsonneault, and Terndrup (2000).

no magnetic braking). In which, for low period systems, the effect of gravitational radiation is around an order of magnitude greater than that from the magnetic braking but for the longer period systems the magnetic braking exceeds that of gravitational radiation by around an order of magnitude (see figure 5.10).

5.7 Conclusions

The disc model used gives results that are fairly consistent with the work described in chapter 4, for an increase in δ from 0.001 to 0.002 $\dot{M}$ increases by around 2.4 times that for the corresponding change in α, but the increase in $\dot{M}$ for an increase in δ from 0.0005 to 0.001 gives around 1.5 times the corresponding change in α. This translates into an increase in P_{min}, around 6.5% for a change in δ from 0.001 to 0.002 compared with a change of around 4% for the same change in α, thus the relative strengths of each parameter appears to be dependent on the range in question. The observed minimum period is quite easily reproduced with reasonable values of $\delta \sim 0.0005$ and $\alpha \sim 0.005$

though the model requires some development for the higher density / temperature discs. Although there appears to be a linear relation between the mass transfer rate and the mass flow rate through the inner edge of the disc, I am unable to classify the effect of a circumbinary disc as that of a CAML as if the linear relation is extended it fails to pass through the origin (if $\dot{M} = 0$ it does not follow that $\Sigma_i \nu_i = 0$).

The work by Willems, Kolb, Sandquist, Taam, and Dubus (2003) presented in section 5.5 shows that the period gap can be reliably reproduced, without the need for the disrupted magnetic braking model, by the inclusion of a circumbinary disc model. The model requires a long characteristic timescale for magnetic braking of the order 10 Gyr, this is around 2 times the length of the characteristic timescale for gravitational radiation, for a system with the secondary in thermal equilibrium at the upper edge of the period gap ($P \sim 3$ hours) and around 10^3 times longer than that for the standard magnetic braking picture (see figure 5.9 with $\gamma = 1$). This agrees nicely with the timescale for magnetic braking prescription of Andronov, Pinsonneault, and Sills (2003) (see section 5.6) with a secondary mass of around $0.3 M_\odot$ in which the characteristic timescale for magnetic braking is around 3 times that for gravitational radiation (see figure 5.10). Thus it may be possible to reproduce the observed distribution of CVs by rejecting the disrupted magnetic braking model in favour of the reduced magnetic braking proposed by Andronov et al. (2003) along with the addition of a circumbinary disc model from Spruit and Taam (2001), though this would require circumbinary discs to form in the majority of systems and systems above the gap to be subject to a different value of mass input rate δ than those below the gap.

Chapter 6

Irradiation Driven Wind Loss

In this section I investigate the effects accretion driven irradiation of the secondary (see e.g. van Teeseling and King (1998), King and van Teeseling (1998)). In this, as mass from the secondary is accreted by the primary, gravitational energy is released in the form of an accretion luminosity. If the accretion is sufficient, a point can be reached at which thermonuclear burning may also start, adding to this luminosity. From this the secondary can be heated on the face that is toward the primary, this in turn can cause an additional wind to be driven from the secondary. This wind will add to the mass transfer rate as some will be swept up and accreted by the primary, leading to a feedback mechanism. If the accretion rate due to mass transfer through the L_1 point and the wind is sufficient, there may be steady state burning of hydrogen on the surface of the primary. The additional mass loss from the secondary will have evolutionary consequences, as the star will be further out of thermal equilibrium and the additional orbital angular momentum and mass loss due to the wind may dominate the binary evolution.

6.1 Wind driven evolution of accreting binaries

King and van Teeseling (1998) and van Teeseling and King (1998) present an estimate of the amount of mass loss from an irradiated secondary and relate this to supersoft binaries.

They include a detailed discussion of the 4.126hr supersoft binary 1E0035.4-7230 which should not have thermal-timescale mass transfer, under the standard evolution due to gravitational radiation and magnetic braking, and should not have steady-state burning (see section 1.1.5). Thus some mechanism must increase the mass transfer rate to that for which steady-state burning can occur.

Irradiation of the secondary by an X-ray source will form an extended corona and induce a strong stellar wind (Basko and Sunyaev (1973)). The soft nature of the X-rays in these systems is more effective at driving a wind as most of the energy is absorbed above the photosphere, unlike in hard X-rays, in which most of the energy is absorbed below the photosphere. (Basko and Sunyaev (1973)) show that the mass outflow then falls into two regimes: for low X-ray fluxes (low accretion rate) the mass outflow rate is directly proportional to the flux. For high X-ray fluxes (high accretion rate) the outflow rate will be proportional to the square root of the flux.

The wind loss rate from the secondary due to the accretion luminosity is thus given by

$$\dot{M}_{W2} \simeq -2.3 \times 10^{-3} \phi \frac{R_2}{a} (M_2 \eta_a \eta_s \dot{M}_{Acc})^{\frac{1}{2}} \qquad \frac{M_\odot}{yr}, \tag{6.1}$$

where ($\phi < 1$) is an efficiency factor for the fraction of the secondaries face (face being defined by van Teeseling and King (1998) as the hemisphere of the companion star facing the primary) that is irradiated and the fraction of the wind mass that escapes the system (see section 6.2.1). η_s is a measure of the efficiency of the primary's spectrum in producing ionizing photons (for X-ray radiation temperature of a few 10^5K this gives $\eta_s \simeq 1$, also van Teeseling and King (1998) point out that for irradiation temperatures less than 10^5K $\eta_s \simeq 1$). η_a measures the luminosity produced for each gram of matter accreted on to the primary, relative to the value for hydrogen nuclear shell burning (4.6×10^{18} erg g^{-1}, Iben (1982)), that is

$$\eta_a = \left(\frac{L_{Acc}}{4.6 \times 10^{18}} \right). \tag{6.2}$$

Once again M_2, R_2 and a are the mass of the secondary, the radius of the secondary and the orbital separation in solar units. $\dot{M}_{Acc}$ is the mass accretion rate of the primary in $M_\odot/yr$.

The mass loss rate of the secondary is

$$\dot{M}_2 = \dot{M}_{TR} + \dot{M}_{W2}, \tag{6.3}$$

where $\dot{M}_{TR}$ is the mass transfer rate through the L_1 point, while the rate of change of mass of the primary was set to be

$$\dot{M}_1 = -\dot{M}_{TR}, \tag{6.4}$$

i.e. any wind from the primary and any mass captured from the secondary wind is neglected. In this prescription the terms $\dot{M}_2$, $\dot{M}_{TR}$ and $\dot{M}_{W2}$ all have negative values (a loss) but $\dot{M}_1$ has a positive value (a gain).

In my model I include these additional effects with the inclusion of a CAML, and a fraction of the wind mass swept up by the primary, giving the rate of change of mass of the primary as

$$\dot{M}_1 = -\dot{M}_{TR} + \dot{M}_{W1} - \delta_{Acc}\dot{M}_{W2}, \tag{6.5}$$

where $\delta_{Acc}\dot{M}_{W2}$ is the fraction of the wind driven from the secondary that is swept up by the primary (see section 6.2.1). The same sign convenction applies as in the previous case except that $\dot{M}_1$ may have either sign, the additional term $\dot{M}_{W1}$ also has a negative value (a loss). King and van Teeseling (1998) perform a stability analysis and find that systems are stable if the wind mass loss rate increases more rapidly than the mass transfer rate with increasing mass transfer rate. King and van Teeseling (1998) assume that there is a critical accretion rate, given by

$$\dot{M}_{CR} = 6.3 \times 10^{-8} 10^{-0.8 M_1} \quad M_{\odot} yr^{-1}. \tag{6.6}$$

For accretion rates below this the envelope of the primary expands to a large radius during a shell flash and possibly expels a large fraction of the accreted material (e.g. Fujimoto (1982)). Thus $\dot{M}_{CR}$ is roughly the minimum accretion rate for effective irradiation of the secondary during the hydrogen burning phase. Below this critical accretion rate η_a in equation 6.1 is given as the gravitational release alone as

$$Gm_1/4.6 \times 10^{18} r_1, \tag{6.7}$$

where r_1 and m_1 are the radius and mass of the primary which along with G are in cgs units. Above this critical value of the mass transfer rate

$$\eta_a = 1. \tag{6.8}$$

For 0.6 $M_\odot$ < M_1 < 1.2 $M_\odot$, a good approximation to the white dwarf mass-radius relation is

$$r_1 = 5.6 \times 10^8 M_1^{-1} \quad cm, \tag{6.9}$$

(Nauenberg (1972)). To replace the term R_2/a in equation 6.1, assuming that $R_2 \approx R_L$ then using the Paczyński (1971) approximation for the secondary's Roche lobe

$$R_L = 0.462 \left(\frac{M_2}{M}\right)^{1/3} a, \tag{6.10}$$

for $q \lesssim 1$ and the approximation

$$R_L = 0.462 M_1^{-0.12} M_2^{0.45} M^{-0.33} a, \tag{6.11}$$

(King and van Teeseling (1998)) for $q \gtrsim 1$. Assuming that the fraction of the wind accreted by the white dwarf δ_{Acc} adds to the accretion luminosity, the following expressions for the wind mass loss rate are obtained.

$$-\dot{M}_{W2} = 1.107 \times 10^{-3} M_2^{0.95} M_1^{-0.12} M^{-\frac{1}{3}} \eta_s^{\frac{1}{2}} \phi \dot{M}_{Acc}^{1/2} \quad , \quad \dot{M}_{Acc} > \dot{M}_{CR}, \tag{6.12}$$

$$-\dot{M}_{W2} = 2.53 \times 10^{-4} M_2^{0.95} M_1^{0.88} M^{-\frac{1}{3}} \eta_s^{\frac{1}{2}} \phi \dot{M}_{Acc}^{1/2} \quad , \quad \dot{M}_{Acc} < \dot{M}_{CR}, \tag{6.13}$$

for $q > 1.0$ and

$$-\dot{M}_{W2} = 1.107 \times 10^{-3} M_2^{\frac{5}{6}} M^{-\frac{1}{3}} \eta_s^{\frac{1}{2}} \phi \dot{M}_{Acc}^{1/2} \quad , \quad \dot{M}_{Acc} > \dot{M}_{CR}, \tag{6.14}$$

$$-\dot{M}_{W2} = 2.53 \times 10^{-4} M_2^{\frac{5}{6}} M_1 M^{-\frac{1}{3}} \eta_s^{\frac{1}{2}} \phi \dot{M}_{Acc}^{1/2} \quad , \quad \dot{M}_{Acc} < \dot{M}_{CR}, \tag{6.15}$$

for $q < 1.0$. Here $\dot{M}_{Acc}$ is the mass accretion rate of the white dwarf, which in their case is simply $(-\dot{M}_{TR})$. In the model to follow I add the fraction δ of the wind mass swept up by the primary to this (see section 6.2.1) giving $\dot{M}_{Acc} = -(\dot{M}_{TR} + \delta_{Acc}\dot{M}_{W2})$ all in $M_\odot yr^{-1}$.

6.2 Application to systems below the period gap

In this section I apply the irradiation heating of the secondary as discussed by King and van Teeseling (1998) to short period low mass systems below the period gap, to investigate the effect on the theoretical minimum period. In addition I take into account the effect of a CAML mechanism and of the wind from the secondary that is swept up by the primary. This additional accreted mass adds to the heating of the secondary. I first determine parameterizations for the fraction of the wind δ_{Acc} accreted by the primary and the efficiency factor ϕ.

6.2.1 Determination of δ_{Acc} and ϕ

The parameter δ_{Acc} is the fraction of the wind from the secondary that is accreted by the primary. I thus assume that the wind driven from the secondary is spherically symmetric and that only the material that directly intersects the Roche lobe of the primary, on a radial trajectory from the secondary (this is an idealized prescription as if the wind traveled on radial trajectories it would have a velocity too high to be accreted at this point), is accreted onto the primary (see figure 6.1). If all other mass in the wind is lost to the system I can parameterize δ_{Acc} in the following way.

I assume that the Roche lobe of the primary is spherically symmetric with the volume equivalent radius R_{LB} (shown dotted in figure 6.1). Then the area of the sector of the sphere with radius X centred on the secondary (shown dashed in figure 6.1), where X is the radial distance connecting the centre of the secondary to a tangent on the volume equivalent sphere of the primary's Roche lobe, is given by

$$A_{r_i} = 2\pi(X^2 - r_i X). \tag{6.16}$$

Where r_i is the distance from the centre of the secondary to the plane passing through the intercept of the two spheres (see figure 6.1 $i1$ to $i2$) and from simple trigonometry is given as

$$r_i = a - \frac{R_{LB}^2}{a}. \tag{6.17}$$

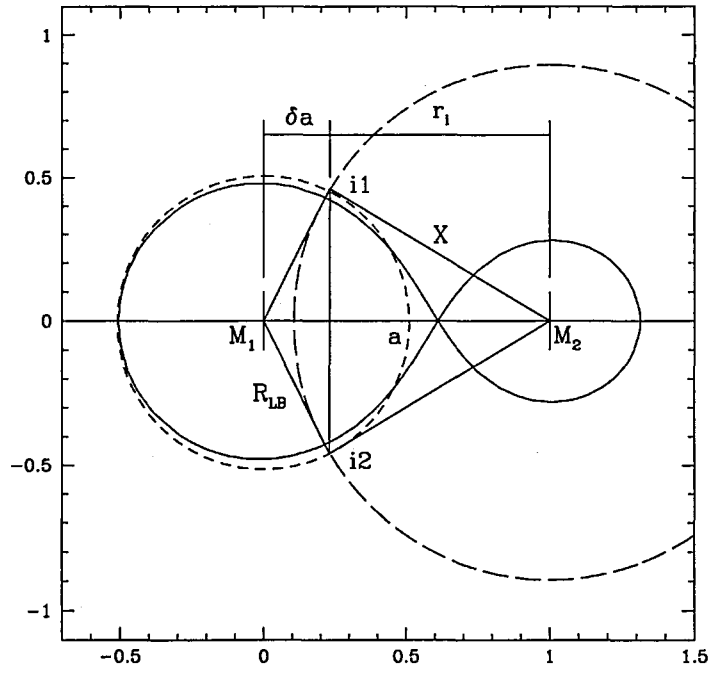

Figure 6.1: Figure defining the fraction of the spherically symmetric wind from the secondary accreted by the primary. R_{LB} is the volume equivalent radius of the primary's Roche lobe (dotted), X is the radius of intercept of the wind with the sphere of radius R_{LB} (dashed).

Along with this as from Pythagoras

$$X = (a^2 - R_{LB}^2)^{1/2}, \tag{6.18}$$

I obtain

$$A_{r_i} = 2\pi \left(a^2 - R_{LB}^2 - \left(a - \frac{R_{LB}^2}{a} \right) (a^2 - R_{LB}^2)^{\frac{1}{2}} \right) \tag{6.19}$$

Thus the fraction of the wind that is intersected by the volume equivalent Roche lode of the primary is simply the fraction

$$\delta_{Acc} = \frac{A_{r_i}}{A_{sc}} = \frac{1 - (a - \frac{R_{LB}^2}{a})(a^2 - R_{LB}^2)^{-\frac{1}{2}}}{2}, \tag{6.20}$$

where A_{SC} is the area of the sphere of radius X. Thus the rate of accretion due to the additional wind is $\delta_{Acc}\dot{M}_{W2}$.

If I assume that all the wind from the secondary is lost to it (none is reaccreted) the parameter ϕ can be taken as the fraction of the face of the secondary that is illuminated. I thus use a similar argument to the one used to find δ_{Acc}, to find the area of the face of the secondary that is illuminated by the primary. I Assume a point like primary, the radius of the secondary equals the Roche radius, and that the accretion disc is sufficiently thin as to not obscure the face of the secondary (see van Teeseling and King (1998), van Teeseling, Reinsch, Pakull, and Beuermann (1998)). Using figure 6.1 as a reference, with M_2 and M_1 reversed and R_{LB} replaced by the radius of the secondary R_2. Then the area of the illuminated face is

$$A_{IL} = 2\pi(R_2^2 - \delta a R_2), \tag{6.21}$$

as

$$\delta a = \frac{R_2^2}{a}, \tag{6.22}$$

the illuminated area is thus

$$A_{IL} = 2\pi R_2^2 \left(1 - \frac{R_2}{a}\right). \tag{6.23}$$

Thus the fraction of the face that is illuminated is given by

$$\delta_F = \frac{A_{IL}}{A_F} = \left(1 - \frac{R_2}{a}\right), \tag{6.24}$$

where A_F is the surface area of the face. Obviously the illuminated area of the face does not receive equal heating (points on the face closer to the primary receive more heating than those at further away), though for this investigation I assume that there is equal heating over the whole illuminated area.

6.2.2 Results of numerical experiments

A routine was added to the binary stellar evolution code in which the wind mass loss rate is determined at the start of each iteration of the binary routine. Equations 6.12-6.15 were used to determine the current wind loss rate, where the value of the mass accretion rate $\dot{M}_{Acc}$ was determined from the current mass transfer rate through the L_1 point ($\dot{M}_{TR}$) and the fraction δ of the wind loss rate from the previous iteration of the wind loss routine

($\dot{M}_{W2}|_{old}$) (see equation 6.25). Clearly for systems below the period gap the accretion rate is quite low $< 10^{-9} M_{\odot} yr^{-1} \ll \dot{M}_{CR}$ and the mass ratio q is generally less than 1 leaving equation 6.15 as the equation of interest in this model, though the routine includes all possibilities. The mass accretion rate on to the primary for this is given as

$$\dot{M}_{Acc} = \dot{M}_{TR} + \delta_{Acc} \dot{M}_{W2}|_{old} \tag{6.25}$$

If I assume that the fraction $(1 - \delta_{Acc})$ of the wind from the secondary not accreted by the primary is lost to the system and carries with it the specific angular momentum of the secondary.

$$j_2 = \frac{M_1 J}{M_2 M}. \tag{6.26}$$

This gives an angular momentum loss rate due to the wind of

$$\dot{J}_{W2} = \left(\frac{1}{2} + \frac{1}{2} \left(a - \frac{R_{LB}^2}{a} \right) (a^2 - R_{LB}^2)^{-\frac{1}{2}} \right) M_1^2 \left(\frac{Ga}{M^3} \right)^{\frac{1}{2}} \dot{M}_{W2}. \tag{6.27}$$

I varied the free parameter η_s, for the efficiency of the primary's spectrum in producing ionizing photons between 0.5 and 1, and the CAML efficiency between 0.0 and 0.6, the mass transfer is assumed to be nonconservative, ($\alpha = 1.0$, see section 2.2 for description of CAML). The value of η_s expected by van Teeseling and King (1998) is around 1 thus the lower value of 0.5 is used to set a lower limit on the influence on the system.

Table 6.1: Minimum period P_{min} in minutes for the values of η_s and η used in figures 6.2 and 6.3. If η_s and $\eta = 0.0$ this reproduces the effect of no wind and no CAML giving $P_{min} = 64.5$ minutes.

	η			
η_s	0.0	0.2	0.4	0.6
1.0	73.4	74.0	74.6	75.2
0.75	72.6	73.1	73.8	74.5
0.5	71.5	72.0	72.7	73.5

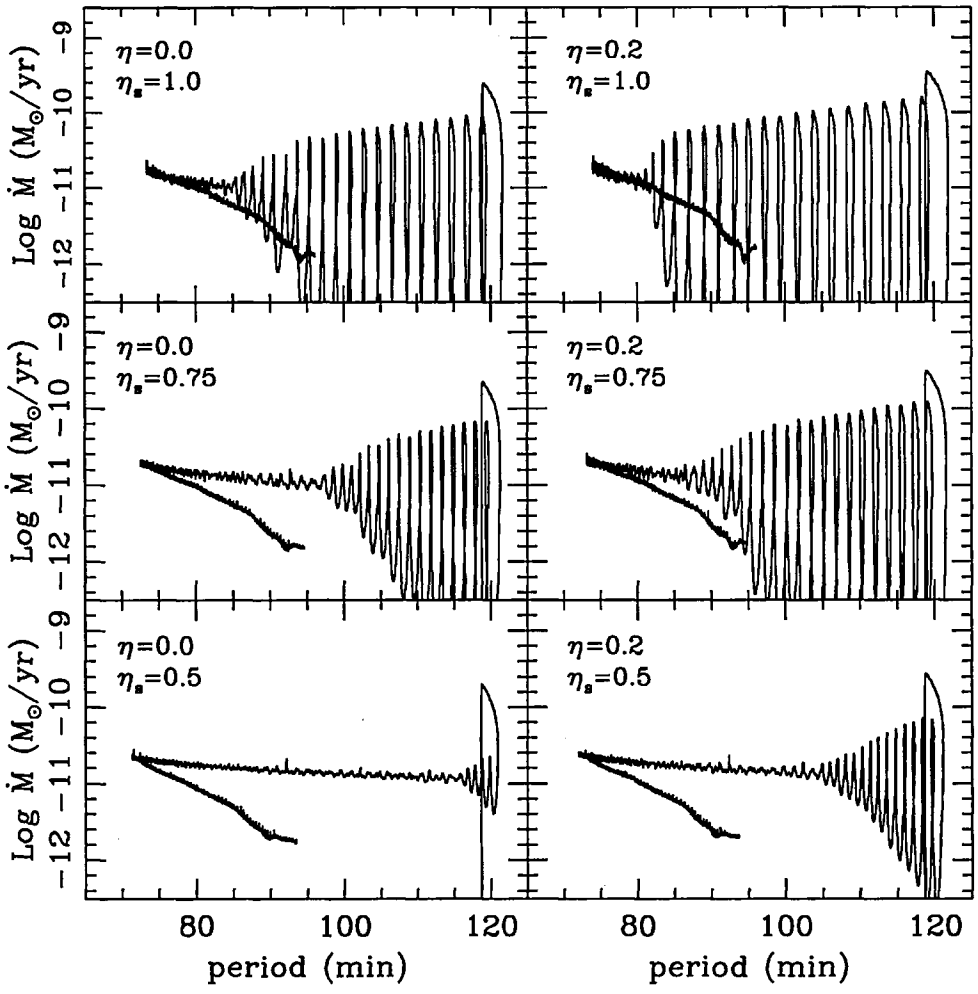

Figure 6.2: Mass transfer rate verses orbital period, for evolutionary sequences subject to irradiation-driven wind loss (for various $\eta_s = 0.5,\ 0.75,\ 1.0$, η_s measures the efficiency of the accretion at producing ionizing photons) and CAML efficiency. Left panels: CAML efficiency $\eta = 0$; Right panels: $\eta = 0.2$.

From figures 6.2 and 6.3 it can be seen that systems exhibit large oscillatory variations in the mass transfer rate for almost all of the parameter space covered. The models were run for various maximum time steps covering the range $10^3 \rightarrow 10^5$ Yrs to ensure that this was not a numerical effect, the results were the same in each case. It should also be noted that the mass transfer rate through the L_1, in the regions of stable mass transfer, is lower than for systems with no irradiation driven wind (see figure 2.5). The lower mass transfer

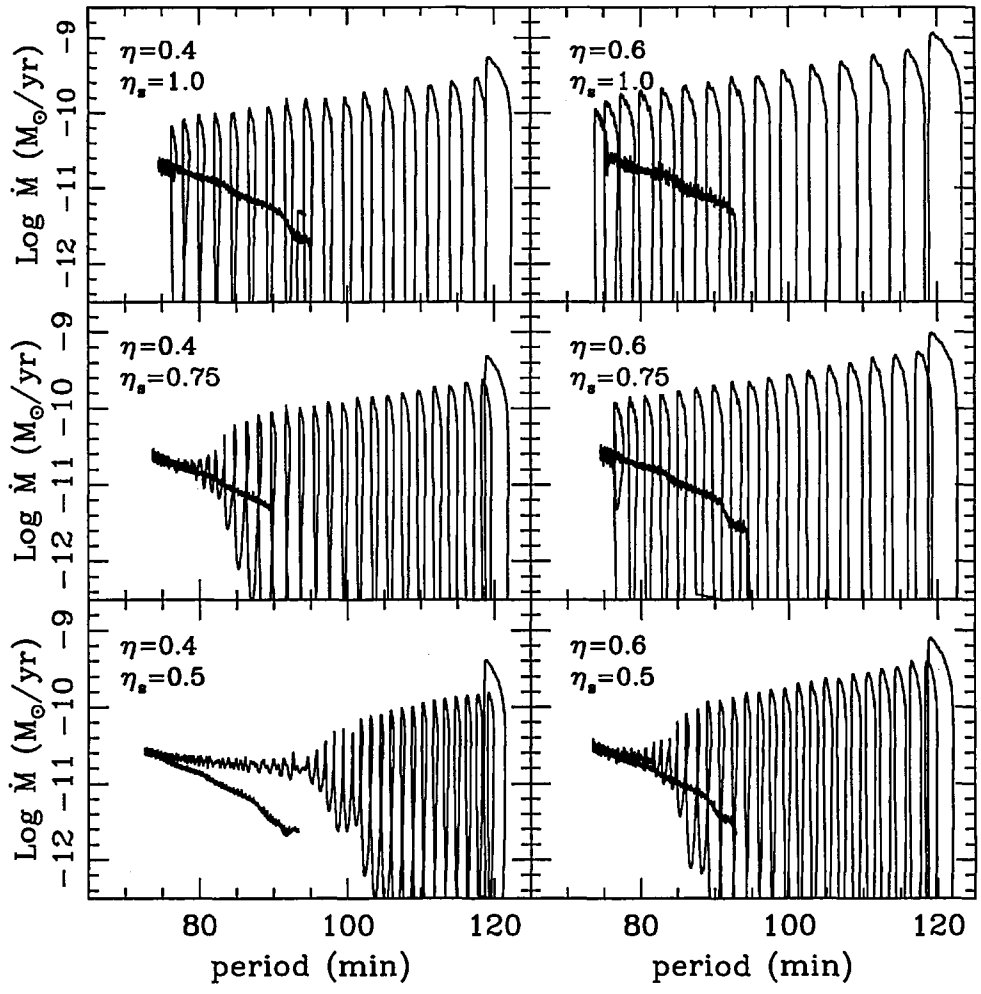

Figure 6.3: Mass transfer rate verses orbital period, for evolutionary sequences subject to irradiation-driven wind loss (for various $\eta_s = 0.5,\ 0.75,\ 1.0$, η_s measures the efficiency of the accretion at producing ionizing photons) and CAML efficiency. Left panels: CAML efficiency $\eta = 4$; Right panels: $\eta = 0.6$.

through the L_1 point is due to the bloating of the secondary as it is further out of thermal equilibrium due to the wind mass loss (see section 2.4.2). Thus the increase in CAML efficiency has a lesser effect on the minimum period for these systems as can be seen in table 6.1 if compared to table 2.1.

From figure 6.4 it can be seen that the wind mass loss rate exceeds the mass transfer rate through the L_1 point by a factor of around 4. The wind mass loss rate for systems

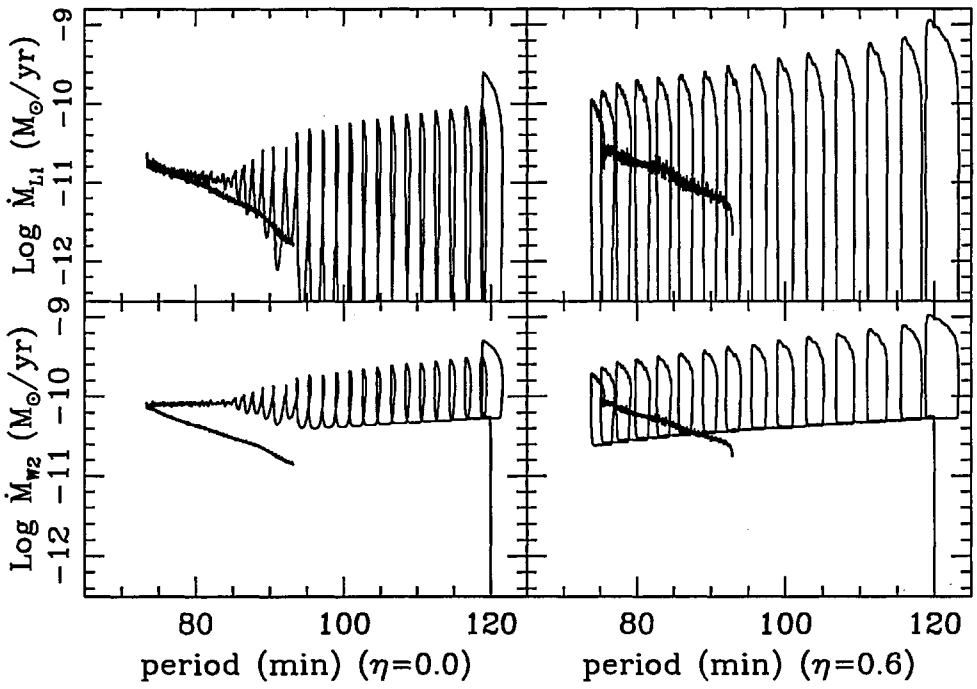

Figure 6.4: Mass transfer rates (top frames) and wind loss rates (bottom frames) for $\eta = 0.0$ and 0.6 and $\eta_s = 1.0$.

above the period bounce also appears to be 'self sustaining'. When the mass transfer rate drops by over 4 orders of magnitude the wind loss rate only falls by just around one order of magnitude, this being to a base value given as follows. If the system has a wind driven from the secondary, initially started by the accretion luminosity from material passing through the L_1 point. Then if the system detaches either by the secondary shrinking or the binary widening, then $\dot{M}_{Acc}$ reduces to $\delta_{Acc}\dot{M}_{W2}$. Using equation 6.15, for $\dot{M}_{Acc} < \dot{M}_{CR}$ and $q < 1$, I get (using the absolute values for $\dot{M}_{W2}$ and $\eta_s = 1.0$)

$$\dot{M}_{W2} = 2.53 \times 10^{-4} M_2^{5/6} M_1 M^{-1/3} \phi (\delta_{Acc} \dot{M}_{W2})^{1/2}. \tag{6.28}$$

Collecting terms this gives

$$\dot{M}_{W2} = 6.4 \times 10^{-8} M_2^{5/3} M_1^2 M^{-2/3} \phi^2 \delta_{Acc}, \tag{6.29}$$

as a minimum wind loss rate once a system has started mass transfer. This equation

converges to a wind loss rate for any given system parameters and therefore sets a lower limit on the mass loss rate of the secondary of $\dot{M}_{W2}$ and a lower limit on the accretion rate of δ_{Acc} times this.

As the fraction of the wind from the secondary accreted on to the primary δ_{Acc} will depend upon many factors. Is the wind mainly from the heated fraction of the secondary or is it isotropically emitted from the whole of the star? Is the wind a fast wind or a slow wind? If the wind is sufficiently fast very little will be accreted by the primary, if it is a slow wind an additional fraction may be swept up by the primary. If the wind is considered to be a fast wind I may take the extreme case in which none of the wind is accreted (see figure 6.5 (left frames) in which $\eta = 0.0$ and $\eta_s = 1.0$. It can be seen that the oscillations have greater magnitude and persist to shorter orbital periods compared with the same system with the original fraction of the intercepted wind being accreted (see figure 6.2).

If I now take the other extreme case in which the wind is is only emitted from the irradiated fraction of the star, and all the material intercepting the Roche lobe of the primary is accreted the fraction δ_{Acc} can be found by replacing A_{SC} in equation 6.20 by the area of the sphere of radius X about the secondary intercepted by the wind from the secondary given as

$$A_{rw} = 2\pi X^2 \delta_F, \tag{6.30}$$

giving

$$\delta_{Acc} = \frac{A_{ri}}{A_{rw}} = \frac{1 - (a - \frac{R_{LB}^2}{a})(a^2 - R_{LB}^2)^{-\frac{1}{2}}}{\delta_F}. \tag{6.31}$$

(see figure 6.5 (Right frames)). From this it can be seen that if the maximum wind is accreted by the primary the following events ensue. As the system comes into contact mass transfer through the L_1 point starts, and the heating of the secondary starts to drive the wind. As a large fraction of this wind is accreted ϕ is small, hence with $\eta = 0.0$ little of the orbital angular momentum carried in the wind is lost from the system. The secondary loses mass at a high rate but its orbit does not shrink rapidly enough and so it detaches from the L_1 point. By now the accretion from the wind is sufficient to dominate

the system and produce a self sustaining wind, preventing the system from coming back into contact.

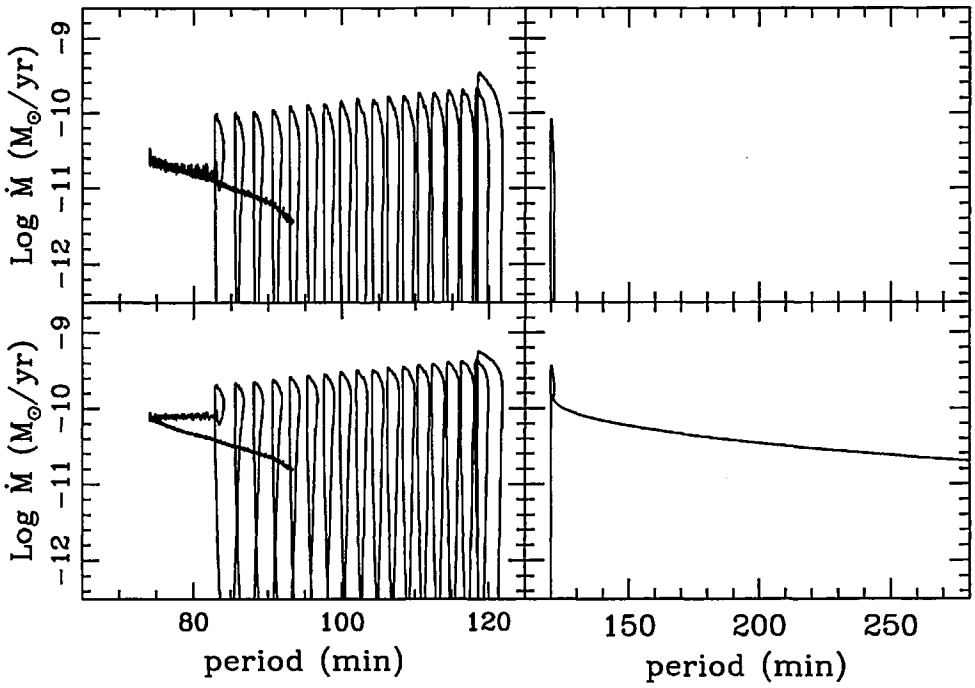

Figure 6.5: Mass transfer rates (top frames) and wind loss rates (bottom frames) for $\delta_{Acc} = 0.0$ (left) and that given by equation 6.31 (right)

6.2.3 Stability considerations

In this section I consider the stability of mass transfer in systems subject to irradiation driven wind loss from the secondary and CAML, in order to try to understand the mass transfer cycles as described in section 6.2.2. I follow the method of King and van Teeseling (1998) and the description for the CAML in section 2.2. The rate of orbital angular momentum loss with the additional wind loss is now the sum of three terms giving

$$\dot{J} = \dot{J}_{sys} + \dot{J}_{CAML} + \dot{J}_{W2}. \tag{6.32}$$

thus from equation 2.12 I obtain

$$\frac{\dot{J}_{sys}}{J}+\frac{\dot{J}_{CAML}}{J}+\frac{\dot{J}_{W2}}{J}=\frac{\dot{M}_1}{M_1}+\frac{\dot{M}_2}{M_2}+\frac{\dot{a}}{2a}-\frac{\dot{M}}{2M}, \tag{6.33}$$

which with the description of the CAML from equation 2.31 I have

$$\frac{\dot{J}_{CAML}}{J}=\frac{\eta b^2\omega\dot{M}_{Acc}}{J}+\frac{\alpha M_2\dot{M}_{Acc}}{M_1M}, \tag{6.34}$$

and from equation 6.27 for the angular momentum lost via the wind from the secondary I obtain

$$\frac{\dot{J}_{W2}}{J}=(1-\delta_{Acc})\frac{M_1\dot{M}_{W2}}{M_2M}. \tag{6.35}$$

Substituting equations 2.18, 6.35 and 6.34 into equation 6.33 and with some rearrangement I obtain

$$\begin{aligned}\frac{\dot{R}_L}{R_L}=2\frac{\dot{J}_{sys}}{J}+2\eta\left(\frac{b}{a}\right)^2\frac{\dot{M}_{Acc}M}{M_1M_2}+2\alpha\frac{M_{Acc}\dot{M}_2}{M_1M}+\\ +2(1-\delta_{Acc})\frac{M_1\dot{M}_{W2}}{M_2M}-2\frac{\dot{M}_1}{M_1}-\frac{5\dot{M}_2}{3M_2}+\frac{2\dot{M}}{3M}.\end{aligned} \tag{6.36}$$

The radius of the secondary R_2 evolves as

$$\frac{\dot{R}_2}{R_2}=\zeta\frac{\dot{M}_2}{M_2}=\zeta\frac{\dot{M}_{TR}}{M_2}+\zeta\frac{\dot{M}_{W2}}{M_2}, \tag{6.37}$$

where ζ is the effective mass-radius index and I neglect the nuclear evolution of the secondary (this is valid for the low mass secondaries below the period gap, $M_2<0.3M_\odot$). Once again for stationary mass transfer it is required that $\dot{R}_L=\dot{R}_2$. This is clearly not true for most of the parameter space covered in figures 6.2 and 6.3. I investigate the region for which the parameter space is stable by assuming stationarity, that is the mass transfer rate does not change. I assume that for systems below the period gap, $M_2<M_1$ and that $\dot{M}_{Acc}<\dot{M}_{CR}$ thus from equations 6.36 and 6.37 along with equation 6.15 I obtain

$$\frac{\dot{R}_2}{R_2}-\frac{\dot{R}_L}{R_L}=\frac{2}{M_2}\left(D\dot{M}_{TR}-B\dot{M}_{W2}-\frac{\dot{J}_{sys}M_2}{J}\right), \tag{6.38}$$

where

$$D=\left(\frac{\zeta}{2}+\frac{5}{6}\right)-\eta\left(\frac{b}{a}\right)^2(1+q)+\frac{2\alpha q}{3(1+q)}-q, \tag{6.39}$$

and

$$B = \left(-\frac{\zeta}{2} - \frac{5}{6}\right) + \frac{(1-\delta_{Acc})}{1+q} - \delta_{Acc}(\alpha-1)q + \\ +(1-\delta_{Acc})\frac{q}{3(1+q)} - \eta\left(\frac{b}{a}\right)^2 \delta_{Acc}(1+q) - \alpha\delta_{Acc}\frac{q^2}{1+q}. \quad (6.40)$$

This group of equations are a more general form of the stability equations from King and van Teeseling (1998) for $M_2 \lesssim M_1$ and by making the assumptions that, mass transfer is conservative ($\alpha = 0.0$), and consequently that there are no CAML losses ($\eta = 0.0$), along with the assumption that the wind losses are negligible these reduce to equations (13) and (14) of their paper. In my case the wind losses are non-negligible (being around 1-4 times the average mass transfer rate through the L_1 point, see figures 6.4 and 6.5). From equation 6.15 and using the magnitudes of the mass transfer rates I obtain,

$$\dot{M}_{W2} = \varepsilon(\dot{M}_{TR} + \delta_{Acc}\dot{M}_{W2})^{1/2}, \quad (6.41)$$

where

$$\varepsilon = 2.53 \times 10^{-4} M_2^{\frac{5}{6}} M_1 M^{-\frac{1}{3}} \eta_s^{\frac{1}{2}} \phi. \quad (6.42)$$

With some rearrangment this gives

$$\dot{M}_{W2}^2 - \varepsilon^2\delta_{Acc}\dot{M}_{W2} - \varepsilon^2\dot{M}_{TR} = 0. \quad (6.43)$$

Using the standard soultion for the quadratic equation in $\dot{M}_{W2}$ I obtain

$$\dot{M}_{W2} = \frac{\varepsilon^2\delta_{Acc} \pm \sqrt{\varepsilon^4\delta_{Acc}^2 + 4\varepsilon^2\dot{M}_{TR}}}{2}. \quad (6.44)$$

If I assume that $\dot{M}_{TR} = 0.0$ this gives the two possible solutions

$$\dot{M}_{W2} = 0, \quad (6.45)$$

or

$$\dot{M}_{W2} = \varepsilon^2\delta_{Acc}, \quad (6.46)$$

substituting back equation 6.46 for ε gives equation 6.29 as expected. If $\dot{M}_{TR} \neq 0.0$ then I may neglect the negative root in equation 6.44 as this would produce a negative wind loss, (a gain) clearly false. This leaves the solution

$$\dot{M}_{W2} = \frac{\varepsilon^2\delta_{Acc}}{2} + \frac{\varepsilon}{2}\left(\varepsilon^2\delta_{Acc}^2 + 4\dot{M}_{TR}\right)^{1/2} \quad (6.47)$$

I now follow the perturbation method used in King and van Teeseling (1998). Starting from equation 6.38 and using $F = \dot{M}_{TR}$ for the general case (relaxing the assumption of stationarity $\dot{R}_L \neq \dot{R}_2$) I have

$$\dot{F} = hF\left[DF - B\dot{M}_{W2} - \frac{\dot{J}_{sys}M_2}{J}\right], \tag{6.48}$$

where

$$h = \frac{2R_2}{HM_2}, \tag{6.49}$$

where H is the scaleheight near the inner Lagrangian point. Substituting equation 6.47 into equation 6.48 gives

$$\dot{F} = hF\left[DF - B\frac{\varepsilon}{2}\left(\varepsilon^2\delta_{Acc}^2 + 4F\right)^{1/2} - B\frac{\varepsilon^2\delta_{Acc}}{2} - \frac{\dot{J}_{sys}M_2}{J}\right], \tag{6.50}$$

This now leads to three possible cases for the term $(\lambda^2\delta_{Acc}^2 + 4F)$ as given below

$$\lambda^2\delta_{Acc}^2 \gg 4F \tag{6.51}$$

$$\lambda^2\delta_{Acc}^2 \simeq 4F \tag{6.52}$$

$$\lambda^2\delta_{Acc}^2 \ll 4F \tag{6.53}$$

I investigate the two extreme conditions.

1:- If $\lambda^2\delta_{Acc}^2 \gg 4F$ then equation 6.50 can be approximated by

$$\dot{F} = hF\left[DF - B\varepsilon^2\delta_{Acc} - \frac{\dot{J}_{sys}M_2}{J}\right]. \tag{6.54}$$

If $F = F_0$ is the stationary solution is given as

$$0 = hF_0\left[DF_0 - B\varepsilon^2\delta_{Acc} - \frac{\dot{J}_{sys}M_2}{J}\right], \tag{6.55}$$

then considering a small perturbation $F = F_0 + u$, $|u/F| \ll 1$ then equation 6.54 gives

$$\dot{u} = h(F_0 + u)\left[D(F_0 + u) - B\varepsilon^2\delta_{Acc} - \frac{\dot{J}_{sys}M_2}{J}\right], \tag{6.56}$$

which by expanding to first order in u reduces to

$$\dot{u} = huF_0D. \tag{6.57}$$

This requires that for stability $D < 0$. For the simple cases of $\alpha = 1.0$ (upper frames in figures 6.2 and 6.3) with the standard $\zeta = 1.0$ for the mass transfering system, from equation 6.39

$$D = \frac{4}{3} - \eta\left(\frac{b}{a}\right)(1+q) + \frac{2q}{3(1+q)} - q, \tag{6.58}$$

which is positive for all values of $0 \leq q \leq 1$ and $0 \leq \eta < 1$ hence unstable to mass transfer over the whole region covered.

2:- For $\lambda^2\delta_{Acc}^2 \ll 4F$ equation 6.50 can be approximated by

$$\dot{F} = hF\left[DF - B\varepsilon F^{1/2} - B\frac{\varepsilon^2\delta_{Acc}}{2} - \frac{\dot{J}_{sys}M_2}{J}\right]. \tag{6.59}$$

Once again I consider the stationary solution $F = F_0$ given as

$$0 = hF_0\left[DF_0 - B\varepsilon F_0^{1/2} - B\frac{\varepsilon^2\delta_{Acc}}{2} - \frac{\dot{J}_{sys}M_2}{J}\right], \tag{6.60}$$

then applying the same small perturbation as previous and expanding to first order in u, equation 6.59 gives

$$\dot{u} = hF_0u\left[D - B\frac{\varepsilon}{F_0^{1/2}}\right]. \tag{6.61}$$

Which for stability requires that

$$D - B\frac{\varepsilon}{F_0^{1/2}} < 0. \tag{6.62}$$

From the provious example I know that D is positive for range of q and η in question. Taking the simple case of $\alpha = 1.0$, $\eta = 0.0$ (upper left frame in figure 6.2) with the standard $\zeta = 1.0$ for the mass transfering system, from equations 6.39 and 6.40 I have

$$D = \frac{4}{3} + \frac{2q}{3(1+q)} - q, \tag{6.63}$$

$$B = -\frac{4}{3} + \frac{(1-\delta_{Acc})}{1+q} + (1-\delta_{Acc})\frac{q}{3(1+q)} - \delta_{Acc}\frac{q^2}{1+q}. \tag{6.64}$$

As ε and $F_0^{1/2}$ are always positive stability requires that B must also be positive, for the regime outlined above this is never true. With the inclusion of the CAML efficiency η the result is even worse (see equation 6.40) and different values of α make little difference to the result. Hence equation 6.62 is always false and the system is unstable to mass transfer.

The third case with $\varepsilon^2\delta_{Acc}^2 \simeq 4F$ is thus the only possible region for which a stable solution may exist. Unfortunately with this equation 6.50 has no easy solution for stability, though on inspection of the stable regions for the models shown in the left frames of figure 6.2, $\varepsilon^2\delta_{Acc}^2$ is of the same order as $4F$.

6.3 Conclusions

It can be seen from table 6.1 that even in systems subject to an irradiation driven wind, where a substantial CAML is considered, the predicted period bounce never reaches that of the observed value. Systems with higher CAML efficiencies are unstable producing extremely high mass transfer rates $\dot{M} > 10^{-7}M_{\odot}/yr$ and hence are not considered. Once systems start mass transfer the irradiation driven wind becomes self sustaining and can be the dominant mechanism in the mass loss of the secondary, being between 1 and 4 times the mass transfer rate from Roche lobe overflow (see figure 6.4). If the extreme cases of accretion of the wind onto the primary are considered I find the following. For zero wind accretion the mass transfer rate due to Roche lobe overflow still displays the cyclic behaviour. In the case of maximum accretion of the wind, with the assumption that only the irradiated region of the star has the wind driven from it, the system is totally dominated by the wind mass loss. After an initial burst of Roche lobe mass transfer the system detaches and mass loss is purely from the self sustaining irradiation driven wind and the system evolves to longer periods.

The two extreme cases are highly unlikely though they demonstrate that, regardless of the actual value of the wind accreted by the primary, the evolution of the system is going to be greatly modified by any irradiation driven wind. The obvious mass transfer cycles predicted by almost all of the models over all periods is highly suggestive of the spread of mass transfer rates observed at a given period in the observed sample of CVs.

Chapter 7

Two separate evolutionary paths for magnetic and non-magnetic CVs?

The increasing number of known CVs with well defined orbital periods is now such that any differences in the distributions of the subclasses should give more meaningful results from statistical tests. In this chapter I investigate the difference in the distributions of magnetic and non-magnetic CV systems.

With the data taken from RKcat, version 7.0 (Ritter and Kolb (2003)) figure 7.1 shows the distributions of CVs over orbital periods $0.67 < P/hr < 7.5$ as a histogram (with 6 minute bins) as well as the corresponding cumulative distributions for ($0.67 < P/hr < 13.4$), all systems (443 systems), polars (74 systems), intermediate polars (34 systems) and non-magnetic (334 systems) CVs including, V1432 Aql, which following the classification given in RKcat could be either a polar or intermediate polar. The cumulative distribution is defined as

$$N_{\Sigma}(> P) = \frac{1}{N_{CV}} \int_{P}^{\infty} N(P')\mathrm{d}P', \tag{7.1}$$

where N_{CV} is the total number of systems in the sample, is independent of any binning and is normalized to unity (see e.g. Kolb (1995)). The features of the distribution of the full sample are discussed in Chapter 1.

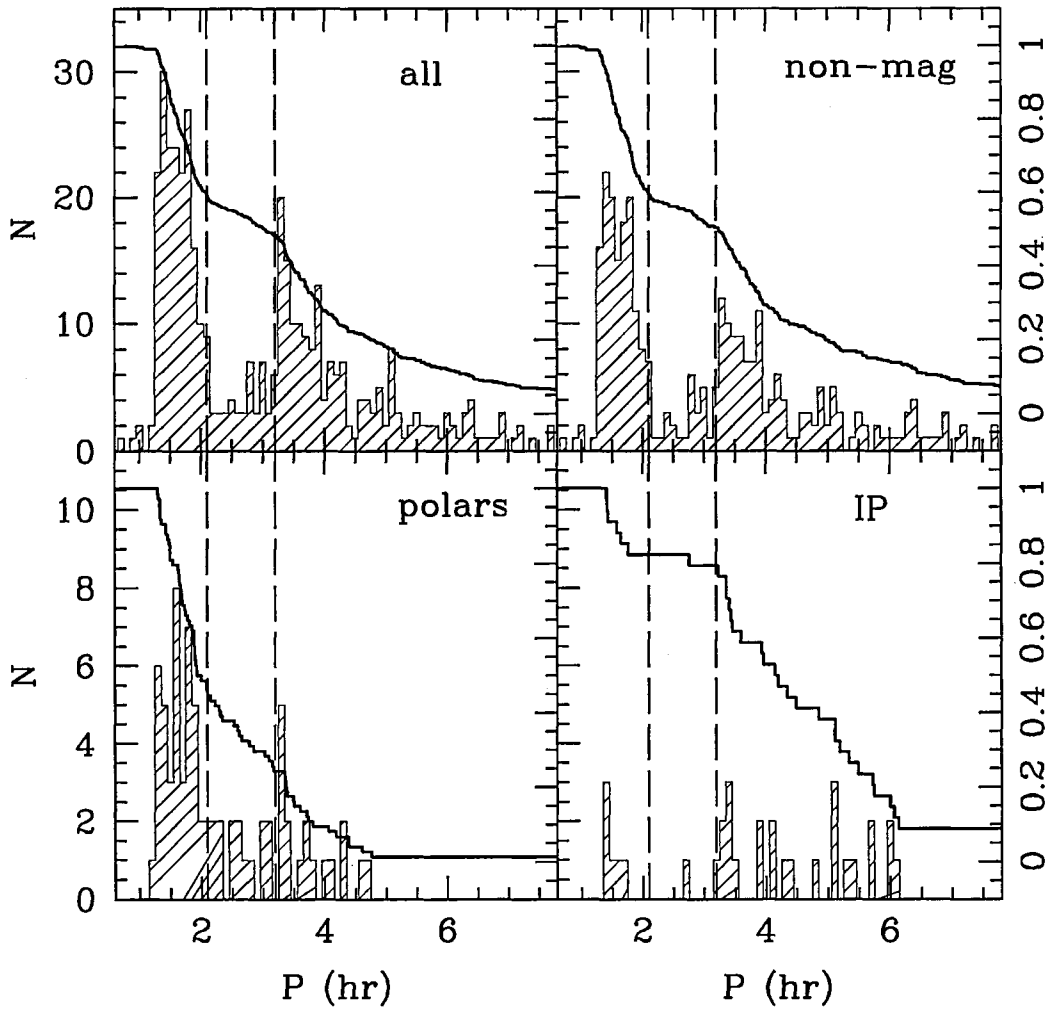

Figure 7.1: Cumulative period distributions (heavy solid lines; scale on right) defined by equation 7.1, and period histograms (hatched; scale on left), for various subgroups of CVs. The vertical dashed lines indicate the period gap for non-magnetic CVs ($2.1 < P/hr < 3.2$).

7.1 Non-magnetic CVs

The period distribution of the non-magnetic systems follows a similar distribution as the full sample, with the period gap in roughly the same period range (approx $2.1 < P/hr < 3.2$). Relatively few non-magnetic CVs are found within the period gap, approx 8.5% compared to approx 40% in the period range $1.3 < P/hr < 2.1$ below the gap (this

compares with approx 11% of the total distribution of CVs which are found within the period gap and approx 41% below the gap).

The main features of additional interest in the distribution are

1:- The cumulative distribution (CDF) below the gap appears to increase linearly with decreasing P (as can be seen in figure 7.2), hence the probability distribution function (PDF) of orbital periods in this region is flat (see Chapter 3). As the mass transfer rate

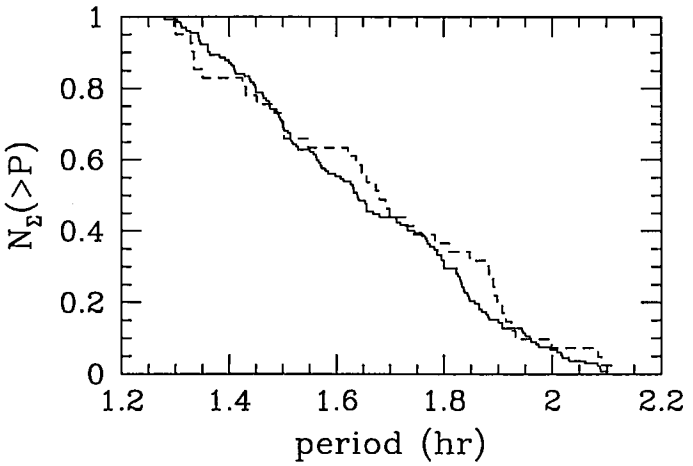

Figure 7.2: Cumulative period distributions below the period gap ($1.3 < P/hr < 2.1$) for polars (dashed line) and non-magnetic systems (solid line).

driven by gravitational radiation alone below the gap is fairly constant (see figure 1.12 middle frame) for systems that have not reached the minimum period, the probability of discovering a system at any period within this range is also constant. If I assume that there are no major selection effects that would distort the shape of the intrinsic PDF then the constancy of the slope of the observed CDF implies that very few non-magnetic systems must form below the gap. The reason for this is as follows: if systems could form with equal probability at any period below the gap, the probability for any system having a given orbital period now, P_o, would consist of a sum of probabilities given from

all systems that formed with orbital periods longer than the given period and evolved to P_o. This would thus give an increasing PDF towards shorter periods. This in turn would cause the slope of the cumulative distribution to increase to shorter periods. This is not observed in the distribution, consistent with the conclusions made in section 3.4.4 on the initial secondary mass spectrum.

2:- The CDF of systems above the gap (see figure 7.3) shows a non-linear increase towards shorter orbital periods. Assuming standard evolution not all this increase can be

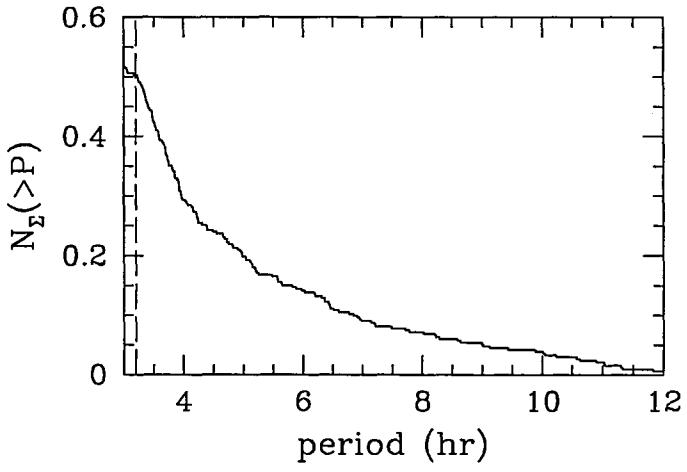

Figure 7.3: Cumulative period distributions for non-magnetic systems in the period range $3 < P/hr < 12$. The vertical dashed line indicates the upper edge of the period gap.

attributed to the change in discovery probability due to the changes in angular momentum loss rate, from gravitational radiation and magnetic braking. If the standard magnetic braking is applied (Verbunt and Zwaan (1981)) then the expected discovery probability (see section 3.1) should follow the trend as shown in figure 7.4. This figure shows a subpopulation of CVs that share a common zero age CV configuration, in which the secondary is a main sequence star and the discovery chance is given by equation 3.3

with $\gamma = 1.0$. This in turn would be expected to give a reduction in the number of

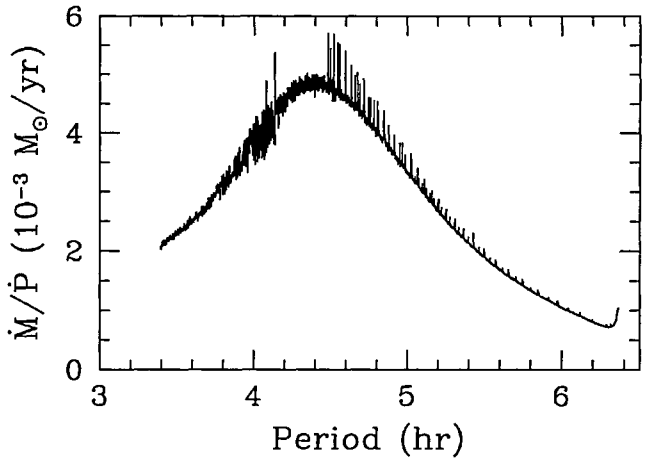

Figure 7.4: The expected discovery rate for systems above the period gap which are subject to the standard full magnetic braking by Verbunt and Zwaan (1981). The spikes in the plot are due to numerical noise.

systems found below around 4.4 hrs, and hence a decrease in the slope of the cumulative distribution below 4.4hs. As can be seen from figure 7.3 no such trend is found. Again if further selection effect are neglected this is consistent with the assumption that CVs do not form with any orbital period shorter than $\sim$ 3.2 hrs.

7.2 Magnetic systems

I split the distribution of magnetic systems into intermediate polars (IPs) and polars as seen in figure 7.1 (lower frames). The number of intermediate polars in the observed distribution is very small, and hence anything we draw from this CDF is somewhat speculative. In IPs there does appear to be a period gap at around the same period range as for non-magnetic systems suggesting that the two types of systems are subject to similar evolutionary effects. I now make the assumption that IPs are the progenitors of polars: as

mass is transferred from the secondary to the primary in IPs the primary is spun up/down to the point that it synchronises with the orbit hence it becomes a polar. Then if IPs form at a similar rate to non-magnetic CVs, but some are lost from the class to become polars, a change in the slope of the CDF at around 5 hours (the period where polars start to be found in any numbers) is expected. If I assume that IPs should have the same distribution as non-magnetics above the gap, then there is a highly suggestive break in the CDF of IPs at around this period (see figure 7.5). A fit to the non-magnetic CDF above the gap was

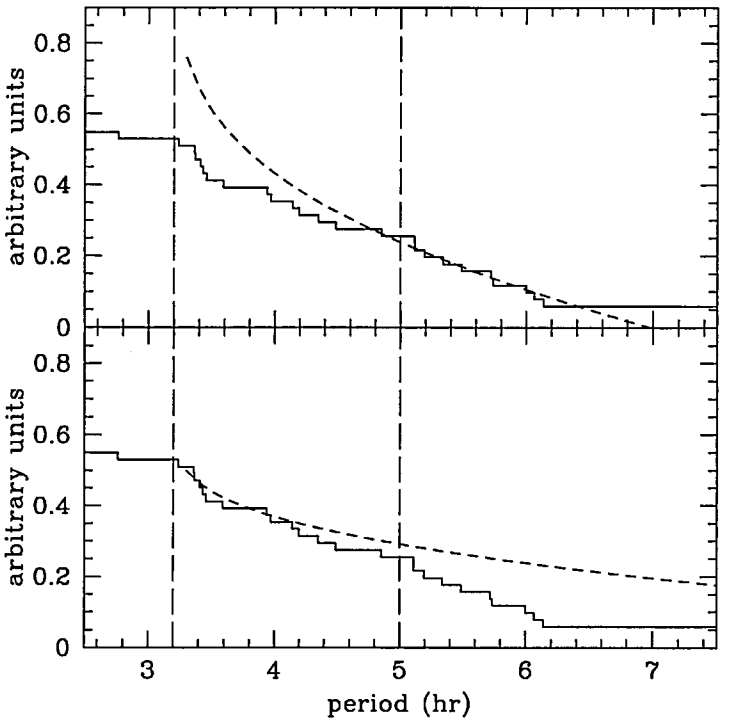

Figure 7.5: Two possible fits of the non-magnetic CDF (dashed) to the intermediate polar CDF (solid): upper frame the model from equation 7.2 is fitted to the IP systems above 5 hrs, lower frame the model from equation 7.2 is fitted to the IP systems below 5 hrs.

produced based on the expression.

$$N_{\Sigma} = \delta_f \int_{3.2}^{13} \frac{1}{P - 2.1} dP, \tag{7.2}$$

where δ_f is a fitting parameter and P is in hours.

Using δ_f this fit was then scaled and compared with the IP CDF above 5 hrs (see figure 7.5 upper frame), and below 5 hrs (see figure 7.5 lower frame). Though with this limited sample the data is not sufficient to draw any firm statistical conclusions as to which if either of the fits has any significance, as the data could just as well (if not better) be fitted by a straight line.

A change in slope at around 5 hrs could also be due to observational selection effects. For any binary system it is required to observe 2 full orbits to determine its period with any certainty. Observation runs are generally $\lesssim 10$ hrs, this weights the sample of CVs with determined orbital periods in favour of the shorter period systems.

It is reasonable to assume that the initial rotation rates of the primaries in pre-CVs are no different than in isolated white dwarfs. Due to the conservation of angular momentum they should have spin periods of around 1 day (Schmidt and Norsworthy (1991), also see Spruit (1998)), and in the absence of an angular momentum loss mechanism the spin period should not change until the onset of mass transfer. Hence virtually any polar, and moreover those found in the gap, must have formed initially as an IP. These systems should take at least 10^6 years to synchronise, from simple angular momentum transfer considerations, [see Frank, King, and Raine (2002), Somerscales, Norton, Wynn, and West (2002)] and, if the secondary is not fully convective, should be subject to the standard magnetic braking prescription during this period. Synchronization may be acheived on a shorter time-scale if a magnetohydrodynamic torque is considered (see Lamb, Aly, Cook, and Lamb (1983)) this mechanism could account for the rapid resychronization rate of nova V1500 Cygni (see Schmidt and Stockman (1991)). Also, if systems become polars at any period within the gap, I would expect to see a non-linear cumulative distribution in the gap, as discussed in section 7.1; this is not seen.

The large number of polars within the range of the period gap for non-magnetic CVs is

suggestive of a separate evolutionary process for polars (approx 21% of polars have orbital periods within the gap, and 55% are below the gap). Polars may not be subject to the disrupted magnetic braking that appears to operate on the non-magnetic and IP systems. One alternative put forward is that polars may be subject to a reduced form of magnetic braking (see Li, Wu, and Wickramasinghe (1994b) and Li, Wu, and Wickramasinghe (1994a)) in which the magnetic field of the primary influences the magnetic field of the secondary causing less open field lines along which material may escape and exert a spin-down torque. This in turn would cause a reduced angular momentum loss rate, compared with standard magnetic braking, thus the secondary is less out of thermal equilibrium than a secondary with the same mass but subject to standard magnetic braking. The radius of the former is therefore smaller, hence the orbital separation and thus orbital period must be smaller for the secondary to fill its Roche lobe. Thus comparing two systems at the same orbital period, one with standard and one with reduced braking, the system with reduced braking will have a higher mass secondary.

The reduced magnetic braking (or alternative form of angular momentum loss) would have to continue to operate until the lower edge of the period gap, thus producing the linear shape of the cumulative distribution found within this period range. At the lower edge of the gap the mass of the secondary would be essentially the same as that for non-magnetic systems now reappearing at this period; from this point on the polars would evolve under gravitational radiation alone. This is consistent with the fact that the observed CDF below the period gap is linear for both the non-magnetics and polars (see figure 7.2), suggesting that the evolution is the same for all systems (implicitly assuming that there are no major differential selection effects). This is also consistent with the results of section 3.2.3 where I found that there is no distinction between magnetic and non-magnetic systems below the gap.

From Warner (1995) it can be seen that the formation probability for polars is dependant upon the synchronization condition (his equation 6.28). This synchronization

condition goes with the inverse cube of the seperation of the two stars.

$$T_{SYNC} \propto \frac{1}{a^3}, \tag{7.3}$$

hence due to Kepler's law is propotional to the inverse square of the orbital period. To test if the polars could be formed from the distribution of non-magnetics a simple scaling of $1/P^2$ was applied to the non-magnetic distribution. The result was normalized to the number of observed polars for comparison, this is shown in figure 7.6 (upper frame).

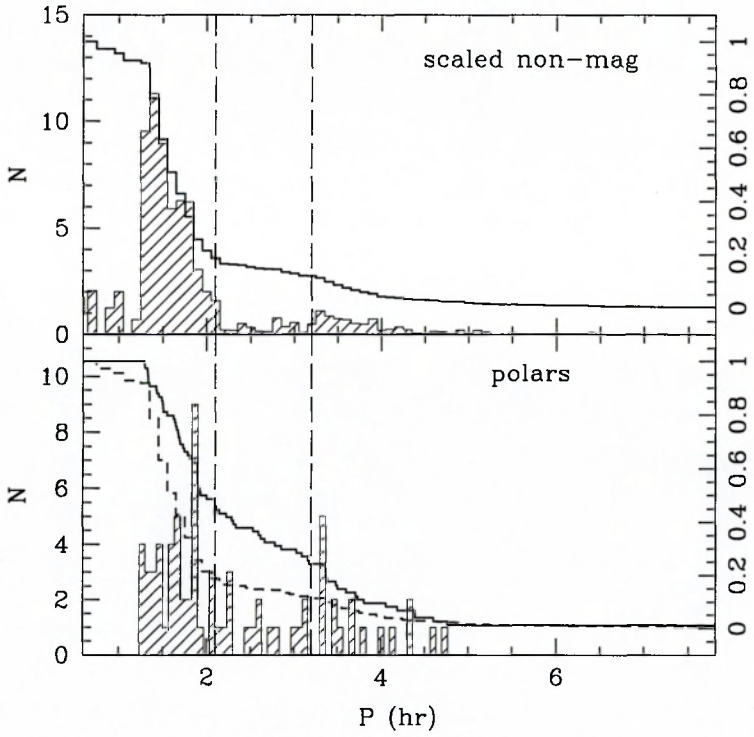

Figure 7.6: Cumulative period distribution for (heavy solid lies; scale on right) and period histograms (hatched; scale on left), for the scaled non-magnetic systems (upper frame) and polar's (lower frame). Short dashed plot indicates scaled distribution for easier comparison.

The period histogram and cumalative distribution of polars is shown in figure 7.6 (lower frame) along with the cumatative distribution of the scaled non-magnetic systems

(short dashed) for easier comparison. A simple KS test was applied to the two cumalative distributions, for $1.2 \leq P(hr) \leq 5$, and gives a KS probability that I can reject the hypothesis that the two distributions are drawn from the same parent distribution of $P_{KS} > 0.999$. The rejection probability is sufficient to say that the distribution of polars is not drawn from the distribution of non-magnetic systems via the simple syncronization condition.

7.3 Statistical comparison

In this section I test the null hypothesis that the distribution of polars and non-magnetic CVs are drawn from the same parent distribution. Due to the relatively small number of systems in the distribution of polars, to use a χ^2 test would require binning the sample into around 20 minute bins to give around 10 systems per bin. This would give very poor resolution and would introduce the problems associated with positioning of the bins that could potentially affect the outcome. I thus used a Kolgomorov-Smirnov (K-S) test. Unlike for the investigation into P_{min} a K-S test is quite appropriate in this situation as the greatest difference in the two distributions is around the mid point.

The test was applied to systems in the range $1.3 < P/hr < 5$, which is populated by polars and non-magnetic CVs (see figure 7.7, upper frame). This gives a K-S probability P_{KS} that I can reject the hypothesis that the two distributions are drawn from the same parent distribution of 0.909. The K-S test was also applied to the distributions of systems below the period gap (see figure 7.2), giving $P_{KS} = 0.267$. The change in K-S probability for distributions with the same lower period ($\sim$ 1.3hrs) and a range of maximum period P_{max} ($2.1 < P_{max}(hr) < 7$) can be seen in figure 7.8. The function $P_{KS}(P_{max})$ exhibits several interesting features: initially the rejection probability increases to a maximum at around 2.8 hrs, then decreases to a (second) minimum at around 3.8 hrs before increasing rapidly once again. This second minimum is due to the non-linear cumulative distributions in both polars and non-magnetic systems. For short P_{max} the cumulative distribution for non-magnetic CVs falls below that for polars (see figure 7.7, lower frame), but for

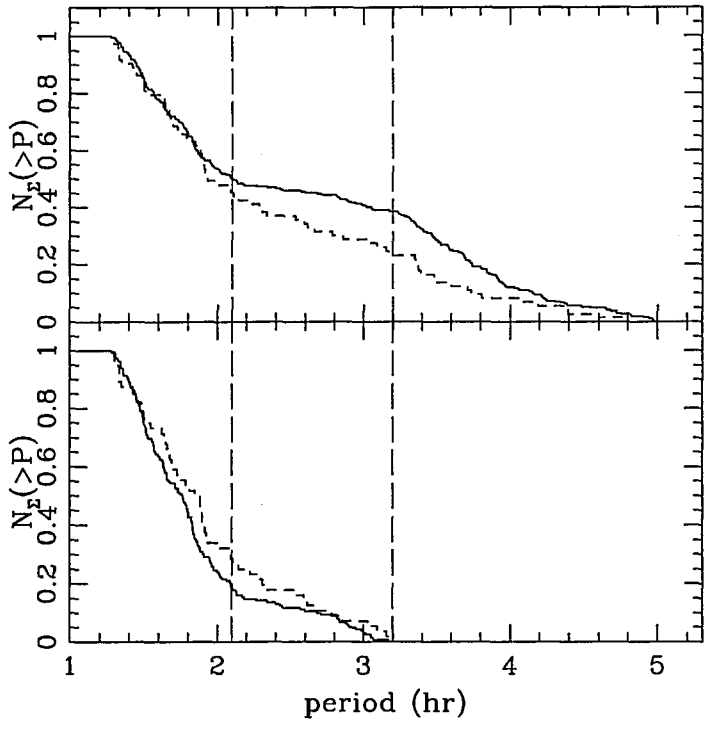

Figure 7.7: Cumulative period distributions for polars (dashed line) and non-magnetic systems (solid line): Top frame, for the period range $1.3 < P/hr < 5$. Bottom frame, for the period range $1.3 < P/hr < 3.2$. The vertical dashed lines indicate the period gap for non-magnetic CVs.

longer P_{max} the cumulative distribution for polars falls below that of non-magnetics (see figure 7.7, upper frame). As the K-S test uses the maximal difference between the two distributions (see section 3.2.1), which has a minimum as the maximal difference moves from being below to above the polar distribution at around 3.8 hrs, thus there is a resonance effect causing the second minimum. This resonance effect would be reduced for sub classes which both experience a period gap at a similar period range. From 5 hrs on the rejection probability tends towards 1 as, from this point on, the cumulative distributions are forced apart, simply due to the lack of polars with orbital periods greater than 5 hrs.

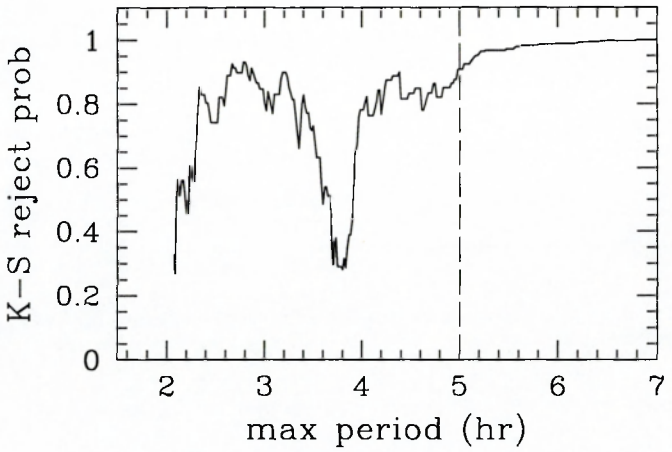

Figure 7.8: Plot of the K-S probability that the hypothesis that as a function of P_{max} the distributions of polars and non-magnetic CVs are drawn from the same parent distribution can be rejected. The K-S test was applied to the observed sample in the period range $1.3 < P/hr < P_{max}$. The vertical dashed line indicates the upper end of the polar distribution at ~ 5 hrs.

7.4 Conclusions

The rejection probability of 0.909, over the orbital period range $1.3 < P/hr < 5$, of the hypothesis that the observed samples of polars and non-magnetic CVs are drawn from the same underlying parent distribution is high, though not high enough to confidently reject this hypothesis. Nontheless it seems likely that the evolution of polars and non-magnetic CVs is the same for periods below the lower edge of the gap, but that they are subject to different types of evolution through the period gap and possibly above the upper edge of the period gap, as is borne out by the resonance effect giving the second minimum in figure 7.8.

Chapter 8

Conclusions

Well, I suppose this is the time for me to say something profound... Nothing comes to mind (O'Neill)

(Stargate SG1, Season Two, 'THE SERPENT'S LAIR')

8.1 General conclusions

This thesis was begun in 2000 with the original idea to investigate what effects winds from the secondary star in CVs could have on the evolution of these systems, and if it was possible to account for the mismatch in observed and theoretically predicted orbital period minimum via this mechanism. In the end this and a number of other mechanisms have been investigated to try to resolve this discrepancy, along with investigating the mismatch in the overall shape of the observed and theoretically predicted short period ($1.3 \lesssim P/hr \lesssim 2.1$) orbital period distribution, the large spread of observed mass transfer rates for any given orbital period and the apparent differences in the orbital period distributions of the magnetic and non-magnetic systems.

The answer to the original problem appears to be 'NO'. On their own winds from the secondary are unable to carry off sufficient angular momentum to raise the minimum period to the observed value. This can be seen from the results of chapter 6 where even

with the high wind loss rates of up to 4 times the mass transfer rate through the L_1 point (around $10^{-10} M_{\odot} yr^{-1}$) this would only raise the calculated minimum period from 66 minutes to around 73 minutes. The effects of a consequential angular momentum loss (CAML) mechanism with reasonable values for the efficiency ($0 \leq \eta \leq 1$, see chapter 2 for details), are also unable to raise the calculated minimum period to above 70 minutes. The two mechanisms investigated which are able on their own to raise the predicted minimum period to that of the observed are, the distortion of the secondary star due to its proximity to the primary, which tends to cause the secondary to become bloated compared to a star of the same mass in isolation, though a bloating factor of around 1.18 is required compared to the expected value of 1.06 (see chapter 2) and the removal of orbital angular momentum into a circumbinary disc (chapter 5). Systems in which the secondary is distorted by 1.18 the amount required to raise the minimum period to the observed value tend to come into contact at longer orbital periods compared to undistorted secondaries, thus the lower edge of the period gap is moved to longer periods. This inconsistency may be overcome if the bloating factor is a function of the mass of the secondary. The circumbinary disc model raises the minimum period to the observed value for quite small disc parameters ($\delta = 0.0005, \alpha = 0.005$) though does require that most if not all systems have developed quite a substantial disc before reaching the period bounce.

It is obviously possible to combine various effects to raise the calculated period bounce to around that of the observed minimum period though any effect has to be able to explain the shape of the observed orbital period distribution at the same time.

As noted the observed orbital period distribution for short period systems displays an almost featureless continuum. Almost any combination of driving mechanisms considered for increasing the predicted period bounce, also give rise to a pronounced pile up of systems in the predicted orbital period distribution at around the minimum period. The exceptions to this are the CV populations that are subject to an age limit, and that evolve under the influence of a circumbinary disc, for certain ranges of parameters. It is possible to smooth out this expected spike by assuming that systems are subject to a spectrum of efficiency values of each mechanism, as seen in chapter 3, though in each case

some additional intrinsic angular momentum loss mechanism (such as remnant magnetic braking) is required to set the minimum period to the observed value. The smoothing out of the spike in this way is never totally convincing. The combination of a spectrum of primary masses and CAML efficiencies gives a reasonably good fit to the observed data, but is still not as good as the assumption of a flat distribution of systems. Some fine tuning of the shape of the parameter spectrum may improve the fit (see section 3.4.5) though the existence of a mechanism that produces such a contrived parameter weighting is dubious.

If sufficiently large values of the viscosity $\alpha \gtrsim 0.007$ and mass input rate $\delta \gtrsim 0.004$ (in each case the other parameter taken as 0.001) for the circumbinary disc are employed the system undergoes an evolution which follows an increasing orbital period for any value of the secondary mass. If so then the implication is that systems below the period gap must form below the gap with orbital periods $P/hr \gtrsim 1.3$, although some mechanism is required to prevent them entering the period gap from the lower edge. Systems with circumbinary discs which undergo nova outbursts may have the circumbinary disc disrupted during the outburst. This could lead to alternate periods, where the evolution follows the standard evolution, (without circumbinary disc) with decreasing orbital period (pre bounce), and phases where the orbital period increases due to the circumbinary disc powered evolution. It is even possible that these systems could have detached phases after a nova outburst. This is similar to the disrupted magnetic braking picture in which the secondary star, which has an artificially large radius due to the high mass loss rate caused by the large angular momentum loss rate, shrinks back inside its Roche lobe with the sudden reduction in angular momentum loss rate. The detaching of the post nova could be further aided by the widening of the binary due to the nova ejection of the envelope.

As noted by Spruit and Taam (2001), if systems are subject to a circumbinary disc evolution with nova outbursts then the mass transfer at any given period would not be determined by the masses of the two stars, but the evolutionary state of the disc. Systems with young or no disc would have lower mass transfer rates than those with large discs at the same orbital period. This could account for the large spread of mass transfer rate

observed in CVs with similar orbital period. Alternatively, as can be seen in chapter 6, the feedback mechanism in the irradiation driven wind case produces large amplitude mass transfer variations for almost the full range of parameters, and the inclusion of additional angular momentum loss mechanisms (e.g. CAML) only cause these variations to increase in amplitude and persist to shorter orbital periods. Systems that are driven by a highly efficient ($\eta \rightarrow 1$) CAML mechanism alone are also be seen to evolve through mass transfer cycles (see section 2.4.1), though these appear confined to the higher secondary mass regions of their evolution.

From chapter 7 it can be seen that there is a distinct possibility that the evolution of polars and non-magnetic systems follow two separate evolutionary paths, thus any mechanism or mechanisms used to explain the minimum period and orbital period distribution of CVs must cater for both cases.

So all in all, it is possible to raise the calculated period bounce to the observed minimum period by various mechanisms or combinations of mechanisms, though in most cases some additional angular momentum loss mechanism or spread of the efficiency values for the given mechanisms is required to reproduce the observed orbital period distribution.

8.2 Directions for future research

I conclude this thesis by outlining some of the areas which I feel warrant further research.

- In my opinion, one of the most promising mechanisms at this point is the orbital braking by a circumbinary disc. There is great potential to help explain the main features of the orbital period distribution of CVs, especially in the light of the increasing evidence of material surrounding binary systems. The following further improvements and applications are apparent:

- An improved opacity and hence viscosity prescription as outlined in section 5.4, along with a more detailed description for the vertical structure of the disc (as started by Dubus, Taam, and Spruit (2002)) and an improved model for the interaction of the binary with the disc.

- Modelling the interaction of nova outbursts with the circumbinary disc, i.e. what magnitude of outburst is required to disrupt the disc and hence how massive could a disc become in the time required for the white dwarf to accrete sufficient material for a nova outburst, what effect would the loss of the circumbinary disc in a disc driven system have on its evolution e.g. would the system undergo periods of detached evolution after a nova outburst due to the reduction in the angular momentum loss.

- The irradiation driven wind model (chapter 6) also deserves further investigation. A more realistic prescription for the wind from the secondary, and for the fraction of the wind that is accreted by the primary should be employed. This model also requires a more refined description for the stability analysis of the mass transfer cycles found below the gap. Also the self sustaining wind at the higher end of the wind accretion in which the systems detach from the L_1 point and evolve purely due to mass loss through the wind is worthy of further investigation.

- Although a crude model for the possible distribution of CVs (see chapter 3) has been calculated for some of the CV driving mechanisms, a full population synthesis model could be extended to include all the driving mechanisms studied in this thesis and hence determine their separate and combined effects on the evolution over the full observed period range for CVs.

8.3 Possible new model for the evolution of CVs

In this section I propose a model that could explain the difference in magnetic and non-magnetic systems along with the difference between systems above and below the period gap using the circumbinary disc model.

I propose that systems evolve under the effects of circumbinary discs and the reduced magnetic braking as discussed in chapter 5. This idea initially started as a result of an investigation into the possible differences between the magnetic and non-magnetic systems above the gap. One of the main and most obvious differences between these two subgroups is the lack of an accretion disc in the magnetic systems. This leads me to propose that

non-magnetic systems above the gap evolve via gravitational radiation, a reduced form of magnetic braking and a circumbinary disc fed via a wind from the disc and a stellar wind from the secondary causing them to bounce before or at the upper edge of the gap. In the case of the magnetic CVs the disc wind is not available to feed the circumbinary disc and hence systems evolve via a different route with lower angular momentum loss enabling them to evolve into the gap. For systems below the gap the mass flow rates are too low to produce a disc wind and hence both magnetic and non-magnetic systems evolve via the same route by gravitational radiation and a reduced circumbinary disc fed via the wind from the secondary. A mechanism to set the lower edge of the gap in non-magnetic systems is difficult to see using this prescription alone. Though I speculate that if some mechanism can cause the mass transfer rate above the gap to drop substantially and for long enough, (e.g. the mass transfer cycles exhibited by systems driven by an irradiation driven wind, see chapter 6) the accretion disc wind could shut down and the circumbinary disc dissipate hence detaching the systems to reappear later at the lower edge of the gap. Alternatively a nova outburst could disrupt the circumbinary disc reducing the angular momentum loss rate and hence the mass transfer rate shutting down the accretion disc wind.

If we accept that systems evolve via the effects similar to that discussed in chapter 5 and by Willems, Kolb, Sandquist, Taam, and Dubus (2003) then fractional mass input rates to a circumbinary disc of $\delta \simeq 0.0003$ and 0.00001 are required above and below the gap respectively. I assume that the rate below the gap can be supplied via the secondary wind (this is around $10^{-15} M_{\odot} yr^{-1}$ for a system below the gap where $\dot{M} \simeq 10^{-10} M_{\odot} yr^{-1}$) with no disc wind. The lack of a disc wind below the gap is probable as Proga, Stone, and Drew (1998) find that for mass flow rates in the disc of less than around $10^{-8} M_{\odot} yr^{-1}$ there is virtually no disc wind whereas above this there is a sharp turn on of the disc wind. Thus systems above the gap are likely to have substantial disc winds. Proga (2003) uses MHD studies of radiation driven winds from accretion discs threaded by axial magnetic fields and finds mass outflow rates in the winds of around 0.001 to 0.1 times the accretion rate. Much of this wind has a high outflow velocity though a fraction has outflow velocities

which may be comparable with that required to form a circimbinary disc (see their figure 1). As can be seen from this only between 0.003 and 0.3 of the disc wind are required to feed a circumbinary disc above the gap.

Due to time restrictions I am unable to test this suggestion/model quantitatively.

REFERENCES

Andronov, N., Pinsonneault, M. H., and Sills, A., 2003. *ApJ, 582*; 358–368.

Artymowicz, P. and Lubow, S. H., 1994. *ApJ, 421*; 651–667.

Baraffe, I. and Kolb, U., 2000. *MNRAS, 318*; 354–360.

Barker, J. and Kolb, U., 2003. *MNRAS, 340*; 623–631.

Basko, M. M. and Sunyaev, R. A., 1973. *Ap&SS, 23*; 117–+.

Bell, K. R., Cassen, P. M., Klahr, H. H., and Henning, T., 1997. *ApJ, 486*; 372–+.

Bell, K. R. and Lin, D. N. C., 1994. *ApJ, 427*; 987–1004.

Cannizzo, J. K. and Reiff, C. M., 1992. *ApJ, 385*; 87–93.

Chabrier, G. and Baraffe, I., 2000. *ARA&A, 38*; 337–377.

Chan, K. L. and Chau, W. Y., 1979. *ApJ, 233*; 950–960.

Copeland, H., Jensen, J. O., and Jorgensen, H. E., 1970. *A&A, 5*; 12+.

Cox, A. N., 2000. *Allen's astrophysical quantities* (Allen's astrophysical quantities, 4th ed. Publisher: New York: AIP Press; Springer, 2000. Editedy by Arthur N. Cox. ISBN: 0387987460).

Crampton, D., Hutchings, J. B., Cowley, A. P., and Schmidtke, P. C., 1997. *ApJ, 489*; 903–+.

Dünhuber, H., 1993. Ph.D. Thesis.

Dünhuber, H. and Ritter, H., 1993. In *NATO ASIC Proc. 403: White Dwarfs: Advances in Observation and Theory*, pp. 359–+.

D'Antona, F., 2001. In *ASP Conf. Ser. 229: Evolution of Binary and Multiple Star Systems*, pp. 21+.

D'Antona, F. and Mazzitelli, I., 1982. *ApJ, 260*; 722–734.

D'Antona, F., Mazzitelli, I., and Ritter, H., 1989. *A&A, 225*; 391–404.

de Kool, M., 1990. *ApJ, 358*; 189–195.

de Kool, M., 1992. *A&A, 261*; 188–202.

Dewi, J. D. M. and Tauris, T. M., 2000. *A&A, 360*; 1043–1051.

Dewi, J. D. M. and Tauris, T. M., 2001. In *ASP Conf. Ser. 229: Evolution of Binary and Multiple Star Systems*, pp. 255–+.

Dubus, G., Taam, R. E., and Spruit, H. C., 2002. *ApJ, 569*; 395–404.

Eggleton, P. P., 1971. *MNRAS, 151*; 351–+.

Eggleton, P. P., 1972. *MNRAS, 156*; 361–+.

Eggleton, P. P. and Pringle, J. E., 1985. *ApJ, 288*; 275–+.

Frank, J., King, A., and Raine, D., 2002. *Accretion power in astrophysics* (Accretion power in astrophysics. 3rd ed. / Juhan Frank, Andrew King and Derek Raine, Cambridge, UK: Cambridge University Press. ISBN 0-521-62957-8, 2002, XIV + 384 pp.).

Fujimoto, M. Y., 1982. *ApJ, 257*; 767–+.

Gänsicke, B. T., Euchner, F., and Jordan, S., 2002. *A&A, 394*; 957–963.

Hameury, J., Menou, K., Dubus, G., Lasota, J., and Hure, J., 1998. *MNRAS, 298*; 1048–1060.

Han, Z., Podsiadlowski, P., and Eggleton, P. P., 1995. *MNRAS, 272*; 800–820.

Henning, T. and Stognienko, R., 1996. *A&A, 311*; 291–303.

Henyey, L. G., Forbes, J. E., and Gould, N. L., 1964. *ApJ, 139*; 306–+.

Howell, S. B., Rappaport, S., and Politano, M., 1997. *MNRAS, 287*; 929–936.

Hurley, J. R., Tout, C. A., and Pols, O. R., 2002. *MNRAS, 329*; 897–928.

Iben, I., 1982. *ApJ, 259*; 244–266.

Iben, I. J. and Livio, M., 1993. *PASP*, *105*; 1373–1406.

Kim, Y. and Demarque, P., 1996. *ApJ*, *457*; 340–+.

King, A. R., 1988. *QJRAS*, *29*; 1–25.

King, A. R., Frank, J., Kolb, U., and Ritter, H., 1997. *ApJ*, *482*; 919–+.

King, A. R. and Kolb, U., 1995. *ApJ*, *439*; 330–336.

King, A. R. and Schenker, K., 2002. In *ASP Conf. Ser. 261: The Physics of Cataclysmic Variables and Related Objects*, pp. 233+.

King, A. R., Schenker, K., and Hameury, J. M., 2002. *MNRAS*, *335*; 513–516.

King, A. R. and van Teeseling, A., 1998. *A&A*, *338*; 965–970.

Kolb, U., 1995. In *ASP Conf. Ser. 85: Magnetic Cataclysmic Variables*, pp. 440–+.

Kolb, U., 2002. In *ASP Conf. Ser. 261: The Physics of Cataclysmic Variables and Related Objects*, pp. 180+.

Kolb, U. and Baraffe, I., 1999. *MNRAS*, *309*; 1034–1042.

Kolb, U. and de Kool, M., 1993. *A&A*, *279*; L5–LL8.

Kolb, U., Rappaport, S., Schenker, K., and Howell, S., 2001. *ApJ*, *563*; 958–970.

Kolb, U. and Ritter, H., 1992. *A&A*, *254*; 213–+.

Kopal, Z., 1959. *Close binary systems* (The International Astrophysics Series, London: Chapman & Hall, 1959).

Kuduz, M., Reinsch, K., Beuermann, K., and Kube, J., 2002. In *ASP Conf. Ser. 261: The Physics of Cataclysmic Variables and Related Objects*, pp. 641–+.

Lamb, F. K., Aly, J.-J., Cook, M. C., and Lamb, D. Q., 1983. *ApJ*, *274*; L71–L75.

Landau, L. and Lifschitz, E., 1958. *The classical theory of fields* (Pergamon press, Oxford).

Li, J. K., Wu, K. W., and Wickramasinghe, D. T., 1994a. *MNRAS*, *270*; 769–+.

Li, J. K., Wu, K. W., and Wickramasinghe, D. T., 1994b. *MNRAS*, *268*; 61–+.

Lin, D. N. C. and Papaloizou, J., 1979. *MNRAS*, *188*; 191–201.

Livio, M. and Pringle, J. E., 1994. *ApJ*, *427*; 956–960.

Magni, G. and Mazzitelli, I., 1979. *A&A*, *72*; 134–147.

Mazzitelli, I., 1989. *ApJ*, *340*; 249–255.

Mazzitelli, I. and Dantona, F., 1986. *ApJ*, *308*; 706–720.

Mestel, L. and Spruit, H. C., 1987. *MNRAS*, *226*; 57–66.

Meyer, F. and Meyer-Hofmeister, E., 1981. *A&A*, *104*; L10+.

Meyer, F. and Meyer-Hofmeister, E., 1999a. *A&A*, *341*; L23–L26.

Meyer, F. and Meyer-Hofmeister, E., 1999b. *A&A*, *346*; L13–L16.

Mouchet, M., Bonnet, J. M., Roueff, E., Beuermann, K., de Martino, D., Desert, J. M., Ferlet, R., Freid, R. E., Gänsicke, B. T., Howell, S. B., Mukai, K., Porquet, D., and Szkody, P., 2003. *A&A*.

Nauenberg, M., 1972. *ApJ*, *175*; 417–+.

Nelson, L. A., Chau, W. Y., and Rosenblum, A., 1985. *ApJ*, *299*; 658–667.

Nomoto, K., 1984. *ApJ*, *277*; 791–805.

Orio, M., della Valle, M., Massone, G., and Oegelman, H., 1997. *A&A*, *325*; L1–L4.

Osaki, Y., 1996. *PASP*, *108*; 39–+.

Paczyński, B., 1971. *ARA&A*, *9*; 183+.

Paczynski, B., 1981. Acta Astronomica, *31*; 1–12.

Paczynski, B. and Sienkiewicz, R., 1981. *ApJ*, *248*; L27–LL30.

Patterson, J., 1984. *ApJS*, *54*; 443–493.

Patterson, J., 2000. *PASP*, *113*; 736.

Plavec, M. and Kratochvil, P., 1964. Bulletin of the Astronomical Institutes of Czechoslovakia, *15*; 165–+.

Politano, M., 1996. *ApJ*, *465*; 338–+.

Pollack, J. B., McKay, C. P., and Christofferson, B. M., 1985. Icarus, *64*; 471–492.

Press, W. H., Teukolsky, S. A., Vetterling, W. T., and Flannery, B. P., 1992. *Numerical recipes in C/Fortran* (Cambridge University Press, Cambridge), 2nd edition.

Pringle, J. E., 1981. *ARA&A*, *19*; 137–162.

Pringle, J. E., 1991. *MNRAS*, *248*; 754–759.

Pringle, J. E. and Wade, R. A., 1985. *Interacting binary stars* (Cambridge Astrophysics Series, Cambridge: Cambridge University Press, 1985, edited by Pringle, J.E.; Wade, R.A.).

Proga, D., 2003. *ApJ*, *585*; 406–417.

Proga, D., Stone, J. M., and Drew, J. E., 1998. *MNRAS*, *295*; 595–+.

Rappaport, S., Joss, P. C., and Verbunt, F., 1983. *ApJ*, *275*; 713–731.

Rappaport, S., Joss, P. C., and Webbink, R. F., 1982. *ApJ*, *254*; 616–640.

Renvoizé, V., Baraffe, I., Kolb, U., and Ritter, H., 2002. *A&A*, *389*; 485–493.

Rezzolla, L., Uryū, K. ō., and Yoshida, S., 2001. *MNRAS*, *327*; 888–894.

Ritter, H., 1988. *A&A*, *202*; 93–100.

Ritter, H., 1990. *A&AS*, *85*; 1179–1256.

Ritter, H., 1996. In *NATO ASIC Proc. 477: Evolutionary Processes in Binary Stars*, pp. 223–+.

Ritter, H. and Burkert, A., 1986. *A&A*, *158*; 161–173.

Ritter, H. and Kolb, U., 1992. *A&A*, *259*; 159–166.

Ritter, H. and Kolb, U., 1998. *A&AS*, *129*; 83–85.

Ritter, H. and Kolb, U., 2003. *A&AS*.

Robinson, E. L., 1976. *ARA&A*, *14*; 119–142.

Rogers, F. J., Swenson, F. J., and Iglesias, C. A., 1996. *ApJ*, *456*; 902–+.

Ruiz, M. T., Rojo, P. M., Garay, G., and Maza, J., 2001. *ApJ*, *552*; 679–684.

Schenker, K., King, A. R., Kolb, U., Wynn, G. A., and Zhang, Z., 2002. *MNRAS*, *337*; 1105–1112.

Schmidt, G. D. and Norsworthy, J. E., 1991. *ApJ*, *366*; 270–276.

Schmidt, G. D. and Stockman, H. S., 1991. *ApJ*, *371*; 749–760.

Schmidtke, P. C. and Cowley, A. P., 1996. *AJ*, *112*; 167–+.

Schreiber, M. R. and Gänsicke, B. T., 2003. *A&A*, p. in print.

Shakura, N. I. and Sunyaev, R. A., 1973. *A&A*, *24*; 337–355.

Silber, A. D., 1992. Ph.D. Thesis.

Sills, A., Pinsonneault, M. H., and Terndrup, D. M., 2000. *ApJ*, *534*; 335–347.

Solheim, J.-E. and Sion, E. M., 1994. *A&A*, *287*; 503–508.

Somerscales, R. V., Norton, A. J., Wynn, G. A., and West, R. G., 2002. In *ASP Conf. Ser. 261: The Physics of Cataclysmic Variables and Related Objects*, pp. 171–+.

Sproats, L. N., Howell, S. B., and Mason, K. O., 1996. *MNRAS*, *282*; 1211–1222.

Spruit, H. C., 1998. *A&A*, *333*; 603–612.

Spruit, H. C. and Ritter, H., 1983. *A&A*, *124*; 267–272.

Spruit, H. C. and Taam, R. E., 2001. *ApJ*, *548*; 900–907.

Spruit, H. C. and van Ballegooijen, A. A., 1982. *A&A*, *106*; 58–66.

Starrfield, S., 1989. *Classical novae*, p. 123 (Chichester: Wiley, 1989, edited by Bode, M.F.; Evans, A.).

Taam, R. E. and Sandquist, E. L., 2000. *ARA&A*, *38*; 113–141.

Taam, R. E., Sandquist, E. L., and Dubus, G., 2003. submitted to *ApJ*.

Taam, R. E. and Spruit, H. C., 2001. *ApJ*, *561*; 329–336.

Thorstensen, J. R., Fenton, W. H., Patterson, J. O., Kemp, J., Krajci, T., and Baraffe, I., 2002. *ApJ*, *567*; L49–L52.

Uemura, M., Kato, T., Ishioka, R., Yamaoka, H., Schmeer, P., Starkey, D. R., Torii, K., Kawai, N., Urata, Y., Kohama, M., Yoshida, A., Ayani, K., Kawabata, T., Tanabe, K., Matsumoto, K., Kiyota, S., Pietz, J., Vanmunster, T., Krajci, T., Oksanen, A., and Giambersio, A., 2002. *PASJ*, *54*; L15–LL18.

Ulla, A., 1994. Memorie della Societa Astronomica Italiana, *65*; 231–+.

van Ballegooijen, A. A., 1982a. *A&A*, *113*; 99–112.

van Ballegooijen, A. A., 1982b. *A&A*, *106*; 43–52.

van den Heuvel, E. P. J., Bhattacharya, D., Nomoto, K., and Rappaport, S. A., 1992. *A&A*, *262*; 97–105.

van Teeseling, A., 1998. In *ASP Conf. Ser. 137: Wild Stars in the Old West*, pp. 385–+.

van Teeseling, A. and King, A. R., 1998. *A&A*, *338*; 957–964.

van Teeseling, A., Reinsch, K., Pakull, M. W., and Beuermann, K., 1998. *A&A*, *338*; 947–956.

Verbunt, F. and Zwaan, C., 1981. *A&A*, *100*; L7–LL9.

Warner, B., 1987. *MNRAS*, *227*; 23–73.

Warner, B., 1995. *Cataclysmic variable stars* (Cambridge Astrophysics Series, Cambridge, New York: Cambridge University Press, —c1995).

Webbink, R. F., 1985. *Interacting binary stars*, chapter Stellar evolution and binaries, pp. 39–70 (Cambridge Astrophysics Series, Cambridge: Cambridge University Press, 1985, edited by Pringle, J.E.; Wade, R.A.).

Wei, J., Jiang, X., Xu, D., Zhou, A., and Hu, J., 2001. Chinese Journal of Astronony and Astrophysics, *1*; 483–486.

Willems, B. and Kolb, U., 2002. *MNRAS*, *337*; 1004–1016.

Willems, B., Kolb, U., Sandquist, E., Taam, R. E., and Dubus, G., 2003. in preparation.

Wynn, G. A., King, A. R., and Horne, K., 1997. *MNRAS*, *286*; 436–446.